

DISCLAIMER

This report was prepared as an account of work sponsored by an agency of the United States Government. Neither the United States Government nor any agency thereof, nor any of their employees, makes any warranty, expressed or implied, or assumes any legal liability or responsibility for the accuracy, completeness, or usefulness of any information, apparatus, product, or process disclosed, or represents that its use would not infringe privately owned rights. Reference herein to any specific commercial product, process, or service by trade name, trademark, manufacturer, or otherwise does not necessarily constitute or imply its endorsement, recommendation, or favoring by the United States Government or any agency thereof. The views and opinions of authors expressed herein do not necessarily state or reflect those of the United States Government.

This report has been reproduced directly from the best available copy.

Available to DOE and DOE contractors from the Office of Scientific and Technical Information, P.O. Box 62, Oak Ridge, TN 37831; prices available from (615) 576-8401.

Available to the public from the National Technical Information Service, U.S. Department of Commerce, 5285 Port Royal Rd., Springfield VA 22161

DOE/BC/14862-14
Distribution Category UC-122

Productivity and Injectivity of
Horizontal Wells

Annual Report for the Period
March 10, 1995 to March 9, 1996

By
Khalid Aziz
Thomas Hewett

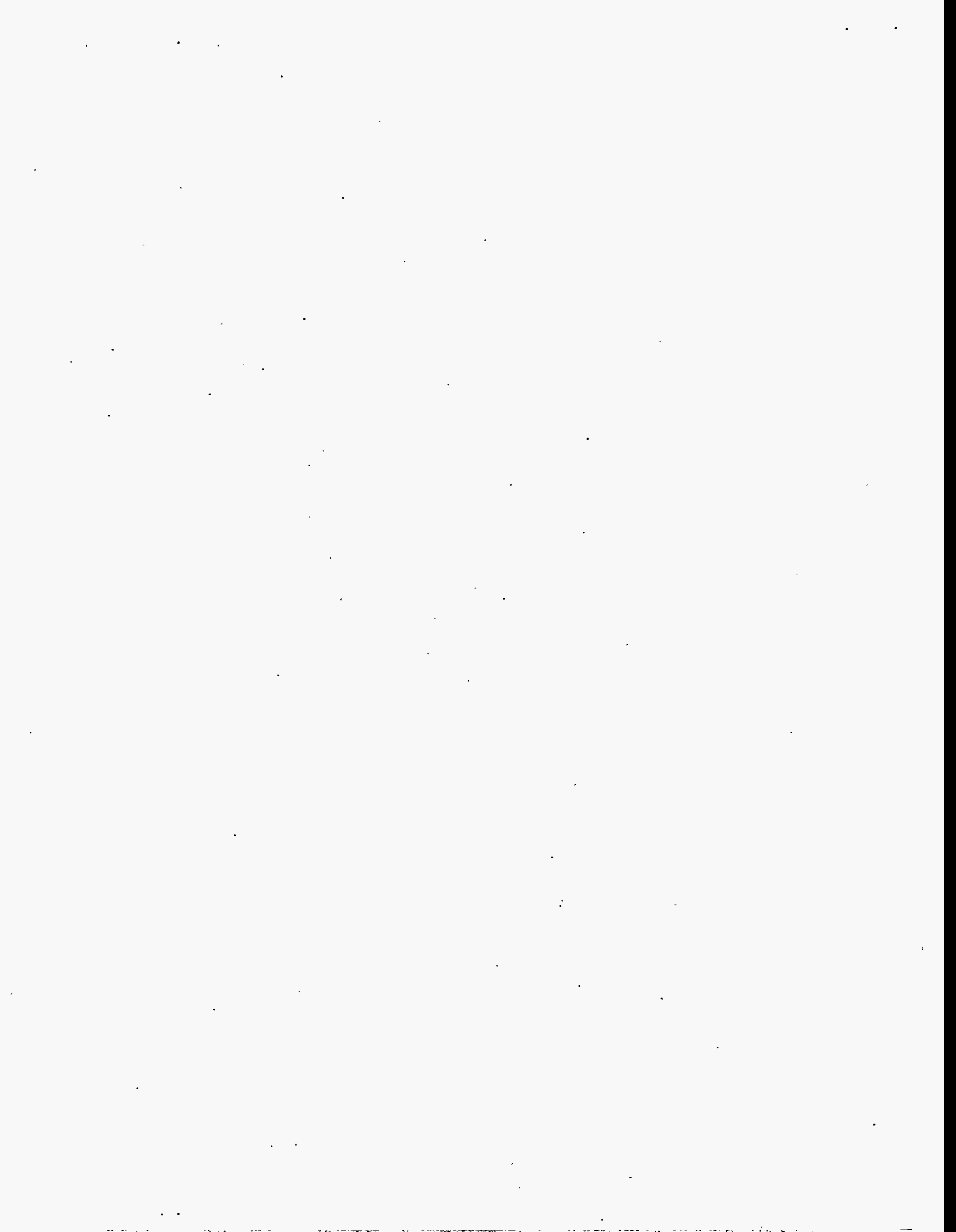
May 1996

Work Performed Under Contract No. DE-FG22-93BC14862

Prepared for
U.S. Department of Energy
Assistant Secretary for Fossil Energy

Thomas B. Reid, Project Manager
Bartlesville Project Office
P.O. Box 1398
Bartlesville, OK 74005

Prepared by
Stanford University
Dept. of Petroleum Engineering
Stanford, CA 94305-2220



Contents

1 Preliminary Analysis of the 1995 Stanford Horizontal Wellbore Experiments	1
1.1 Introduction	1
1.2 Experimental Setup	2
1.3 Analysis of Experimental Data	5
1.3.1 Wellbore Characterization Experiment	5
1.3.2 Single Phase Water Flow with Inflow	7
1.3.3 Air and Water Two-Phase Flow	8
1.4 Mechanisms of Inflow Effect	18
1.5 Model Prediction	20
1.6 Discussion and Conclusions	23
2 Development and Testing of a New Mechanistic Model for Multiphase Flow in Pipes	25
2.1 Introduction	25
2.2 Model description	26
2.2.1 Equilibrium Stratified Flow	26
2.2.2 Annular Mist Flow	29
2.2.3 Intermittent Flow	32
2.2.4 Dispersed Bubble Flow	34
2.2.5 Bubble Flow	34
2.2.6 Froth Flow	35
2.3 Results	35
2.4 Summary and Conclusions	37
3 Well Indices for Horizontal Wells	40
3.1 Introduction	40
3.2 Well Pressure	41
3.2.1 Calculation	41
3.2.2 Validation	41
3.3 Well Index	42
3.3.1 Definition	42
3.3.2 New Model	45
3.3.3 Applications	45
3.4 Conclusions	48

3.5	Appendix: Outline of the 3D Semi-analytical method	51
3.5.1	Description of the Problem	51
3.5.2	Description of the Solution	52
4	Analytical Reservoir/Wellbore Coupling	54
4.1	Previous Work	54
4.2	Modeling	56
4.3	Example Problem	59
4.4	Optimum Well Length	62
4.5	Production Loss vs. Pressure Drop Ratio	66
4.6	Conclusions	70
5	Correlations for Cresting Behavior in Horizontal Wells	73
5.1	Introduction	73
5.2	Mathematical Model	75
5.2.1	General Equations	75
5.2.2	Assumptions	76
5.2.3	Boundary Conditions	77
5.2.4	Dimensionless Variables	77
5.2.5	Parameters	79
5.3	Literature Review	80
5.3.1	Steady-State Solutions	80
5.3.2	Transient Solutions	82
5.4	Development of Equations	87
5.5	Water Cresting Correlations	88
5.5.1	Breakthrough Time	90
5.5.2	Water-Oil Ratio	93
5.5.3	Optimum Grid	93
5.6	Conclusions	98
6	Critical Rates for Simultaneous Gas and Water Cresting in Horizontal Wells	105
6.1	Introduction	105
6.2	Considerations for Horizontal Wells	106
6.2.1	Procedure for Calculating Critical Cresting Rates	107
6.3	Example Problem	107
6.4	Concluding Remarks	109

List of Figures

1.1	Wellbore section used for the 1995 horizontal flow experiments	3
1.2	Average measured wellbore internal diameter for each section	3
1.3	Comparison between predicted and measured pressure at different wellbore locations	6
1.4	Pressure drop for single phase water flow with inflow	7
1.5	Water inflow effect on pressure drop—comparison between two flows with same total water flow rate	8
1.6	Comparison among different fanning friction factors	8
1.7	Air axial flow rate effect—two-phase axial flow with no inflow	9
1.8	Air axial flow rate effect—two-phase axial flow with water inflow	10
1.9	Air inflow flow rate effect—water axial flow with air inflow	10
1.10	Air inflow flow rate effect—two-phase axial flow with air inflow	10
1.11	Air inflow flow rate effect—comparison between air axial flow and air inflow	11
1.12	Water axial flow rate effect—two-phase axial flow with no inflow	11
1.13	Water axial flow rate effect—water axial flow with air inflow	11
1.14	Water axial flow rate effect—two-phase axial flow with water inflow	12
1.15	Water axial flow rate effect—two-phase axial flow with air inflow	12
1.16	Water axial flow rate effect—two-phase axial flow and inflow	12
1.17	Two-phase inflow rate effect—comparison between two-phase axial flow with and without two-phase inflow	13
1.18	Two-phase inflow pattern specification	14
1.19	Two-phase inflow pattern effect—low flow rate case	14
1.20	Two-phase inflow pattern effect—high flow rate case	14
1.21	Difference between the measured pressure drop and its real value	15
1.22	Pipe inclination effect—single-phase water flow	16
1.23	Pipe inclination effect—water axial flow with air inflow	16
1.24	Pipe inclination effect—two-phase axial flow with air inflow	16
1.25	Pressure drop comparison at 1.0 MMscfD air and 7.0 MbpD water flow rates	17
1.26	Inflow effect on boundary layer	19
1.27	Inflow effect on kinetic energy	19
1.28	Inflow effect on flow pattern	19
1.29	Segmented model approach	21
1.30	Comparison between model prediction and measurement—air & water axial flow	21
1.31	Comparison between model prediction and measurement—water axial flow with air inflow	22

1.32	Comparison between model prediction and measurement—air & water axial flow with air inflow	22
1.33	Comparison between model prediction and measurement—air & water axial flow and inflow	23
2.1	Momentum balance with two segregated fluids	26
2.2	Characteristics of annular-mist flow	30
2.3	Intermittent flow model	32
2.4	Comparison of calculated liquid volume fraction with experimental data . . .	36
2.5	Comparison of calculated pressure gradient with experimental data	36
3.1	Flow regimes of a mildly laterally penetrating horizontal well	42
3.2	Comparison between a classical 2D solver and the 3D solution for one fully penetrating well (2D problem) in the middle of the reservoir	43
3.3	Comparison between a classical 2D solver and the 3D solution for an injector and a producer	44
3.4	Comparison between Eclipse and the 3D solution for a single fully penetrating well	44
3.5	Variations of r_0 with time for Eclipse and for the new model for a 3D problem	47
4.1	Flow Rate vs. Well Length: Single Phase Oil	60
4.2	Flow Rate vs. Well Length: Two-Phase Flow, GOR=1000 SCF/STB, Homogeneous Flow Model Used	61
4.3	Flow Rate vs. Well Length: Two-Phase Flow, GOR=1000 SCF/STB, Beggs & Brill Correlation Used	62
4.4	Comparison Plot With Different Models For Wellbore Pressure Drop (Fixed Drawdown of 15 psi)	63
4.5	Horizontal Well Divided Into Three Sections	64
4.6	Effect of Wellbore Roughness With 15 psi Drawdown	66
4.7	Effect of Wellbore Roughness With 25 psi Drawdown	67
4.8	Effect of Viscosity	68
4.9	Effect of Permeability	69
5.1	Comparison of breakthrough time correlation and simulation results	92
5.2	Comparison of various correlations for breakthrough time	94
5.3	Effect of production rate in WOR as a function of time	95
5.4	Effect of mobility ratio in WOR as a function of time	95
5.5	Effect of lateral reservoir size in WOR as a function of time	96
5.6	Effect of well height in WOR as a function of time	96
5.7	Effect or oil relative permeability exponent in WOR as a function of time . .	97
5.8	Comparison of WOR correlation and simulation results for a dimensionless rate of 0.7	97
5.9	Comparison of WOR correlations and simulation results for a dimensionless rate of 0.7	99
5.10	Effect of vertical block dimension in WOR as a function of time	99

6.1	Schematic of the water and gas coning problem in vertical wells as considered by Piper and Gonzalez	105
6.2	Variation of critical oil rate versus distance to the top of the completion for vertical wells	106
6.3	Comparison of the shape of interface between simulation and the semi-analytical method for both gas and water crests	108

List of Tables

1.1	Experiments Conducted in 1995	4
1.2	Overall Pressure Drop Comparison	18
1.3	Inflow Pattern Effect at High Flow Rate	18
2.1	Comparison with Experimental Data	37
2.2	Flow Pattern Distribution in Experimental Data	37
3.1	Geometric Parameters Used for Validation (A)	41
3.2	Geometric Parameters Used for Validation (B)	42
3.3	Geometric Parameters Used for Validation (C)	43
3.4	Geometric Parameters Used for Validation (D)	45
3.5	Rock and Fluid Properties	45
3.6	Parameters Used in the Application Examples	46
4.1	Parameters Used in Example Problems	59
5.1	Assumptions and BC used to get steady-state solutions. Refer to sections 5.2.2 and 5.2.3	82
5.2	Assumptions and BC used to get transient solutions. Refer to sections 5.2.2 and 5.2.3	85
5.3	Dimensionless variables used to get transient solutions. Refer to section 5.2.4	86
5.4	Parameters used to develop BT and WOR correlations. Refer to section 5.2.5	86
5.5	Basic data set for simulation runs	90
5.6	Dimensionless BT and parameters C and m of Equation 5.73 for each simulated data. A blank entry indicates that parameter has same value of reference case (first row)	91
5.7	Correlations for BT using equation 5.72 with each parameter for the reference case.	92
5.8	Variations in BT and N_{pd} with grid size for the reference case.	94
6.1	Comparison of Critical Rates from the Method and the Simulation	108

Management Summary

1. DOE Approval

The DOE approval for the annual renewal of the research grant to the Stanford Project on the *Productivity and Injectivity of Horizontal Wells* was received in early March 1995. The Project formally commenced on March 10, 1993. Mr. Thomas Reid is the DOE Project Manager in Bartlesville and Mr. John Augustine is the DOE Contracts Officer in Pittsburgh.

2. Industrial Affiliates Program

The DOE Project operates in association with an Industrial Affiliates program on horizontal wells, for which oil company membership has also continued during 1995. The membership during this year comprised the following organizations:

Amoco (USA)
AGIP (Italy)
ARTEP/IFP (France)
BP Exploration (USA)
Chevron (USA)
INTEVEP (Venezuela)
Marathon (USA)
Mobil (USA)
Norsk Hydro (Norway)
Petrobras America (Brazil)
Phillips Petroleum (USA)
Texaco (USA)
Union Pacific Resources (USA)
US Department of Interior/
Minerals Management Service (USA)

3. Project Goals

The Project has eight principal goals to be studied and developed over a five year period. These goals are as follows:

TASK 1: Advanced Modeling of Horizontal Wells - Develop special gridding techniques and associated averaging algorithms for accurate simulation of HW-performance.

TASK 2: Investigate and Incorporate the Effects of Reservoir Heterogeneities - Study impacts of various types of heterogeneity and develop methods for incorporating their effects in both fine grid and coarse grid models.

TASK 3: Develop Improved Methods for Calculating Multi-Phase Pressure Drops within the Wellbore - Plan, execute, and interpret two-phase flow experiments at an oil company research facility, and use results to analyze/validate a new two-phase model.

TASK 4: Pseudo-Functions - Define improved methods for computing two-phase pseudo-functions for effective relative permeabilities for coarse grid blocks near an HW - determine sensitivities to heterogeneities, flow conditions, skin factors, etc.

TASK 5: Develop Multi-Well Models - Develop numerical techniques and software in a parallel computing architecture capable of interactively coupling multiple detailed HW-models to a large scale reservoir simulator.

TASK 6: Test HW-Models with Field Examples - Work with affiliate's member companies to establish HW-modeling capabilities from field measurements, particularly for pathological problem cases.

TASK 7: EOR Applications - Provide and implement practical HW aspects into modeling of EOR processes - miscible gas, steam displacement, in-situ combustion.

TASK 8: Application Studies and Their Optimization - Seek field opportunities for HW's and study their best implementation in various reservoir scenarios e.g., multiple laterals, hydraulic fracture variants, etc.

Tasks 1, 3, and 4 were the primary focus of activities in 1995, and the annual report is therefore written around these three tasks, which are also ongoing in 1996. Some of our principal achievements are summarized below.

4. Large-Scale Flow Loop Experiments

The funding from the Industrial Affiliates Project is mainly expended on a series of large scale experiments in an outdoor flow loop being conducted at the Marathon Research Center in Littleton, Colorado. Contractual arrangements have continued with Marathon to undertake these experiments, for which a substantial part of the costs (~ 50%) is born by Marathon. In 1995, extensive modifications were made to the rig in order to (1) perform high gas rate experiments (up to 1.7 MMscf/day from the previous high of 0.5 MMscf/day), (2) reduce entrance effects by making the inlet pipe diameter to conform with the test section diameter of 6.2 inches and extending the inlet length by 8 ft, (3) add the capability of running experiments at small downflow inclination angles, and (4) enhance and automate the data acquisition system. The inflow section of the model was also extended from 40 ft to 75 ft, thus allowing for the gathering of more data involving radial perforation flow. The higher gas rates were achieved by using three compressors which were rented for this purpose and the separator was improved to handle the higher gas rates. The fluids in all the experiments were water and air. More than 230 two-phase flow experiments were performed. These experiments include single phase axial water flow with the inflow of water or air, two-phase axial flow with no radial influx, two-phase axial flow with the inflow of water or air, and finally two-phase axial flow with various arrangement of the influx of water and air through perforations. In addition to horizontal flow experiments, some of the experiments were also carried out at +2° (upflow) and -2° (downflow). Differential pressures were recorded along the wellbore using Rosemount pressure transmitters. Three nuclear densitometers were also employed in an attempt to measure the in-situ liquid fractions at three locations along the wellbore model. The observed flow regimes as seen through the transparent acrylic pipe

were recorded on video tape for every experiment resulting in about 60 hours of recording. These data are being used to check the physical flow regimes in the two-phase flow analysis and modeling. The experimental work was financed by the Industrial Consortium for this project.

5. Improved Theoretical Modeling of Two-Phase Flow within the Wellbore

Advances have been made in the mechanistic model under development at Stanford. Stratified flow and annular mist flow regimes have been studied in detail resulting in new and improved correlations for these two flow patterns. Namely, in the case of stratified flow, new correlations for wall friction factor have been developed while studies on the annular mist flow have resulted in new correlations for liquid fraction entrained and gas-liquid interfacial factors. The many features of the Stanford mechanistic model are being tested against data from many sources including our own two-phase flow experiments. A general flow model has recently been developed for modeling single phase axial flow with single phase fluid influx. Two separate and detailed reports on this aspect of the project will be submitted to be published as technical reports. One report will describe a general single phase flow model with inflow recently developed and the other will cover the Stanford multiphase mechanistic model. Various improvements have also been made to the many features of the Stanford multiphase flow database. This work is supported partially by the Stanford Reservoir Simulation Industrial Affiliates Program (SUPRI-B).

6. Well Indices and Pseudo-Functions

It is not generally established which techniques are best employed to generate well indices which tie the well pressure to the grid block pressures for realistic horizontal and multilateral wells of complex profile. We have been studying this problem analytically in 1995 and will continue in 1996 where horizontal wells with complex profiles can be modeled using a continuous point source solution. This approach has many significant applications: (1) the analytical solution can be used to calculate exact well indices for use in a simulator, and (2) we can compute shape factors for horizontal wells of any trajectory (e.g., dual laterals) which provide an easy way to estimate the well productivity index in the transient and the pseudo steady-state flow regimes.

7. Well Indices and Pseudo-Functions

Another research work started in 1995 is to develop a coarse grid method which can be used to accurately study breakthrough times of horizontal wells and possibly the subsequent gas or water production behavior. The method should be fairly general and also be able to accurately model the actual movement of a water or a gas front on coarse grids. One way to accomplish this is to incorporate a breakthrough correlation to act as a pseudo function on a coarse grid. We are currently developing general breakthrough correlations based on fine grid simulations and analytical approaches.

8. Analytical Reservoir/Wellbore Coupling

While simulators can be used to predict the performance of horizontal wells, simple models are needed to quickly respond to such questions as: What is the optimum length of a horizontal well? What is the relative effect of wellbore friction, and various reservoir and fluid parameters on well performance. A simple and flexible model to answer such questions has been developed and a sensitivity study was conducted. It is shown that while long horizontal wells, high permeabilities, low drawdowns and high flow rates tend to increase the effect of wellbore pressure loss on productivity, high fluid viscosities tend to decrease this effect. The model uses an integrated treatment of flow in the reservoir and the well which allows for easy accommodation of any flow model in the well and in the reservoir.

9. Coning and Cresting Methods

We have extended our previous semi-analytical solution method for calculating critical cresting oil rates to the case of simultaneous water and gas cresting. Simulations on test problems show very good agreement with the predictions of the method.

10. Generalized Gridding Methods

Work on developing a 3D generalized flexible gridding code has progressed well during 1995 and is near completion. A control volume based finite difference scheme for reservoir simulation has been developed. Full, anisotropic and asymmetric permeability can readily be handled and the permeability tensor can vary from block to block, both in magnitude and direction. Thus it will be of great value in modeling fluid flow in reservoirs where principal permeability directions vary between beds or within a bed. The scheme can be used with Voronoi grids in 2D, control volume finite element (CVFE) type grids in 2D and 3D and Variations of CVFE type grid.

An object oriented reservoir simulator called FLEX has been written to implement and test various gridding schemes. Two-phase oil/water flow simulations both in 2D and 3D have been done to validate the numerical approach used in this work. Results from FLEX on tests involving homogeneous full symmetric tensors were identical to those from commercial simulators Eclipse and Imex. Flex is currently being further tested for more complex problems, which include aligning gridblocks along streamlines, use of upscaled diagonalized permeabilities in 2D and 3D, use of full (anisotropic and asymmetric) tensors obtained from upscaling, etc. The modularity of FLEX allows easy incorporation of changes or additions. The Ph.D. dissertation on this research will be published as a technical report.

11. Effects of Heterogeneities on Flow Performance

Our previous studies had shown that the complex flow paths induced by a producing horizontal well in the presence of horizontal shales could not be represented on a coarsened regular grid. A method based on the calculation of streamlines for single phase flow subjected to the actual boundary conditions was developed to modify the geometry of the coarsened grid blocks to remove the non-physical flows resulting in negative transmissibilities. This approach was shown to provide an accurate means of calculating well flow rates for given pressure drawdowns, whereas conventional methods were in error by significant percentages.

This method was also extended to calculations for multiphase flow in two dimensions. A semi-analytical approach to defining appropriate multiphase flow properties has been devised which is fast, accurate, and does not require a solution of the multiphase flow equations on a high resolution reservoir model with subsequent averaging. The multiphase method has been extended to three dimensions and the continuing work will focus on using this approach for defining scaled up multiphase flow properties in three dimensions.

12. Affiliates Progress Review Meeting

An annual review meeting for member companies in the Stanford Horizontal Well Project was held at Stanford on October 19-20, 1995. This meeting was well attended and member companies made presentations on their horizontal well interests and activities on the second day. The next meeting is scheduled for October 10 and 11, 1996, to be right after the SPE Fall Meeting, for the benefit of travel arrangements for overseas members.

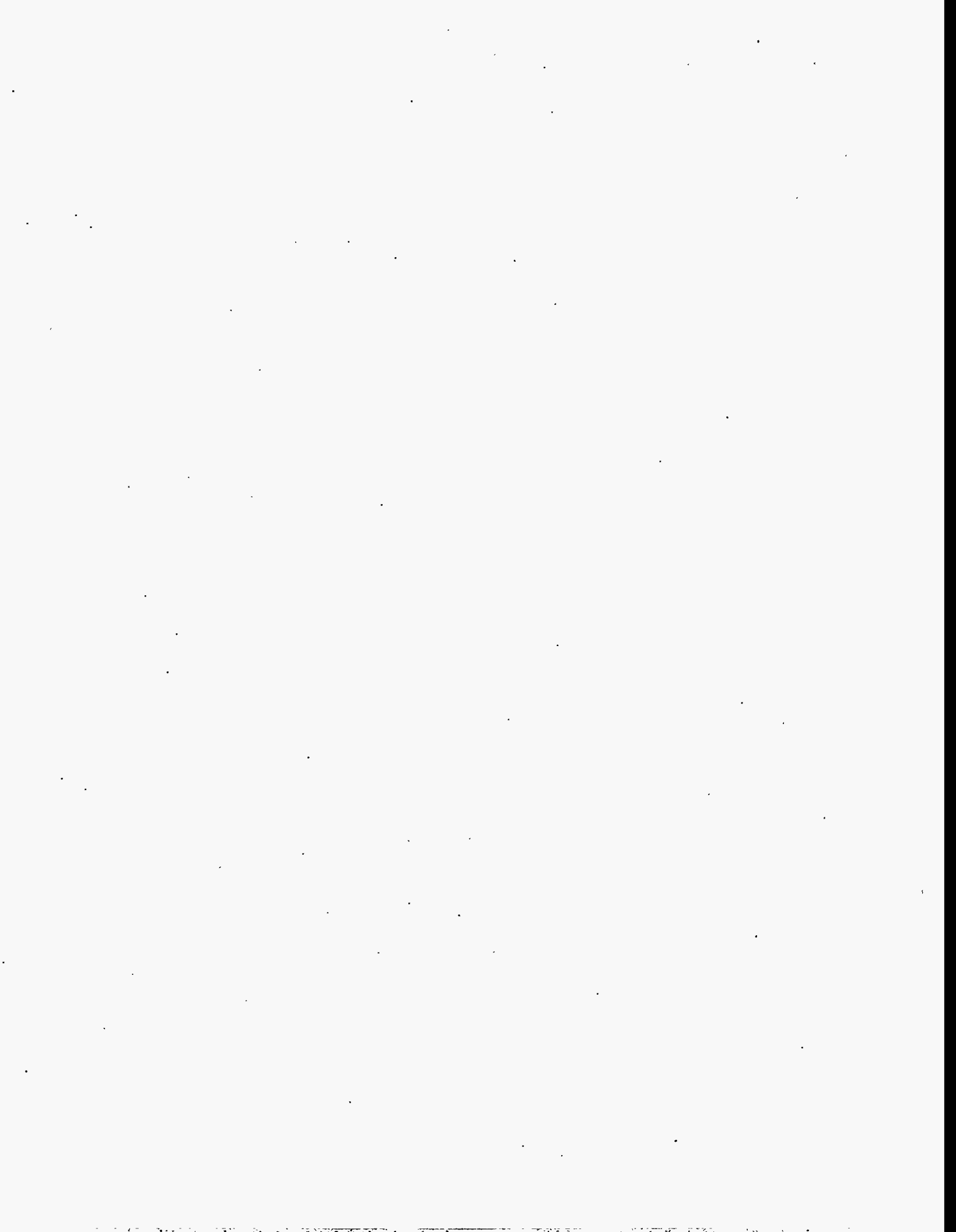
13. Presentations at Conferences, etc.

A number of presentations were made at various technical conferences and forums:

1. "*Use of Simulators for Horizontal Well Evaluation*" presented at 1995 SPE Forum on Horizontal Well Evaluation and Performance Assessment - Snowmass CO, July 30-August 4
2. Two presentations on *Reservoir Management* and *The Way Forward* presented at 1995 SPE Forum on Horizontal Wells: Problems and Solutions - Dubai, UAE, Nov 25-30.

We also attended the following meetings:

- SPE Karachi Section Meeting on Use of Horizontal and Non-Conventional Wells for Oil and Gas Field Development held, at Islamabad Office of Occidental of Pakistan in Karachi on November 23 and December 8, 1995.
- BP Workshop on Non-Conventional Wells where Stanford Horizontal Well Project was discussed, held on Feb 20-22, 1996 in Seattle, Washington.



1. Preliminary Analysis of the 1995 Stanford Horizontal Wellbore Experiments

by *Liang-Biao Ouyang, Sepehr Arbabi, and Khalid Aziz*

Abstract

Brief introduction and analysis of the 1995 Stanford Horizontal Wellbore experiments is presented. The influence of inflow on wellbore flow for both single phase and two-phase cases is investigated. Different mechanisms, including boundary layer effect, kinetic energy effect, and flow pattern effect, have been proposed to explain inflow effect. Comparison between measurement and prediction by existing mechanistic models or empirical correlations is also performed.

1.1 Introduction

Over the last decade horizontal wells have become a well established technology for the recovery of oil and gas. They have become increasingly attractive for production from thin reservoirs, naturally fractured reservoirs, reservoirs with gas and water coning problems, offshore environments where various wells are drilled from a central platform, as well as in the enhanced oil recovery practices such as steam injection.

Modeling of horizontal wells poses additional challenges, one of which is the determination of the frictional pressure drop along the wellbore. The pressure drop due to friction is usually neglected in classical reservoir simulation models. However, practical examples have shown that in many cases the inclusion of wellbore friction is essential for the correct prediction of well performance. For horizontal wells, the frictional pressure drop becomes even more significant, since the drilling technology now allows wells to be several thousands of feet long. Thus the frictional pressure drop over the production portion of the well will be much larger in horizontal wells compared to that in vertical wells.

Depending on the completion method used in a horizontal well, fluid may enter the wellbore radially through perforations at various locations, which alters the flow behavior along the wellbore and complicates the modeling of the problem. For single phase flow, Ouyang & Aziz [1] have shown that influx through well perforations increases the wall friction for the laminar flow regime and decreases the wall friction for the turbulent flow regime. This means that the frictional pressure drop can be larger or smaller than that for no influx or no-wall-flow situations depending on the flow regime present in the wellbore. In addition, as the distance between adjacent perforations may not be long enough to achieve a stabilized velocity profile, the flow characteristics and the pressure gradient in a horizontal wellbore may change with location. The flow behavior in a horizontal wellbore, with an increasing flow rate along it due to influx, and the relationship between pressure drop and influx from reservoir are some of the most important but unsolved issues in the engineering analysis of horizontal wells. Furthermore, in certain cases, gas and liquid flow simultaneously in horizontal wellbores under different flow patterns. Since various

flow patterns behave differently when no influx is present through the pipe walls, with inflow the problem will become much more complicated.

Literature survey leads to the following observations:

- No correlations exist for determining the wall friction factors for single phase and multiphase fluid flow in a wellbore with inflow or outflow through perforations.
- The accelerational and inflow-directional pressure drops are neglected in most of the single wellbore flow models or wellbore-reservoir coupling models.
- The wall friction shear is usually evaluated by using the friction factor correlations for pipe flow without mass transfer through the pipe wall. Therefore, the impact of mass transfer through the pipe wall on the wall friction is not included.
- No mechanistic model has been developed to predict the flow characteristics, such as flow pattern, liquid holdup and pressure drop in multiphase wellbore flow with the presence of inflow or outflow through perforations.

In order to investigate the influence of inflow on single phase and multiphase wellbore flow behaviors, experiments have been designed and performed in 1994 for oil-nitrogen and in 1995 for air-water flow in a 100 feet-long horizontal wellbore model at the Marathon Oil Company's Littleton facility. This report focuses on a preliminary analysis of the 1995 Stanford Horizontal Wellbore Experiments for multiphase flow. A separate report will be presented on the new single phase wellbore flow model and new wall friction factor correlations which have been developed at Stanford (Ouyang & Aziz, [1]).

1.2 Experimental Setup

The horizontal wellbore flow model can be sketched as shown in Figure 1.1. The wellbore test section is 100 feet long and consists of twenty 5-foot sections. The perforations begin at the 85-foot location and end at the 10-foot location. Figure 1.2 shows the average measured wellbore inside diameters for each section. From this figure it can be seen that the wellbore internal diameters range from 6.15 inch to about 6.30 inch, this range is smaller than that of the wellbore employed for the 1994 experiments. Except for the 20-25 feet section, the 55-60 feet section and the 80-95 feet section, variation in the pipe internal diameter is quite small (less than 0.05 inch).

A total of 134 experiments have been conducted (Table 1.1) which can be classified as:

- Single phase water flow without inflow – calibration experiment (series 0)
- Single phase water axial flow with water inflow (series IA1–IA3)
- Air and water two-phase flow
 1. Air-water axial flow without inflow (series IIA1–IIA3)
 2. Water axial flow with air inflow (series IIB1–IIB3)
 3. Air-water axial flow with single phase inflow
 - Water inflow (series IIC1a–IIC1c)
 - Air Inflow (series IIC2a–IIC2b)
 4. Air and water axial flow with air and water inflow (series IID1a–IID3b)

For each experimental run, axial flow and inflow flow rates; the liquid fractions at 11.25 feet, 36.25 feet, and 61.25 feet locations; pressure drops every 10 feet and 50 feet; pipe inclination angle; inlet and outlet temperatures and pressures were measured and recorded automatically into a Microsoft Excel file for later analyses. For most experiments, data were recorded for at least 10 minutes after reaching stabilized flow. The flow along the whole wellbore was video-taped and the flow patterns at 11.25 feet, 36.25 feet and 61.25 feet locations were also recorded.

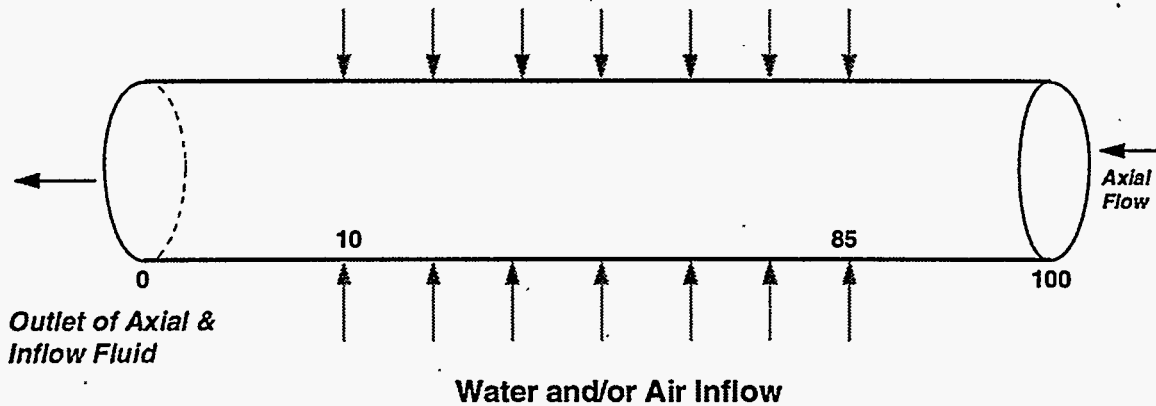


Figure 1.1: Wellbore Section Used for the 1995 Horizontal Flow Experiments

Average Measured Wellbore Inside Diameter

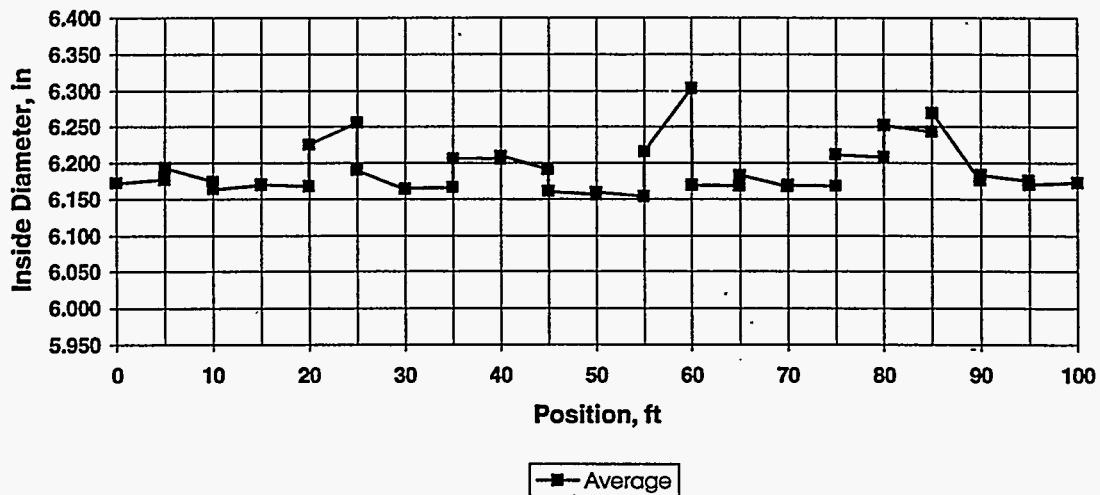


Figure 1.2: Average Measured Wellbore Internal Diameter for Each Section

Table 1.1: Experiments Conducted in 1995

Experiment Series	Exp. Number	Angle	Axial Flow		Inflow		Inflow Location	
			water	air	water	air	water	air
0	1	0	17.1		N/A		N/A	
Wellbore Char.	2	0	30		N/A		N/A	
IA1	3	0	6.9		3.4		10. - 85.	
Water inflow (L)	4	0	10.3		3.4		10. - 85.	
IA2	5	0	6.9		6.9		10. - 85.	
Water inflow(M)	6	0	10.3		6.9		10. - 85.	
IA3	A5	0	13.7		10.3		10. - 85.	
Water inflow(H)	A6	0	17.1		10.3		10. - 85.	
IIA1	7	0/-2/+2	3.4	0.5	N/A		N/A	
Air core flow	8	0/-2/+2	6.9	0.5	N/A		N/A	
low rate	9	0/-2/+2	10.3	0.5	N/A		N/A	
	10	0/-2/+2	13.7	0.5	N/A		N/A	
IIA2	11	0/-2/+2	3.4	1.0	N/A		N/A	
Air core flow	12	0/-2/+2	6.9	1.0	N/A		N/A	
Intermediate	13	0/-2/+2	10.3	1.0	N/A		N/A	
	14	0/-2/+2	13.7	1.0	N/A		N/A	
IIA3	15	0/-2/+2	3.4	1.7	N/A		N/A	
Air core flow	16	0/-2/+2	6.9	1.7	N/A		N/A	
high rate	17	0/-2/+2	10.3	1.7	N/A		N/A	
	18	0/-2/+2	13.7	1.7	N/A		N/A	
IIB1	19	0/-2/+2	3.4			0.5	10. - 85.	
Air Inflow	20	0/-2/+2	6.9			0.5	10. - 85.	
low rate	21	0/-2/+2	10.3			0.5	10. - 85.	
	22	0/-2/+2	13.7			0.5	10. - 85.	
IIB2	23	0/-2/+2	3.4			1.0	10. - 85.	
Air Inflow	24	0/-2/+2	6.9			1.0	10. - 85.	
Intermediate	25	0/-2/+2	10.3			1.0	10. - 85.	
	26	0/-2/+2	13.7			1.0	10. - 85.	
IIB3	27	0	3.4			1.7	10. - 85.	
Air Inflow	28	0	6.9			1.7	10. - 85.	
high rate	29	0	10.3			1.7	10. - 85.	
	30	0	13.7			1.7	10. - 85.	
IIC1a	31	0/-2/+2	3.4	0.5	3.4		10. - 85.	
Air core flow	32	0/-2/+2	6.9	0.5	3.4		10. - 85.	
water inflow	33	0/-2/+2	10.3	0.5	3.4		10. - 85.	
	34	0/-2/+2	13.7	0.5	3.4		10. - 85.	
IIC1b	35	0/-2/+2	3.4	1.0	3.4		10. - 85.	
Air core flow	36	0/-2/+2	6.9	1.0	3.4		10. - 85.	
water inflow	37	0/-2/+2	10.3	1.0	3.4		10. - 85.	
	38	0/-2/+2	13.7	1.0	3.4		10. - 85.	

Table 1.1: Experiments Conducted in 1995 (continued)

Experiment Series	Exp. Number	Angle	Axial Flow		Inflow		Inflow Location	
			water	air	water	air	water	air
IIC1c	39	0	3.4	1.7	3.4		10. - 85.	
Air core flow	40	0	6.9	1.7	3.4		10. - 85.	
water Inflow	41	0	10.3	1.7	3.4		10. - 85.	
	42	0	13.7	1.7	3.4		10. - 85.	
IIC2a	43	0/-2/+2	3.4	0.5		0.5		10. - 85.
Air core flow	44	0/-2/+2	6.9	0.5		0.5		10. - 85.
air Inflow	45	0/-2/+2	10.3	0.5		0.5		10. - 85.
	46	0/-2/+2	13.7	0.5		0.5		10. - 85.
IIC2b	47	0/-2/+2	3.4	0.5		1.0		10. - 85.
Air core flow	48	0/-2/+2	6.9	0.5		1.0		10. - 85.
air Inflow	49	0/-2/+2	10.3	0.5		1.0		10. - 85.
	50	0/-2/+2	13.7	0.5		1.0		10. - 85.
IID1a	51	0	3.4	0.5	3.4	0.5	10. - 47.5	47.5 - 85
	52	0	13.7	0.5	3.4	0.5	10. - 47.5	47.5 - 85
IID1b	53	0	3.4	0.5	3.4	0.5	10. - 47.5	47.5 - 85
	54	0	13.7	0.5	3.4	0.5	10. - 47.5	47.5 - 85
IID2a	55	0	3.4	0.5	3.4	0.5	47.5 - 85	10 - 47.5
	56	0	13.7	0.5	3.4	0.5	47.5 - 85	10 - 47.5
IID2b	57	0	3.4	0.5	3.4	0.5	47.5 - 85	10 - 47.5
	58	0	13.7	0.5	3.4	0.5	47.5 - 85	10 - 47.5
IID3a	59	0	3.4	0.5	3.4	0.5	10 - 78.7	16.3 - 85
	60	0	13.7	0.5	3.4	0.5	10 - 78.7	16.3 - 85
IID3b	61	0	3.4	0.5	3.4	1.0	10 - 78.7	16.3 - 85
	62	0	13.7	0.5	3.4	1.0	10 - 78.7	16.3 - 85
Total	134							

1.3 Analysis of Experimental Data

1.3.1 Wellbore Characterization Experiment

As can be imagined, the effective wellbore roughness will be altered (becomes higher) due to the perforations drilled in the wellbore. The determination of the effective wellbore pipe roughness is an important issue for data analysis.

Kloster [2] experimentally studied flow resistance in a perforated pipe without inflow through the perforations by using a pipe of $6\frac{5}{8}$ inch OD and 17-feet in length. The pipe had a perforated section of 14-feet long with a perforation density of 180 holes per foot. The Reynolds

number covered in his study ranged from 60,000 to 450,000. He found that friction factor vs Reynolds number relationship didn't exhibit the characteristics of regular pipe flow. The friction factor for perforated pipe did not decrease with increasing Reynolds number for the whole Reynolds number range investigated. It reached a local maximum between $Re = 160,000$ and $Re = 220,000$ where the friction factor increased about 60–70% over the value determined by Reynolds number and pipe roughness. For Reynolds number less than 160,000, the friction factor increased about 55%, while it increased about 25–45% for Reynolds number greater than 220,000. Su & Gudmundsson [3] measured the mass flow rates and water column heights for single phase water flow along a vertical tube. For comparison purposes, both the experimental data for flow before and after perforation drilling were measured. Based on their measurement, Su & Gudmundsson [3] introduced a roughness function which was correlated as a function of the perforation/casing diameter ratio.

Although the analyses associated with the above two studies for single phase water flow in a perforated pipe need to be improved, the observations do imply that the effective pipe roughness is augmented by perforations.

In order to determine the effective pipe roughness for the wellbore used in our experiments, two characterization experimental runs (series 0), one with water flow rate of 17.5 MbpD, and the other with water flow rate of 30.0 MbpD, were performed. By changing the effective pipe roughness, the best match between prediction and measurement of the pressure drops for each section can be achieved. The best match is referred here to the point where either the minimum absolute difference or the minimum absolute relative difference between prediction and measurement is reached. Figure 1.3 shows the comparison between measurement and prediction obtained from two effective pipe roughnesses, 6.8×10^{-5} feet which is derived from the minimum of absolute difference, and 9.8×10^{-5} feet which is derived from the minimum of absolute relative difference. The comparison indicates that the effective pipe roughness of 9.8×10^{-5} feet gives better prediction. Analysis for the 17.5 MbpD water flow rate case leads to a value of the effective pipe roughness very close to that for the 30 MbpD water flow rate case.

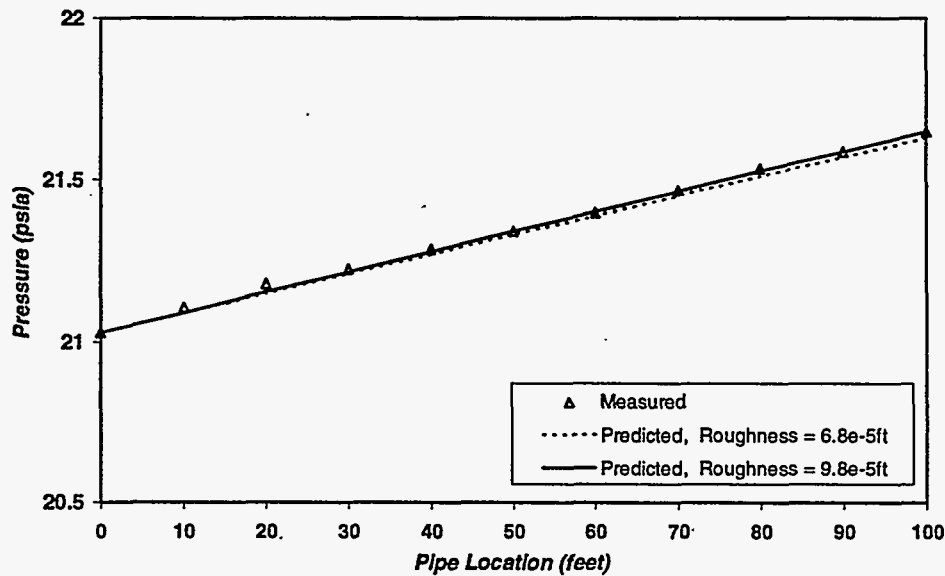


Figure 1.3: Comparison between Predicted and Measured Pressure at Different Wellbore Locations

1.3.2 Single Phase Water Flow with Inflow

Figure 1.4 compares pressure drops for different combinations of water axial and inflow rates. It can be observed that the higher the axial water flow rate, or the higher the water inflow rate, the higher the pressure drops. A more revealing comparison is displayed in Figure 1.5, where two single phase water flows with the same amount of total water flow rate of 17.5 MbpD, one with only axial water flow, the other with 10.5 MbpD of axial flow and 7.0 MbpD of inflow, are compared. Along the first half of the wellbore, the pressure drops for the 10 feet sections with no inflow are higher than for the case with inflow, while along the second half of the wellbore pressure drops for the case with no inflow are lower than for the case with inflow. Note that from the inlet (100 feet location) up to the 10 feet wellbore location, the average local water velocity is always higher for the case with no inflow than for the case with inflow. Therefore it is very natural to conclude from Figure 1.5 that inflow increases the pressure drop along the wellbore. As used by some researchers, such as Shapiro et al. [4], Kays & Crawford [5], the apparent friction factor can be introduced here to describe the pressure drop along the wellbore. Then the above observation is equivalent to saying that inflow increases the apparent friction factor. The statement is correct but dangerous, since it is easy for engineers to get the impression that inflow increases wall friction. Figure 1.6 demonstrates why the impression is inappropriate. It shows the change of three friction factors with wellbore locations, the total (apparent) friction factor obtained on the basis of measurements, the actual friction factor obtained from measurement and new single phase wellbore flow model (Ouyang & Aziz, [1]), and the no-wall-flow friction factor obtained from the Colebrook-White [6, 7] equation by using local Reynolds number and effective pipe roughness. The apparent friction factor is larger than the no-wall-flow friction factor, but the actual friction factor is smaller than the no-wall-flow friction factor. In other words, the wall friction factor is reduced (not augmented) by inflow. This can be easily explained by the inflow and outflow influence mechanisms detailed in Ouyang & Aziz [1], it is a result of the existence of turbulent flow in all the single phase water flow experiments.

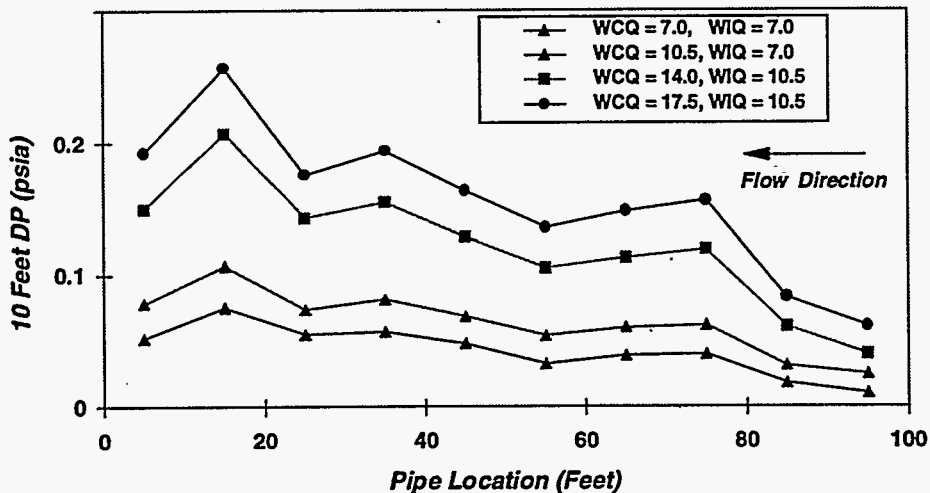


Figure 1.4: Pressure Drop for Single Phase Water Flow with Inflow

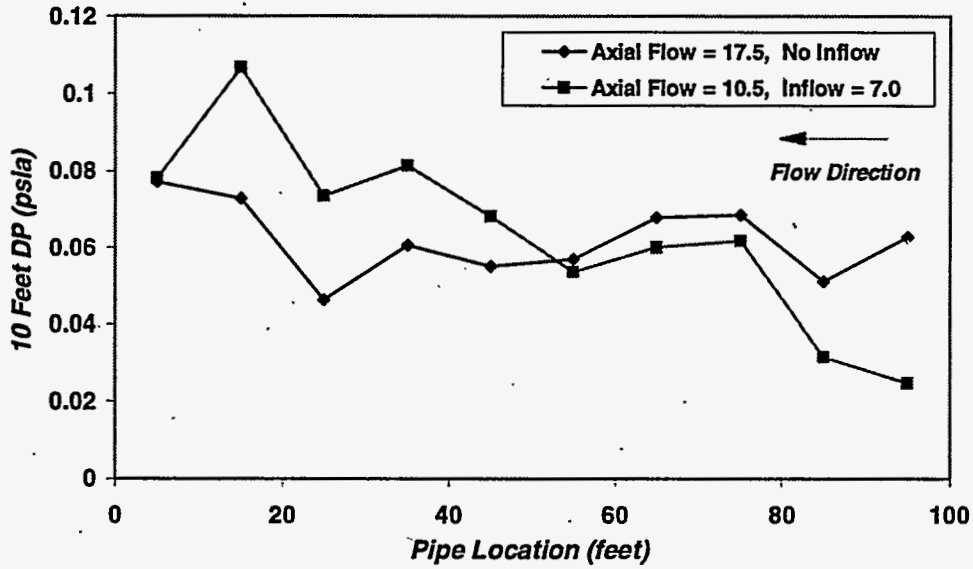


Figure 1.5: Water Inflow Effect on Pressure Drop--Comparison between Two Flows with Same Total Water Flow Rate

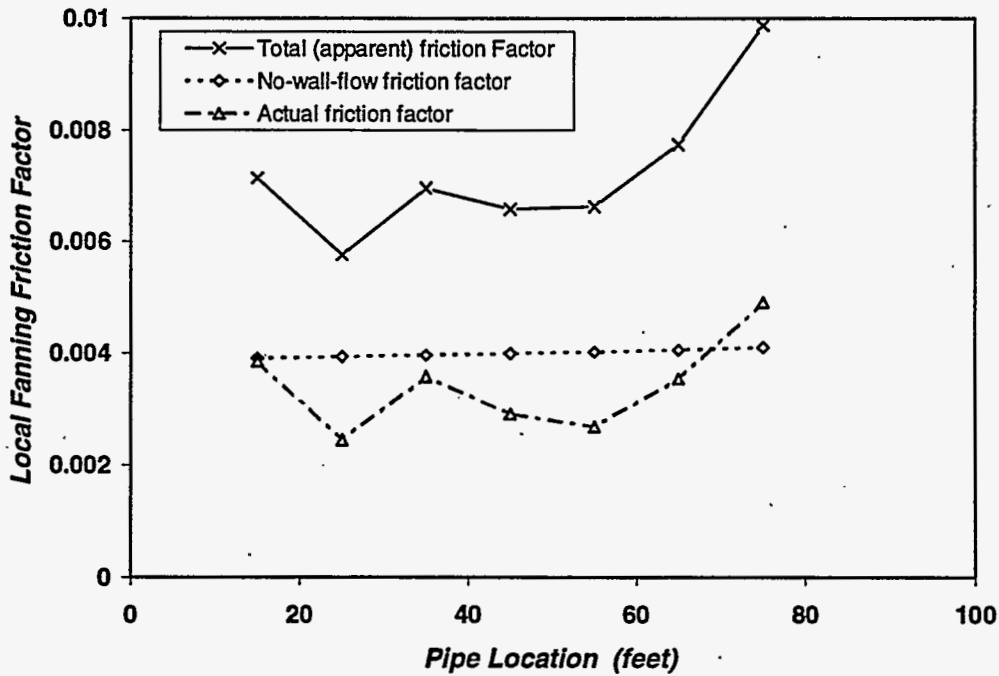


Figure 1.6: Comparison among Different Fanning Friction Factors

1.3.3 Air and Water Two-Phase Flow

For simplicity, the following notation is used in the plots shown in this section
 WCQ: Water axial flow rate, in MbpD (thousand barrels per day);

- WIQ: Water inflow rate, in MbpD;
- WQ: Water flow rate, either water inflow rate or water axial flow rate, in MbpD;
- ACQ: Air axial flow rate, in MMscfD (million standard cubic feet per day);
- AIQ: Air inflow rate, in MMscfD;
- AQ: Air flow rate, either air inflow rate or air axial flow rate, in MMscfD;
- WAQ: Water and air flow rates, i.e., WAQ = (WCQ, ACQ; WIQ, AIQ).

Air axial flow rate effect. Figure 1.7 shows pressure drop over each 10 feet section for two-phase axial flow without air or water inflow through perforations, where the water flow rate is held constant while the air flow rate is increased from about 0.5 MMscfD to 1.7 MMscfD. The overall pressure drop along the wellbore increases from 1.147 psia to 2.236 psia when the air axial flow rate increases from 0.5 MMscfD to 1.7 MMscfD. Figure 1.8 shows the influence of air axial flow on pressure drop for two-phase axial flow with water inflow. Again, increasing of axial air flow rate leads to the increasing of pressure drop.

Air inflow rate effect. The air inflow rate effect on two-phase wellbore flow is shown in Figures 1.9 and 1.10. Both figures indicate that the higher the air inflow rate, the higher the pressure drop. It is interesting to compare two wellbore flows with the same total air and water flow rates, one with only air and water axial flow, while the other with water axial flow and air inflow. As shown in Figure 1.11, the overall pressure drop in the first case where no inflow is present is lower than that for the latter case with inflow. The main reason for this difference is due to the inflow effect on the accelerational and frictional pressure drops, because flow patterns observed for both cases are the same, i.e., slug flow along most of the wellbore.

Water axial flow rate effect. Similar to the influence of air axial flow rate, the increase of water axial flow rate also leads to the increasing of pressure drop in each 10 feet section. This is shown for two-phase axial flow without inflow in Figure 1.12, for water axial flow with air inflow in Figure 1.13, for two-phase axial flow with water inflow in Figure 1.14, for two-phase axial flow with air inflow in Figure 1.15, and for two-phase axial flow with two-phase inflow in Figure 1.16.

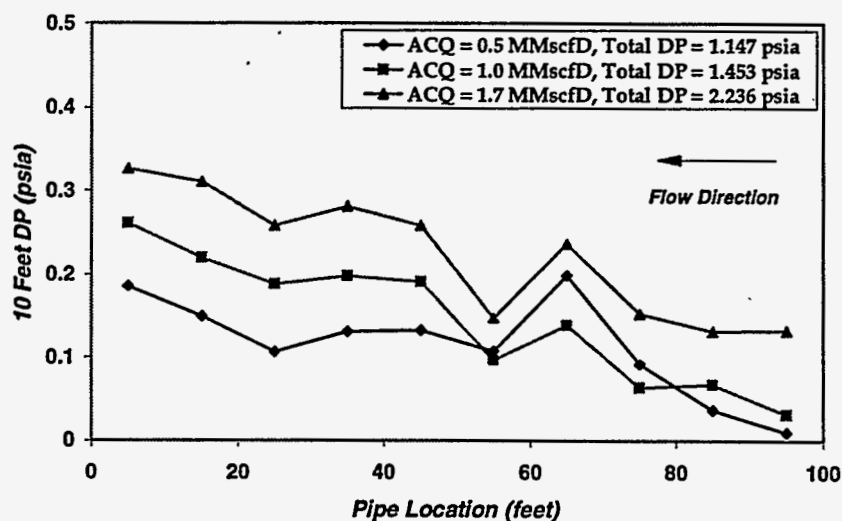


Figure 1.7: Air Axial Flow Rate Effect --Two-Phase Axial Flow with No Inflow (WCQ = 14.0MbpD)

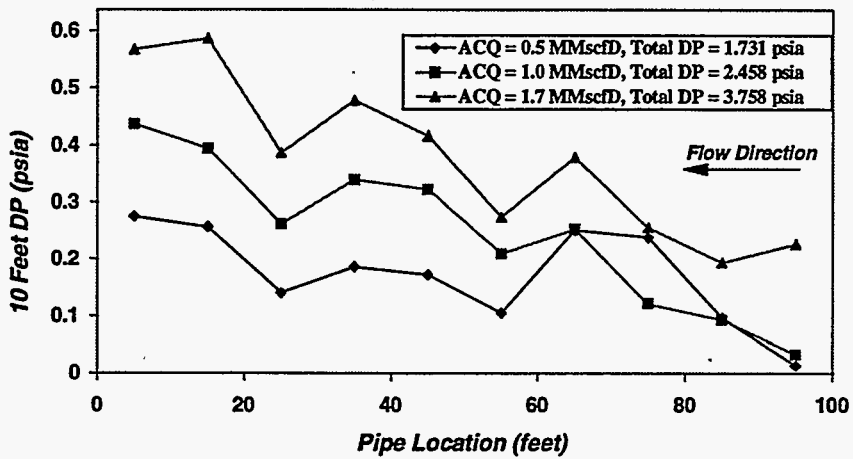


Figure 1.8: Air Axial Flow Rate Effect --Two-Phase Axial Flow with Water Inflow (WCQ = 14.0 MbpD, WIQ = 3.5 MbpD)

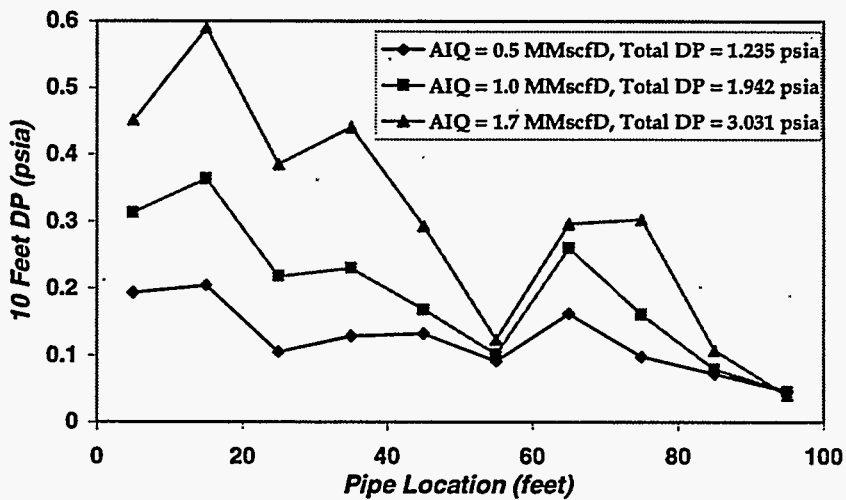


Figure 1.9: Air Inflow Flow Rate Effect --Water Axial Flow with Air Inflow (WCQ = 14.0 MbpD)

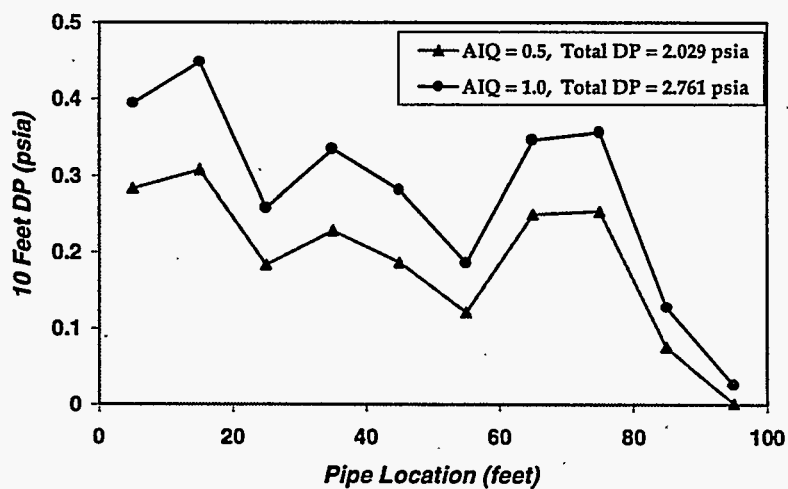


Figure 1.10: Air Inflow Flow Rate Effect --Two-Phase Axial Flow with Air Inflow (WCQ = 14.0 MbpD, ACQ = 0.5 MMscfD)

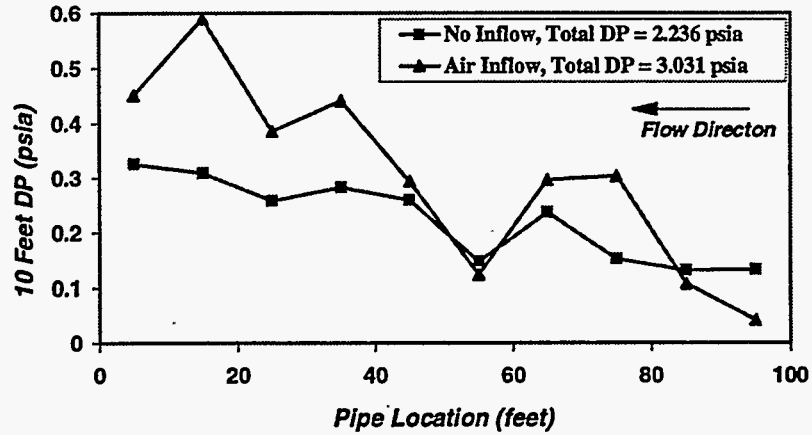


Figure 1.11: Air Inflow Flow Rate Effect --Comparison between Air Axial Flow and Air Inflow (WCQ = 14.0 MbpD, AQ = 1.7 MMscfD)

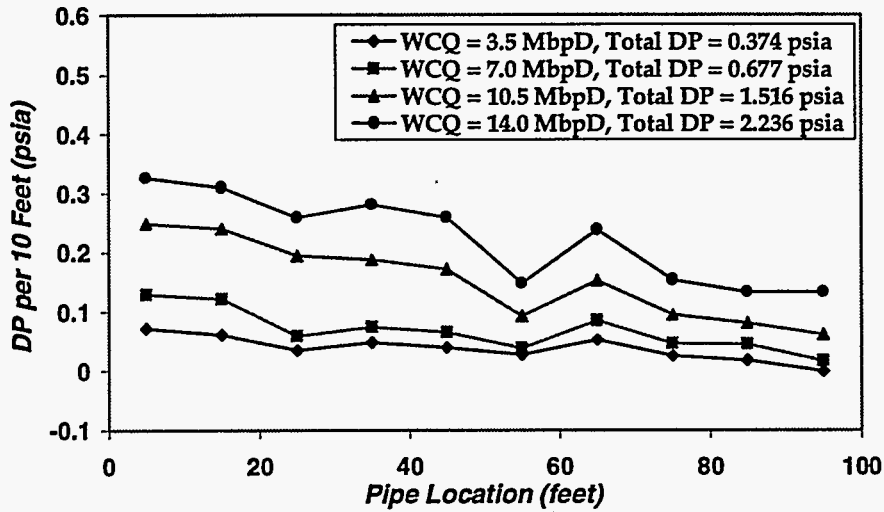


Figure 1.12: Water Axial Flow Rate Effect --Two-Phase Axial Flow with No Inflow (ACQ = 1.7 MMscfD)

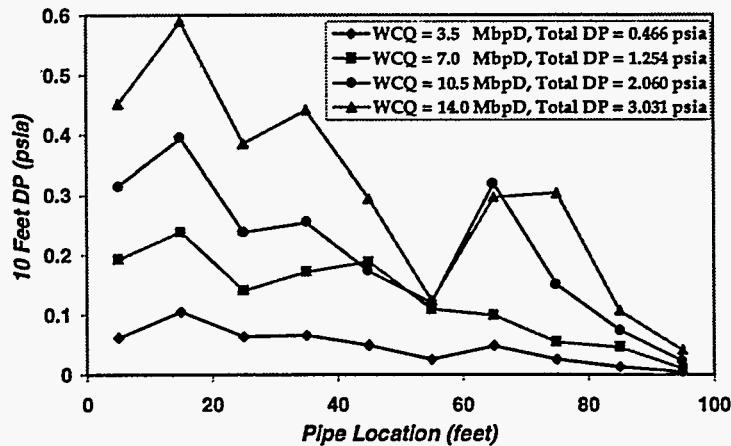


Figure 1.13: Water Axial Flow Rate Effect --Water Axial Flow with Air Inflow (AIQ = 1.7 MMscfD)

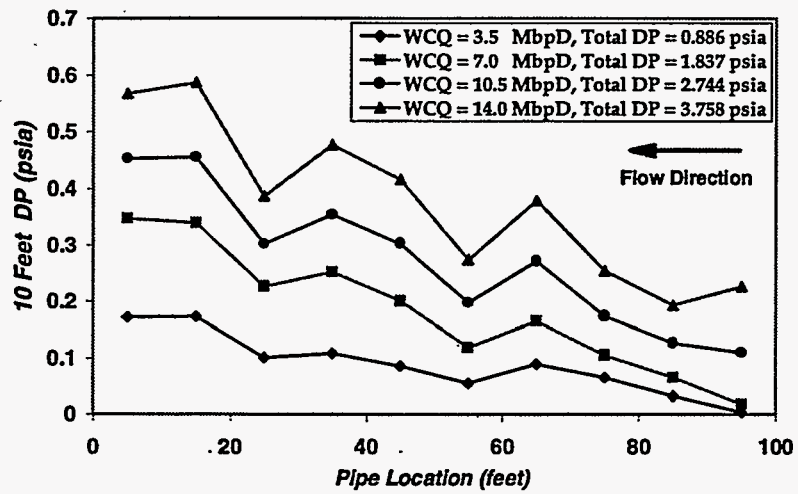


Figure 1.14: Water Axial Flow Rate Effect --Two-Phase Axial Flow with Water Inflow .
(ACQ = 1:7 MMscfD, WIQ = 3.5 MbpD)

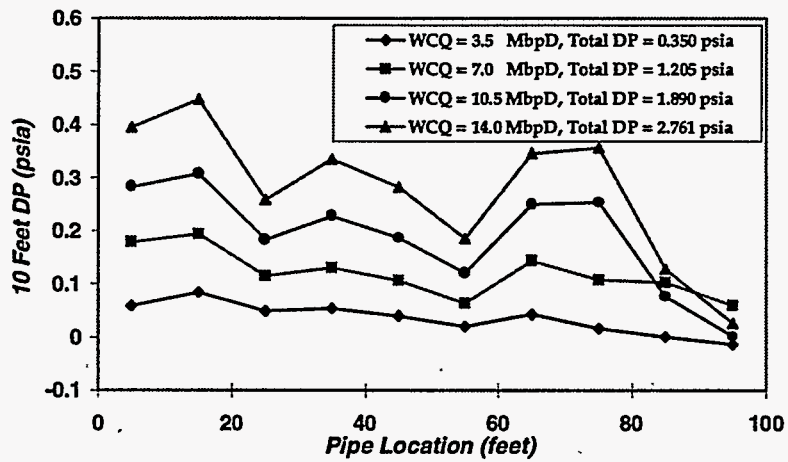


Figure 1.15: Water Axial Flow Rate Effect --Two-Phase Axial Flow with Air Inflow
(ACQ = 0.5 MMscfD, AIQ = 1.0 MMscfD)

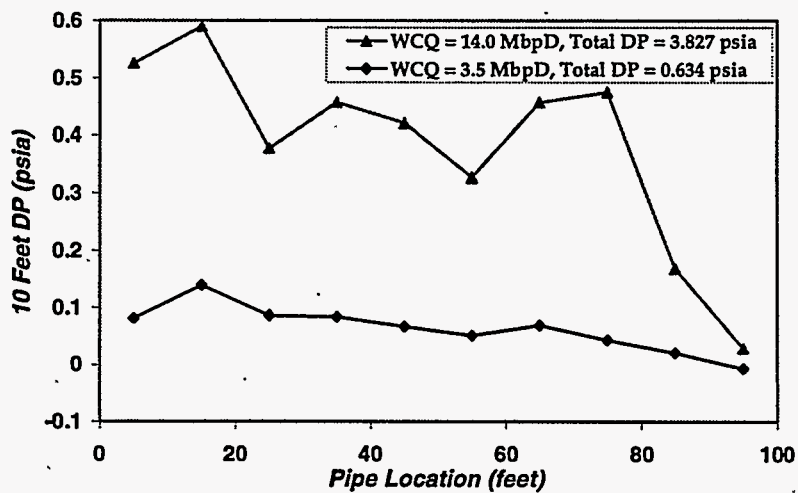


Figure 1.16: Water Axial Flow Rate Effect --Two-Phase Axial Flow and Inflow
(ACQ = 0.5 MMscfD, WIQ = 3.5 MbpD, AIQ = 1.0 MMscfD)

Two-phase inflow effect. The inflow not only affects the accelerational and frictional pressure drops for two-phase wellbore flow, it may also modify the flow pattern present in the wellbore. As a result the pressure drop may not increase with air or water inflow. An example of this situation is given in Figure 1.17. The total wellbore pressure drop for the case without inflow is even higher than for the case with inflow. This observation is different from what was observed for single phase flow (Figure 1.5). Therefore, the flow pattern change plays an important role in the pressure drop along the wellbore for two-phase flow.

Inflow pattern effect. Inflow pattern is referred in this report to the air and water inflow distribution along the perforated part of the wellbore. Three inflow patterns were implemented in the 1995 experiments (Figure 1.18):

- Pattern #1: Air inflow in the first half (47.5–85 feet part), water inflow in the second half (10–47.5 feet part);
- Pattern #2: Water inflow in the first half (47.5–85 feet part), air inflow in the second half (10–47.5 feet part);
- Pattern #3: Alternating air and water inflow distribution along the whole perforated part.

Figures 1.19 and 1.20 show the influence of inflow pattern on the pressure drop for both low and high flow rate cases. For the low flow rate case, the overall pressure drop along the wellbore for inflow pattern #2 is 0.8 psia, which is about twice that for inflow pattern #1 and inflow pattern #3. Such a significant difference is related to the change in flow pattern. Even when the air and water axial and inflow rates are the same, the flow patterns observed are different for different inflow patterns. Stratified wavy flow occurs along the whole wellbore for both inflow patterns #1 and #3, whereas slug flow is observed along a part of the wellbore for inflow pattern #2. For the high flow rate case, slug flow occurs for all three inflow patterns, as a consequence the overall pressure drops along the wellbore are about the same (Figure 1.20).

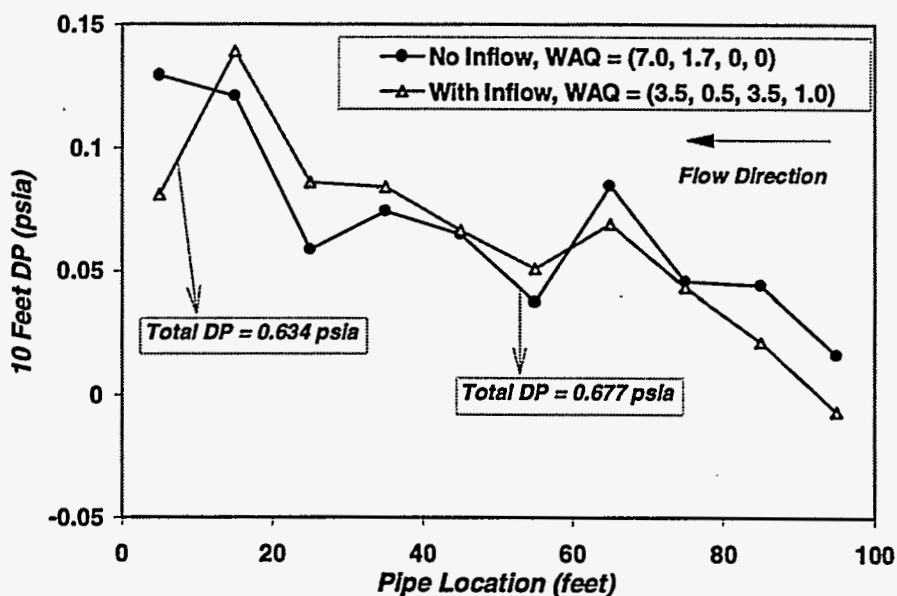


Figure 1.17: Two-Phase Inflow Rate Effect --Comparison between Two-Phase Axial Flow with and without Two-Phase Inflow

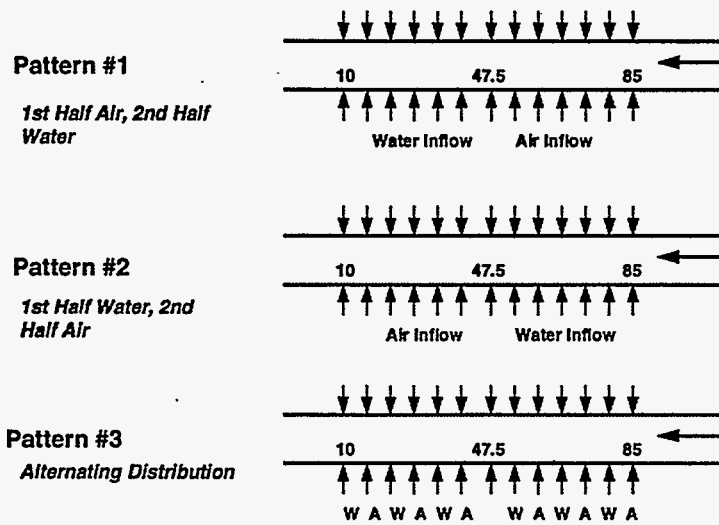


Figure 1.18: Two-Phase Inflow Pattern Specification

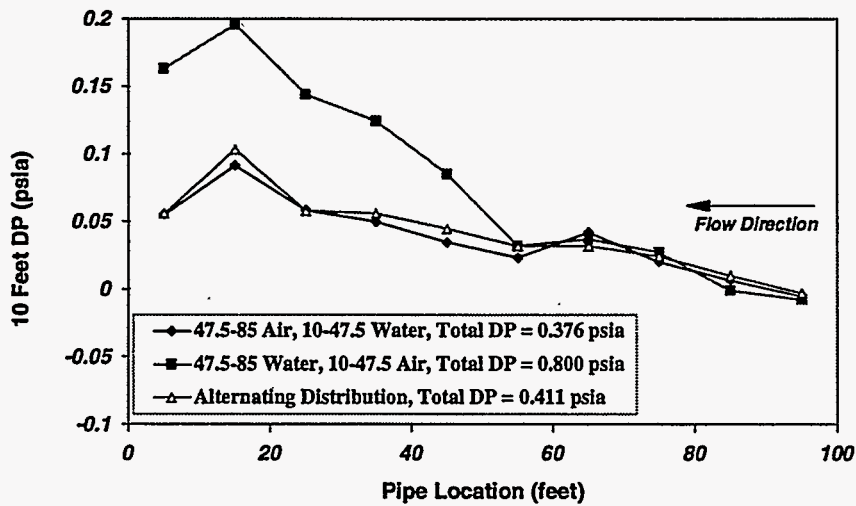


Figure 1.19: Two-Phase Inflow Pattern Effect--Low Flow Rate Case, WAQ = (3.5, 0.5, 3.5, 0.5)

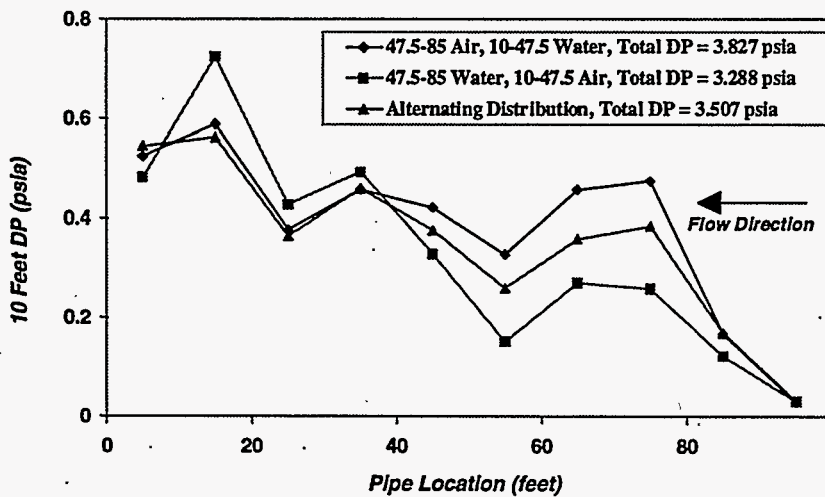


Figure 1.20: Two-Phase Inflow Pattern Effect--High Flow Rate Case, WAQ = (14.0, 0.5, 3.5, 1.0)

Pipe inclination effect. As shown in Figure 1.21, the measured pressure drop along a certain wellbore section (section AA₁B₂B) is different from the actual pressure drop along the same section,

$$(\Delta P)_{\text{measured}} = (\Delta P)_{12} = (\Delta P)_{AB} + (\Delta P)_{HH,AB}$$

The actual hydrostatic pressure drop is considered to be the pressure drop between cross-section AA₁ and cross-section BB₂, which may differ from the hydrostatic pressure drop between point A and point B. Furthermore, the pressure drop between point A and point B can be different from the pressure difference between the average pressure at cross-section AA₁ and cross-section BB₂ (the latter pressure drop is what is obtained from model predictions). The actual hydrostatic pressure drop is dependent upon the fluid distribution (flow pattern) in the section, while the pressure difference between cross-section AA₁ and cross-section BB₂ depends on the pressure distribution over both cross-sections.

Figure 1.22 compares the 10 feet no-hydrostatic pressure drops for single phase water axial flow with inflow in upward (pipe inclination angle = 2 degree), downward (pipe inclination angle = -2 degree) and horizontal wellbores. The no-hydrostatic pressure drops are defined as the sum of all pressure drop components along the section except the gravitational one. The figure shows that the no-hydrostatic pressure drops for all three wellbore orientations are identical, which means that, as expected, the pipe inclination only affects the hydrostatic pressure drop term under single phase flow conditions. For two-phase or multiphase flow, pipe inclination plays an important role in the flow pattern and thus the overall pressure drop, the no-hydrostatic pressure drops, as well as the hydrostatic pressure drops (Figures 1.23 and 1.24).

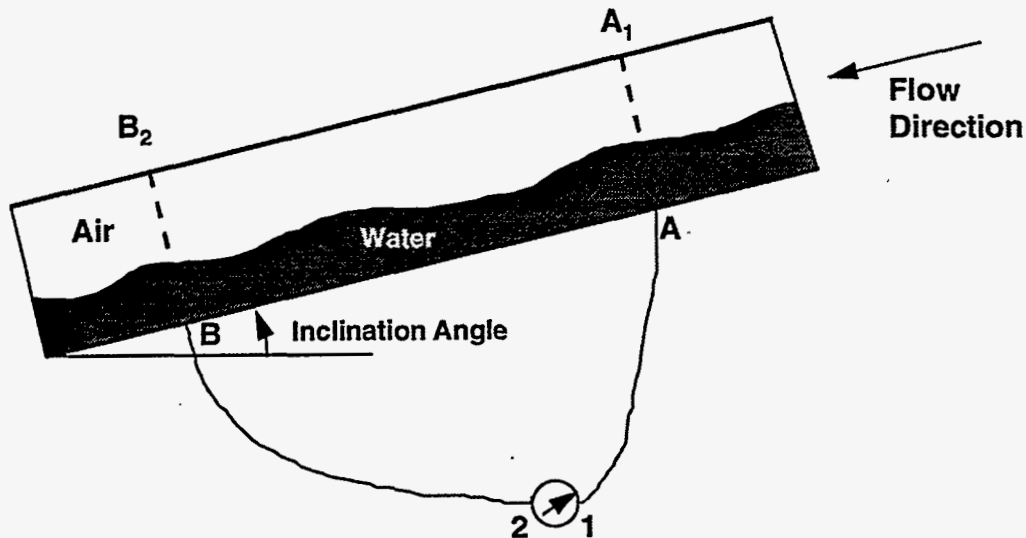


Figure 1.21: Difference between the Measured Pressure Drop and Its Real Value

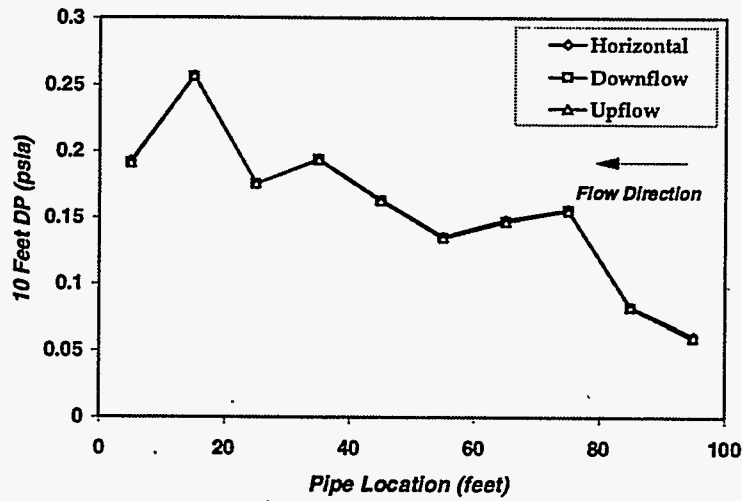


Figure 1.22: Pipe Inclination Effect--Single Phase Water Flow

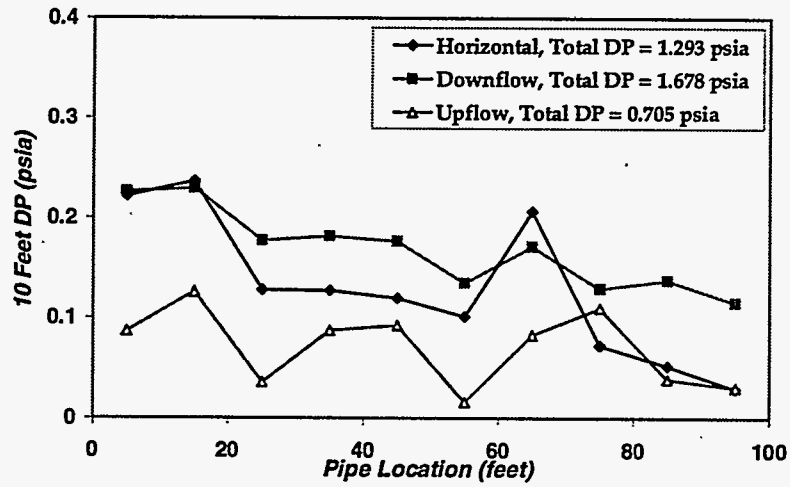


Figure 1.23: Pipe Inclination Effect--Water Axial Flow with Air Inflow, (WCQ = 10.5, AIQ = 1.0)

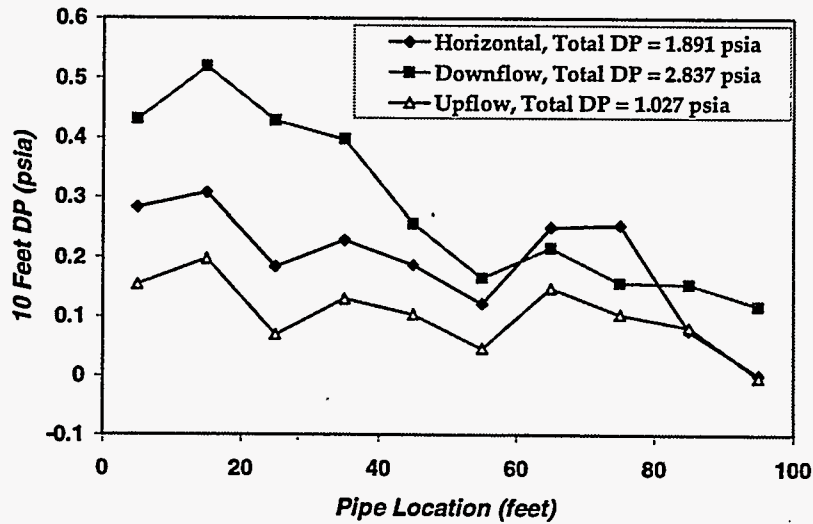


Figure 1.24: Pipe Inclination Effect--Two-Phase Axial Flow with Air Inflow (WCQ = 10.5 MbpD, ACQ = 0.5 MMscfD, AIQ = 1.0 MMscfD)

Brief summary. As discussed above, many factors come into effect when the two phases flow in the wellbore, among them are axial air and water flow rates, air and water inflow rates, inflow pattern, pipe inclination, and as can be anticipated, fluid properties, pipe geometry as well as perforation density and geometry. Figure 1.25 compares pressure drops for different air and water flow arrangements in the wellbore where the total air and water flow rates are 1.0 MMscfD and 7.0 MbpD respectively. The overall pressure drops along the wellbore are listed in Table 1.2. Both Figure 1.25 and Table 1.2 show that pressure drops change significantly with flow arrangement. The overall pressure drop ranges from 0.2992 psia to 0.8891 psia. Under the condition of air and water flow rates of 1.0 MMscfD and 7.0 MbpD, the flow format corresponding to the water axial flow with air inflow and that corresponding to air and water axial flow give the highest overall pressure drop, while with air and water axial flow the lowest overall pressure drop is obtained.

It should be noted that influences of different parameters on wellbore flow behavior are interrelated and depend upon specific flow conditions. For example, the effect of two-phase inflow pattern is affected by flow rates. For the low flow rate case, the overall pressure drop along the wellbore in the inflow pattern #2 is about two times that in inflow pattern #1 and inflow pattern #3 (Table 1.2), whereas the overall pressure drops in all three inflow patterns are about the same for the high flow rate case as shown in Table 1.3.

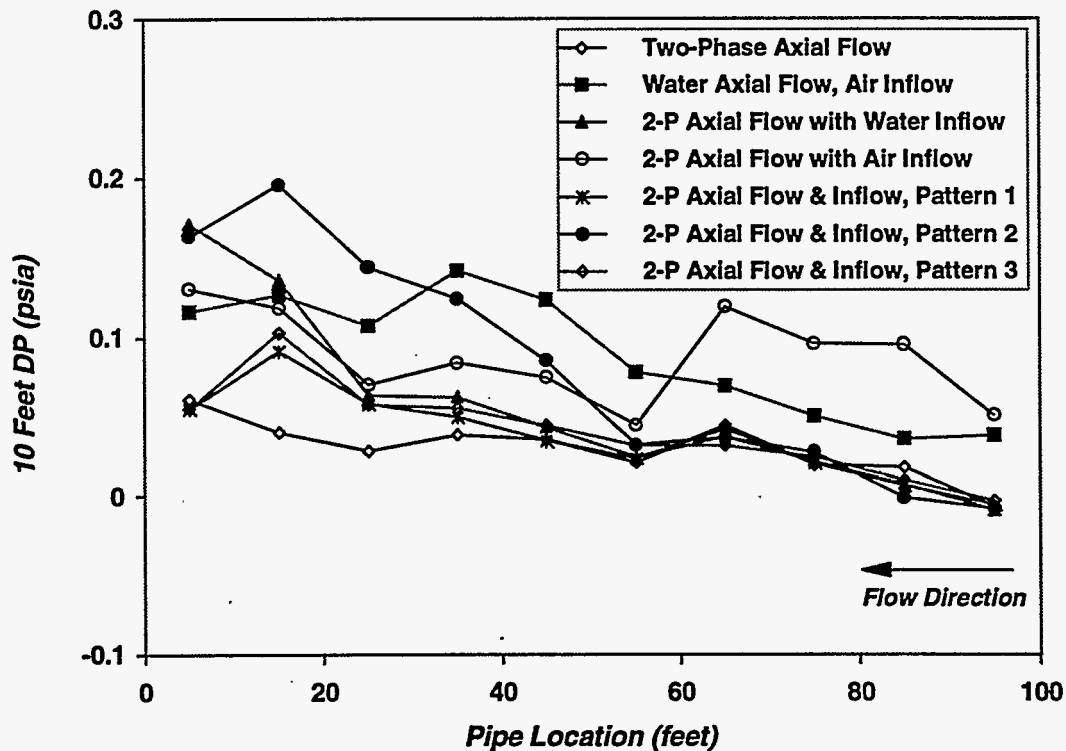


Figure 1.25: Pressure Drop Comparison at 1.0 MMscfD Air and 7.0 MbpD Water Flow Rates

Table 1.2: Overall Pressure Drop Comparison

Flow Format	Overall Pressure Drop along the Wellbore (psia)
Water axial flow, air inflow	0.8891
Air and water axial flow with air inflow	0.8856
Air and water axial flow and inflow, pattern #2	0.8001
Air and water axial flow with water inflow	0.5575
Air and water axial flow and inflow, pattern #3	0.4108
Air and water axial flow and inflow, pattern #1	0.3763
Air and water axial flow	0.2993

Table 1.3: Inflow Pattern Effect at High Flow Rate
WAQ = (14.0, 0.5, 3.5, 1.0)

Flow Format	Overall Pressure Drop along the Wellbore (psia)
Air and water axial flow and inflow, pattern #1	3.827
Air and water axial flow and inflow, pattern #3	3.507
Air and water axial flow and inflow, pattern #2	3.288

1.4 Mechanisms of Inflow Effect

Three different but interdependent mechanisms for inflow affect two-phase wellbore flow:

- *Boundary layer effect* (Figure 1.26). Inflow disturbs the fluid flow near the pipe wall and thus changes the velocity profiles in each cross-section, as a result the wall friction is altered. Based on Ouyang & Aziz [1], for single phase flow, inflow increases the axial velocity gradient near the pipe wall and hence increases the wall friction for laminar flow, whereas the opposite is true for turbulent flow.
- *Kinetic energy effect* (Figure 1.27). Inflow provides the energy needed to accelerate the fluid flow along the wellbore. This effect is found to be very important for all the 1995 single phase water axial flow with water inflow experiments. The accelerational pressure drop accounts for about the same percentage in the total pressure drop as the frictional pressure drop component (Ouyang & Aziz, [1]).
- *Flow pattern effect* (Figure 1.28). As can be anticipated, inflow affects the flow pattern by two different means:
 1. The inflow changes air and water flow rates in a specific cross-section, as a result the superficial air and water velocities are both changed, which leads to the flow pattern change along different cross sections;

2. The inflow enhances the radial velocity component and affects the fluid flow near the pipe wall. The flow pattern transition mechanisms for pipe flow with no inflow may be invalid for wellbore flow due to the inflow influence.

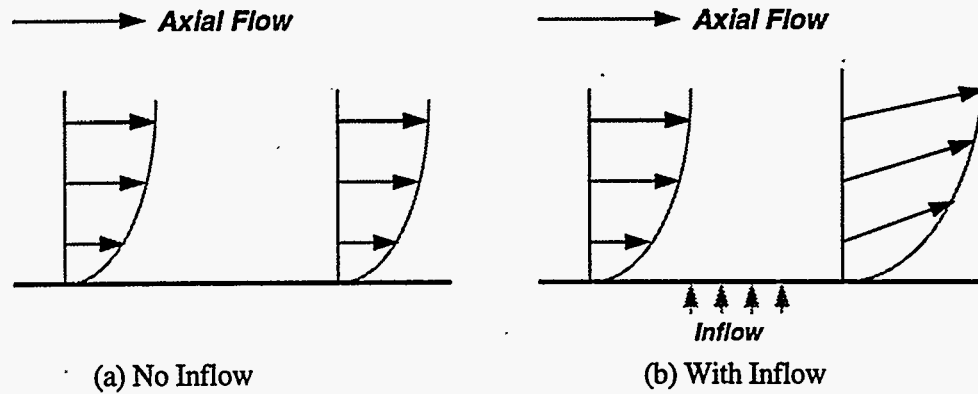


Figure 1.26: Inflow Effect on Boundary Layer

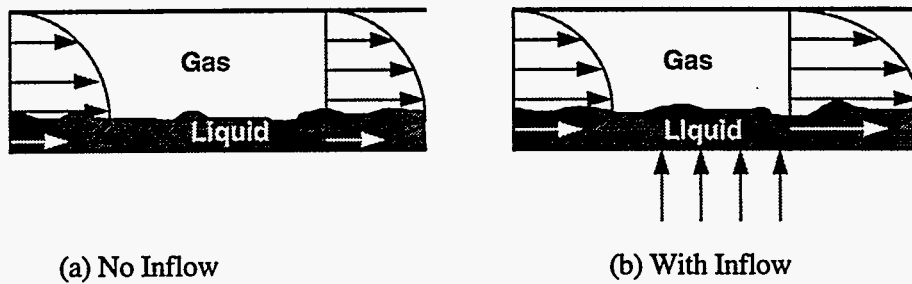


Figure 1.27: Inflow Effect on Kinetic Energy

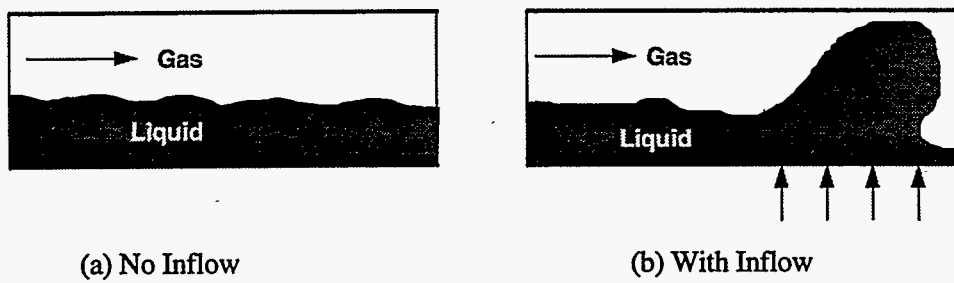


Figure 1.28: Inflow Effect on Flow Pattern

1.5 Model Prediction

All the existing flow pattern, pressure drop and liquid holdup prediction models and correlations have been developed for multiphase pipe flow where no inflow occurs. For two-phase flow in pipes with no inflow, the flow pattern should not change along the pipe provided that the superficial velocities for both phases are kept unchanged, and that the stabilized flow has been reached. This is not true for two-phase wellbore flow with mass transfer through perforations. For this situation, the flow pattern is expected to change with pipe location even under stabilized flow conditions. Moreover, wall friction and kinetic energy also change due to inflow (see last section). Therefore, new mechanistic models or empirical correlations should be developed to handle multiphase flow in the completed portion of a wellbore. So far, no such models or correlations have been reported in the literature.

For the time being, the segmented model approach as shown in Figure 1.29 is used to predict flow pattern, pressure drop, and liquid holdup by using existing mechanistic models or correlations. But it should be noted that:

- no existing models or correlations account for the inflow effect;
- empirical correlations used in mechanistic models, such as wall friction factor, interfacial friction factor, liquid entrainment fraction correlations, intended for pipe flow without inflow, may lead to large deviations for wellbore flow; and
- transition criteria in existing mechanistic models may be invalid for wellbore flow, as a result the flow patterns predicted may be incorrect.

The procedure involved in the segmented model approach consists of the following steps:

1. Divide the wellbore into small segments; the smaller the segment, the more accurate the predictions.
2. Begin with the well toe, add the air and water inflow rates dQ_L and dQ_G in the segment to the inlet air and water axial flow rates Q_L and Q_G , respectively.
3. Compute the average superficial velocities for both phases.
4. Determine the flow pattern in the segment based on the superficial velocities.
5. Calculate the pressure drop and liquid holdup in the segment.
6. Repeat steps 2–5 until reaching the well heel.
7. Sum up to get information on flow pattern and liquid holdup along the wellbore and the pressure drop along any section of interest.

Five models or empirical correlations are used to predict pressure drop and liquid holdup,

- Stanford Mechanistic Model (Petalas & Aziz, [8])
- Beggs & Brill Model [9]
- Beattie & Whalley Model [10]
- Dukler et al. Model [11]
- Homogeneous Model (used in Eclipse reservoir simulator)

The first two models also provide flow pattern predictions.

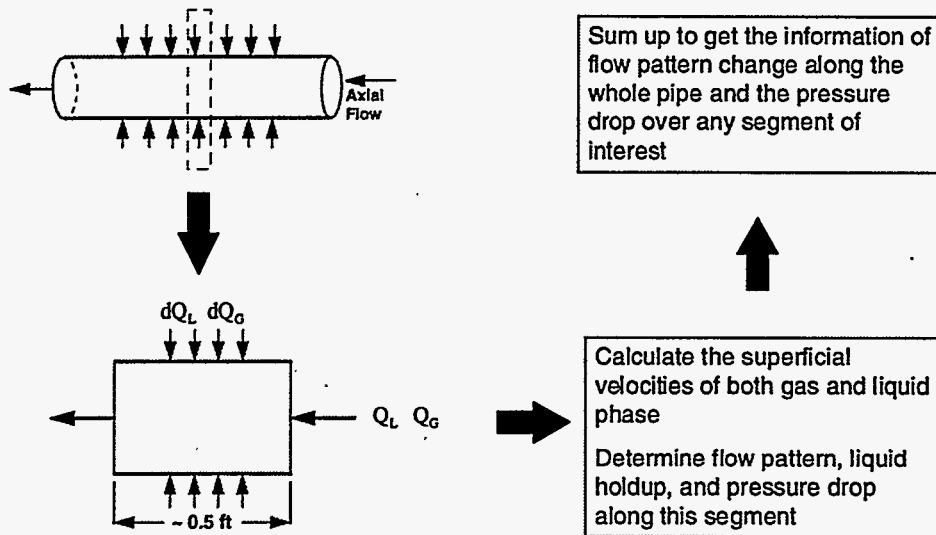


Figure 1.29: Segmented Model Approach

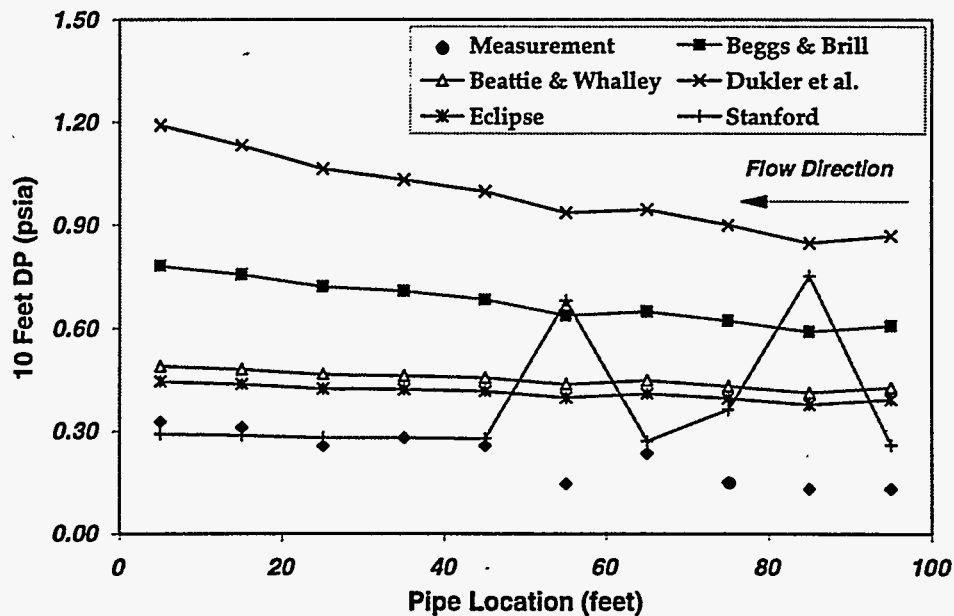


Figure 1.30: Comparison between Model Prediction and Measurement
—Air & Water Axial Flow (Experiment No 18, Horizontal Case)

Comparisons of every 10 feet pressure drops between measurement and prediction for air and water two-phase flow with or without inflow are shown in Figures 1.30–1.33. Figure 1.30 is for air and water axial flow without inflow, from which it can be seen that all the models except the Stanford mechanistic model predict higher pressure drops than measurements. The Beattie & Whalley [10] model and the homogeneous model used in Eclipse reservoir simulator predict close pressure drops which are still larger than measured values, while the Dukler et al. [11] model and

the Beggs & Brill [9] model give much higher values of the pressure drop. The Stanford model predicts satisfactory results for pressure drops along the second half (downstream) of the wellbore (50–100 ft), but overpredicts pressure drops in the first half (0–50 ft). Note that the predicted flow pattern changes along the first half of the wellbore, as a result the pressure drops vary significantly. For water axial flow with air inflow (Figure 1.31), air and water axial flow with air inflow (Figure 1.32), or air and water axial flow with air and water inflow (Figure 1.33), no existing model can provide satisfactory predictions. In most situations, the models underestimate pressure drop for the first half of the wellbore, while overestimate pressure drop for the second half.

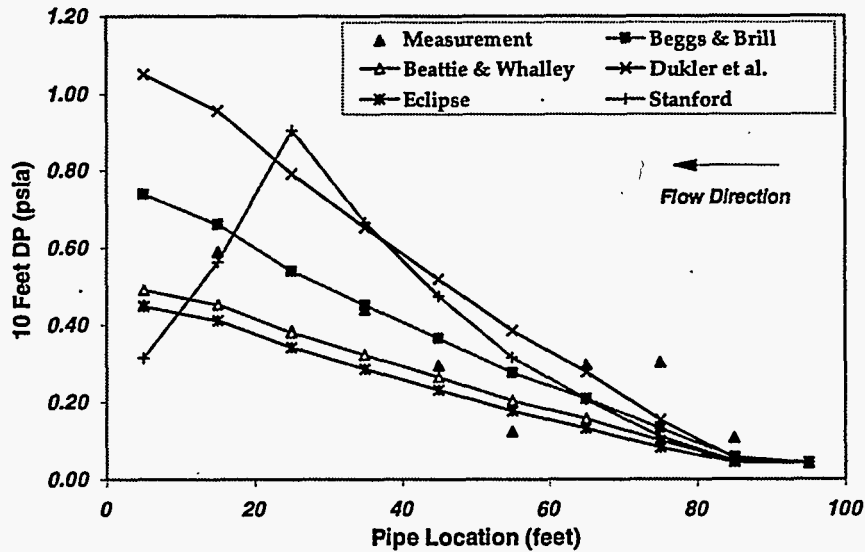


Figure 1.31: Comparison between Model Prediction and Measurement
—Water Axial Flow with Air Inflow (Experiment No 30, Horizontal Case)

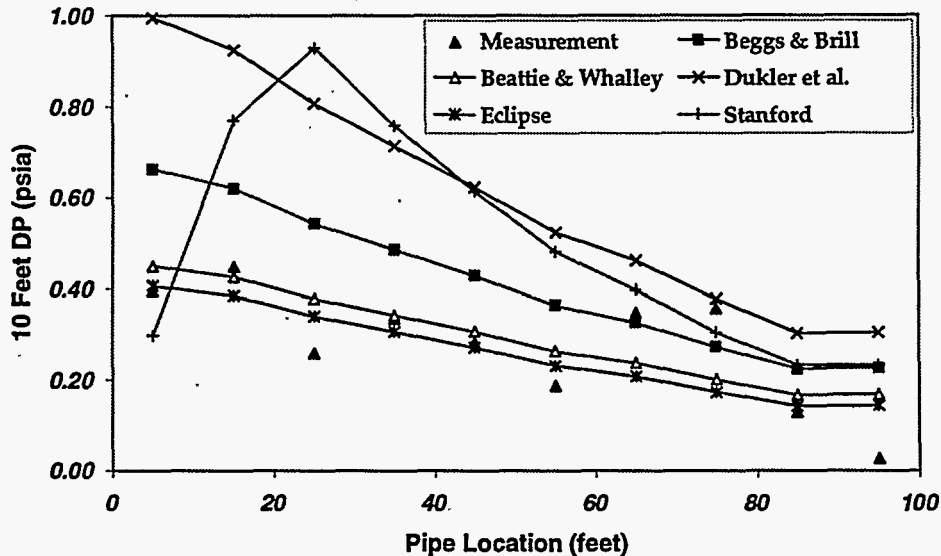


Figure 1.32: Comparison between Model Prediction and Measurement
—Air & Water Axial Flow with Air Inflow (Experiment No 50, Horizontal Case)

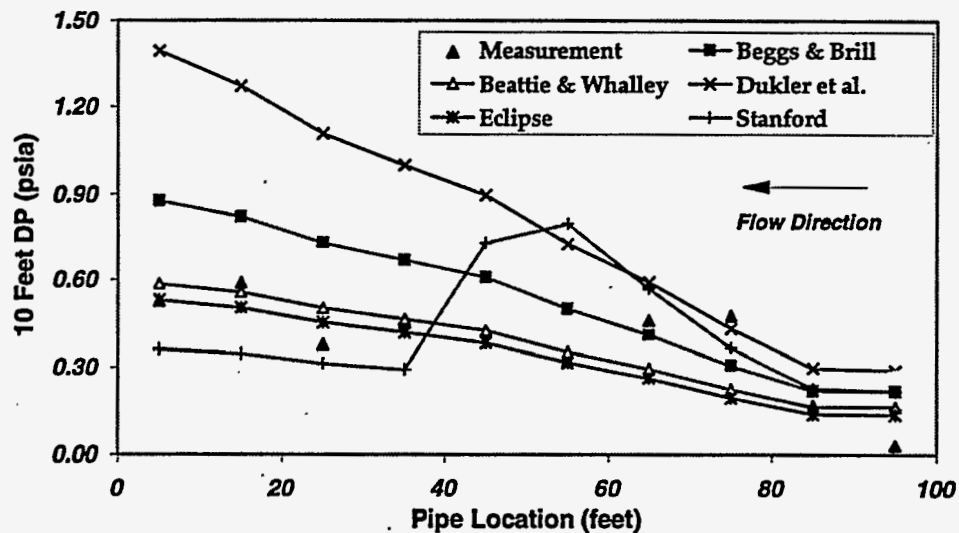


Figure 1.33: Comparison between Model Prediction and Measurement
—Air & Water Axial Flow and Inflow (Experiment No 54, Horizontal, Pattern #1)

1.6 Discussion and Conclusions

Inflow has a significant impact on single phase flow in pipes. The wall friction shear is found to be reduced by inflow for turbulent flow. The accelerational pressure drops are quite large and comparable to the frictional components in all the single phase experiments. Therefore, both the accelerational and frictional pressure drops should be considered in studying the fluid flow along a wellbore.

The influence of inflow on air-water two-phase pipe flow is not so straightforward as in the single phase flow case. Many parameters come into play, among which are air and water axial flow rates, air and water inflow rates, two-phase inflow pattern, pipe inclination, fluid properties, pipe geometry as well as perforation density and geometry. Effects of different parameters are interrelated.

Three mechanisms, boundary layer effect, kinetic energy effect, and flow pattern effect, have been proposed to explain the influence of inflow. For single phase flow, only the first two mechanisms control the inflow characteristics, while all the three mechanisms affect two-phase flow.

A segmented method has been suggested to predict flow pattern, pressure drop and liquid holdup by using the existing mechanistic models or empirical correlations. Unfortunately, substantial differences between measurements and predictions have been observed. The reasons for this are: (a) existing models or correlations do not account for the inflow effect; (b) correlations for wall friction factors, interfacial friction factor and liquid entrainment fraction were proposed for gas-liquid two-phase pipe flow without inflow, as a consequence they may not be appropriate for air and water wellbore flow where inflow occurs; and (c) transition criteria in

existing mechanistic models may be invalid for wellbore flow with influx, and the flow patterns predicted may be incorrect.

References

- [1] Ouyang, L-B., and Aziz, K. "General Single Phase Wellbore Flow Model for Horizontal, Vertical and Slanted Well Completions," DOE Technical Report, in preparation, (1996)
- [2] Kloster, J. "Experimental Research on Flow Resistance in Perforated Pipe," M. S. report, Norwegian Institute of Technology, (1990)
- [3] Su, Z., and Gudmundsson, J. S. "Friction Factor of Perforation Roughness in Pipes," paper SPE 26521, presented at the 68th SPE Annual Technical Conference and Exhibition, Houston, Texas, Oct 3-6, (1993)
- [4] Shapiro, A. H., Siegel, R., and Kline, S. J. "Friction Factor in the Laminar Entry Region of a Smooth Tube," Proc. Second U. S. National Congress of Applied Mechanics, Ann Arbor, MI, June 14-18, 733-741, (1954)
- [5] Kays, W. M., and Crawford, M. E. *Convective Heat and Mass Transfer*, McGraw-Hill Co., New York, 601pp, (1993)
- [6] Colebrook, C. F. "Turbulent Flow in Pipes, with Particular Reference to the Transition Region between the Smooth and Rough Laws," *J. Inst. Civil Engineering (London)*, vol 12, 133-156, (1939)
- [7] Colebrook, C. F., and White, C. M. "Experiments with Fluid Friction in Roughened Pipes," *Proc. Roy. Soc. (London)*, vol 161A, 367-381, (1937)
- [8] Petalas, N., and Aziz, K. "Development and Testing of a New Mechanistic Model for Multiphase Flow in Pipes," Second International Symposium on Numerical Methods for Multiphase Flows, ASME Fluids Engineering Division Summer Meeting, San Diego, California, July 7-11, (1996)
- [9] Beggs, H. D., and Brill, J. P. "A Study of Two-Phase Flow in Inclined Pipes," *Trans. AIME*, vol 256, 607, (1973)
- [10] Beattie, D. R. H., and Whalley, P. B. "A Simple Two-Phase Frictional Pressure Drop Calculation Method," *Int. J. Multiphase Flow*, vol 8, no 1, 83-87, (1982)
- [11] Dukler, A. E., Wicks, M., and Cleveland, R. G. "Frictional Pressure Drop in Two Phase Flow: A. A Comparison of Existing Correlations for Pressure Loss and Holdup," *AIChE J.*, vol 10, 38, (1964)

2. Development and Testing of a New Mechanistic Model for Multiphase Flow in Pipes

by Nicholas Petalas and Khalid Aziz[†]

Abstract

The use of mechanistic models for multiphase flow calculations is expected to greatly improve our ability to predict pressure drop and holdup in pipes. In this paper, a new model is developed which can be used for all pipe geometries and fluid properties. The model lends itself to implementation in a computer program in that a significant number of calculations are required and several of these require iterative procedures. The performance of the model over a wide range of conditions has been evaluated through the use of three dimensional surface plots. Comparisons with laboratory as well as field data have also exhibited good results. This work has also identified the need for further work in this area.

2.1. Introduction

Empirical models often prove inadequate in that they are limited by the range of data on which they were based and, generally, cannot be used with confidence with the types of fluids or under the types of conditions encountered in the field. Furthermore, many such models exhibit large discontinuities⁴ at the flow pattern transitions and this can lead to convergence problems when these models are used for the simultaneous simulation of petroleum reservoirs and associated production facilities. Mechanistic models, on the other hand, are based on fundamental laws and thus can provide for more accurate modeling of the geometric and fluid property variations. Most mechanistic models begin by assuming that a particular flow regime is present. By solving the momentum balance equations for certain quantities that determine its characteristics, the stability of the flow pattern is examined. If the chosen flow pattern is shown to be stable, the procedure is terminated, the pressure drop and phase volume fractions being obtained directly from the momentum balance equations. If the flow pattern cannot exist under the specified conditions, a new flow pattern is assumed and the procedure is repeated until a stable flow pattern is determined.

To date, many of the models presented in the literature are either incomplete^{6,15}, in that they only consider flow pattern determination, or are limited in their applicability to all pipe inclinations^{3,18}. A new model has been developed which overcomes these limitations.

For most of the flow patterns considered, one or more empirical closure relationships are required even when a mechanistic approach is used. Where correlations available in the literature are inadequate for use in such models, new correlations must be developed.

A large amount of data has been collected through the use of a Multiphase Flow Database developed at Stanford University. This database program allows the user to specify criteria which

[†] This paper was submitted for publication at the Second International Symposium on Numerical Methods for Multiphase Flows of the Fluids Engineering Division of the ASME to be held in San Diego on July 7-11, 1996.

limit the range of data selected and to output the results using a number of different formats. The database presently contains over 20,000 laboratory measurements and approximately 1800 measurements from actual wells. The required empirical correlations were developed based on these data and they reflect changes in pipe diameter, fluid properties and pipe inclination (upward and downward inclinations are represented).

2.2. Model Description

The development of mechanistic models to predict the behavior of multiphase systems started with the pioneering work of Taitel and Dukler¹⁵ (1976). While they dealt only with flow pattern predictions, these ideas have been extended here to obtain comprehensive design techniques. The basic flow patterns considered in this approach are:

- Stratified Smooth
- Stratified Wavy
- Intermittent (slug, elongated bubble, plug)
- Annular Mist (annular flow with dispersed bubbles)
- Bubble
- Dispersed Bubble
- Froth or Churn

2.2.1. Equilibrium Stratified Flow

The geometrical aspects of this kind of flow are shown in Figure 2.1.

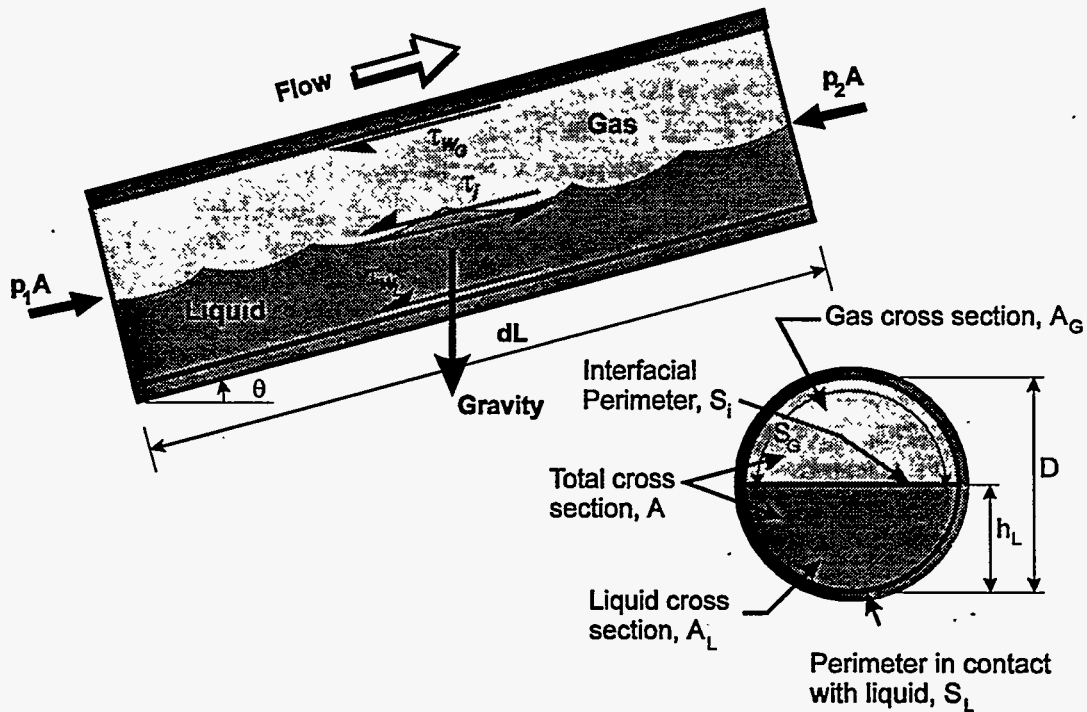


FIGURE 2.1 - MOMENTUM BALANCE WITH TWO SEGREGATED FLUIDS

Momentum balance can be written on the liquid and gas phases contained in a control volume. After taking the limit as $\Delta L \rightarrow 0$ the two momentum balance equations may be expressed as:

$$-A_L \left(\frac{dp}{dL} \right) - \tau_{wL} S_L + \tau_i S_i - \rho_L A_L \frac{g}{g_c} \sin \theta = 0 \quad \text{Eq. 2.1}$$

and

$$-A_G \left(\frac{dp}{dL} \right) - \tau_{wG} S_G - \tau_i S_i - \rho_G A_G \frac{g}{g_c} \sin \theta = 0 \quad \text{Eq. 2.2}$$

The shear stress terms can be expressed in terms of friction factors:

$$\tau_{wL} = \frac{f_L \rho_L V_L^2}{2g_c}, \quad \tau_{wG} = \frac{f_G \rho_G V_G^2}{2g_c}, \quad \text{and} \quad \tau_i = \frac{f_i \rho_G V_i |V_i|}{2g_c} \quad \text{Eq. 2.3}$$

The friction factors for the gas and liquid phases are evaluated from the single phase relationships by using the Colebrook⁹ correlation with the following definitions of Reynolds number and hydraulic diameter:

$$\text{Re}_L = \frac{D_L \rho_L V_L}{\mu_L}, \quad D_L = \frac{4A_L}{S_L} \quad \text{Eq. 2.4}$$

$$\text{Re}_G = \frac{D_G \rho_G V_G}{\mu_G}, \quad D_G = \frac{4A_G}{S_G + S_i} \quad \text{Eq. 2.5}$$

Following the approach used by Taitel and Dukler,¹⁵ the momentum balance equations can be combined and expressed in dimensionless form leading to the following expression which can be solved to determine the equilibrium liquid height:

$$X^2 F_2 - F_1 + 4Y = 0 \quad \text{Eq. 2.6}$$

The quantity, X, is the Lockhart-Martinelli parameter:

$$X^2 = \frac{\left(\frac{dp}{dL} \right)_{SL}}{\left(\frac{dp}{dL} \right)_{SG}} = \frac{f_{SL} V_{SL}^2 \rho_L}{f_{SG} V_{SG}^2 \rho_G} \quad \text{Eq. 2.7}$$

The remaining quantities are given by:

$$Y = \frac{(\rho_L - \rho_G) g \sin \theta}{\left(\frac{dp}{dL} \right)_{SG} g_c} \quad \text{Eq. 2.8}$$

$$F_1 = \left(\frac{f_G}{f_{SG}} \right) \tilde{V}_G^2 \left\{ \frac{\tilde{S}_G}{\tilde{A}_G} + \frac{f_i}{f_G} \frac{\tilde{V}_i^2}{\tilde{V}_G^2} \left(\frac{\tilde{S}_i}{\tilde{A}_G} + \frac{\tilde{S}_i}{\tilde{A}_L} \right) \right\} \quad \text{Eq. 2.9}$$

$$F_2 = \left(\frac{f_L}{f_{SL}} \right) \tilde{V}_L^2 \frac{\tilde{S}_L}{\tilde{A}_L} \quad \text{Eq. 2.10}$$

Normally it is assumed that the superficial gas velocity is much higher than the interface velocity. This simplification however, is only valid for horizontal or uphill flow where gas moves much faster than liquid. To provide for a more general application, here it is assumed that the interface velocity is given by the difference of the average phase velocities, i.e.

$$V_i = (V_G - V_L) \quad \text{Eq. 2.11}$$

The interfacial friction factor is obtained from the modification of the Duns and Ros method by Baker et al⁵.

The simplifications imposed by Taitel and Dukler, i.e., that $f_i \approx f_G$, $V_G \gg V_L$, and that the friction factors can be approximated by the smooth-pipe correlation of Blasius, limit the applicability of their model and are not made in this model. Furthermore, since the values of X and Y are dependent on pressure gradients, which are in turn dependent on pipe roughness, the evaluation of the effect of roughness based on dimensionless plots of liquid height versus X for various values of Y is not trivial. An iterative procedure is required where for a given value of Y , the value of X required to obtain a desired dimensionless liquid height is determined. The results thus obtained are relevant only for the specific set of fluid properties and pipe roughness analyzed. Our results show that the effect of roughness can be significant, even for very small values of Y .

The stability of the stratified flow pattern can be determined once the liquid height is known. The approach used by Taitel and Dukler, using an extension of the Kelvin-Helmholtz wave stability theory is also used in this model. This attempts to predict the gas velocity at which waves on the liquid surface are large enough to bridge the pipe:

$$V_G = \left(1 - \frac{h_L}{D}\right) \sqrt{\frac{(\rho_L - \rho_G)gA_G \cos\theta}{\rho_G \frac{dA_L}{dh_L}}} \quad \text{Eq. 2.12}$$

or, in dimensionless form:

$$F^2 \left[\frac{\tilde{V}_G^2}{(1 - \tilde{h}_L)^2 \tilde{A}_G} \frac{d\tilde{A}_L}{d\tilde{h}_L} \right] \geq 1 \quad \text{Eq. 2.13}$$

where $F = \frac{V_{SG}}{\sqrt{Dg \cos\theta}} \sqrt{\frac{\rho_G}{\rho_L - \rho_G}}$, $\frac{d\tilde{A}_L}{d\tilde{h}_L} = \sqrt{1 - (2\tilde{h}_L - 1)^2}$

Xiao¹⁸ et al. suggest that this mechanism of wave growth for the transition to intermittent flow may not be applicable for large diameter pipes where the entrainment deposition process is more dominant. At steep downward inclinations, Barnea⁶ proposes a mechanism whereby stratified flow can change to annular, even at relatively low gas rates. This occurs when the liquid height is small and the liquid velocity is high. Liquid droplets are sheared off from the wavy interface and may be deposited on the upper pipe wall, eventually developing into an annular film. The condition for this type of annular flow is given as:

$$V_L > \sqrt{\frac{gD(1 - \tilde{h}_L) \cos\theta}{f_L}} \quad \text{Eq. 2.14}$$

Although no distinction is made in this model between stratified smooth and stratified wavy flow for the purposes of determining pressure drop and liquid volume fraction, the transition between these two regimes is considered. Taitel and Dukler propose that waves will form on the liquid surface once the gas velocity is increased beyond:

$$V_G \geq \sqrt{\frac{4\mu_L(\rho_L - \rho_G)g \cos\theta}{s\rho_L\rho_G V_L}} \quad \text{Eq. 2.15}$$

where the sheltering coefficient, s , is given as 0.01. Xiao et al. and in the present model, s is taken as 0.06, based on a study by Andritsos¹. This value is said to be more suitable, especially for gas flow with high viscosity liquids.

During downflow, waves can develop on the flowing liquid even in the absence of interfacial shear from the gas flow. The criterion for the appearance of waves can be expressed in terms of a critical Froude number which varies from 0.5 to 2.2 depending on roughness and whether the flow is laminar or turbulent. Barnea⁶ recommends a limiting value of 1.5 for the critical Froude number. When interfacial effects are considered in the calculation of the liquid height, this limit can predict smooth flow even at high liquid rates where the flow is known to be wavy. Reducing the limit to 1.4 resolves this problem. Thus the transition from stratified smooth to wavy flow based on this mechanism is:

$$Fr = \frac{V_L}{\sqrt{gh_L}} > 1.4 \quad \text{Eq. 2.16}$$

Barnea also notes that theory and experiment both suggest that stratified smooth flow does not exist for downward inclinations greater than $\sim 5^\circ$.

The solution of the momentum balance equations produces multiple roots when the pipe inclination is positive. Xiao et al.⁵ assume that the lowest root is the physical one. It has been observed however, that in certain circumstances the roots are in close proximity and it is not possible to discern which root is the physical one. It is believed that the cause of the multiple root phenomenon and our inability to establish which of the roots is the physical one is perhaps due to the inadequacies of the stratified flow model. For this reason, the present model limits stratified flow to horizontal and downhill angles only.

If the flow is shown to be stratified, the liquid volume fraction may be evaluated from:

$$E_L = \frac{A_L}{A} = \frac{4\tilde{A}_L}{\pi} \quad \text{Eq. 2.17}$$

The pressure drop can be obtained directly from either one of the momentum balance equations (Eq. 2.1 or Eq. 2.2).

2.2.2. Annular Mist Flow

The approach presented here is based on the work of Oliemans¹³ et al. (1986), and Xiao¹⁸ et al. (1990), who in turn have used the work of many previous investigators. The model is based on the assumption of a constant film thickness and no slip between the liquid droplets in the gas core and the gas phase. It does however account for the entrainment of the liquid in the gas core (Figure 2.2).

Momentum balance on the liquid film and gas core with liquid droplets yields:

$$-A_f \left(\frac{dp}{dL} \right) - \tau_{wL} S_L + \tau_i S_i - \rho_L A_f \frac{g}{g_c} \sin \theta = 0 \quad \text{Eq. 2.18}$$

and

$$-A_c \left(\frac{dp}{dL} \right) - \tau_i S_i - \rho_c A_c \frac{g}{g_c} \sin \theta = 0 \quad \text{Eq. 2.19}$$

The shear stresses for this case are given by:

$$\tau_{wL} = \frac{f_f \rho_L V_f^2}{2g_c}, \text{ and } \tau_i = \frac{f_i \rho_c (V_c - V_f)^2}{2g_c} \quad \text{Eq. 2.20}$$

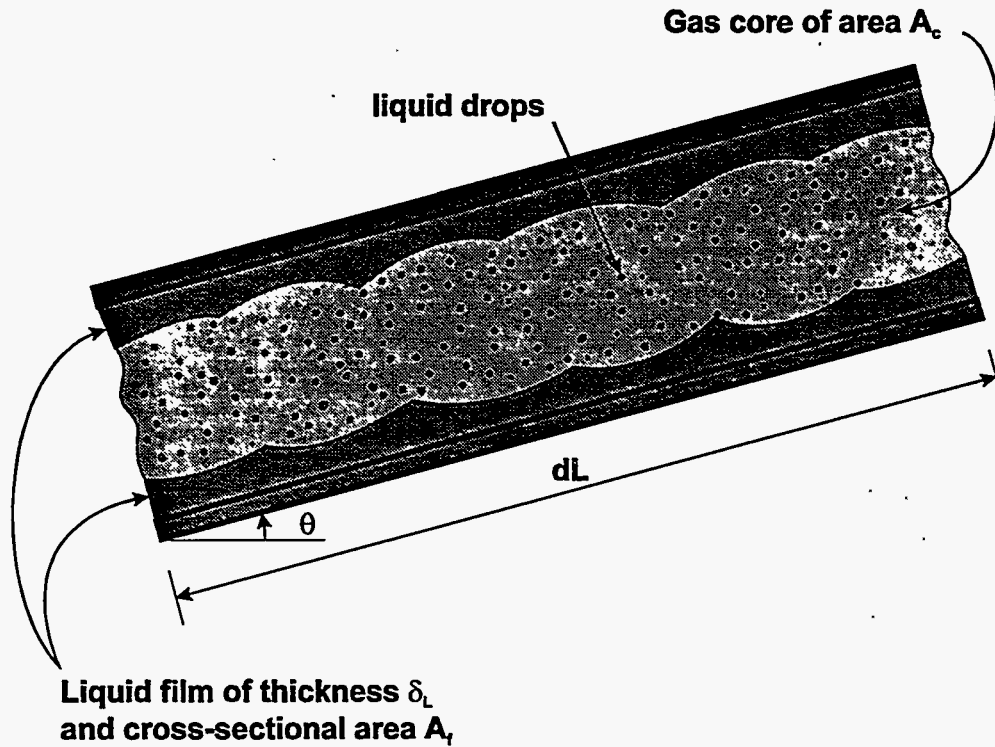


FIGURE 2.2 - CHARACTERISTICS OF ANNULAR-MIST FLOW

As was done for stratified flow, the following equation can be solved for the dimensionless film thickness, δ_L :

$$X^2 F_2 - F_1 + 4Y = 0 \text{ where} \quad \text{Eq. 2.21}$$

$$Y = \frac{(\rho_L - \rho_c) g \sin \theta}{\left(\frac{dp}{dL}\right)_{SG} g_c}$$

$$F_1 = \left(\frac{f_i}{f_{SG}}\right) \frac{\rho_c}{\rho_G} \tilde{V}_{gf}^2 \tilde{S}_i \left(\frac{1}{\tilde{A}_f} + \frac{1}{\tilde{A}_c}\right)$$

$$F_2 = \left(\frac{f_f}{f_{SL}}\right) \tilde{V}_f^2 \frac{\tilde{S}_L}{\tilde{A}_f} \text{ and } \tilde{V}_{gf} = \left(\frac{V_c - V_f}{V_{SG}}\right)$$

The velocities of the liquid film and of the gas core are given by:

$$V_f = V_{SL} (1 - FE) \frac{A}{A_f} = V_{SL} \frac{(1 - FE)}{4\tilde{\delta}_L (1 - \tilde{\delta}_L)} \quad \text{Eq. 2.22}$$

$$V_c = (V_{SG} + V_{SL}FE) \frac{A}{A_c} = \frac{(V_{SG} + V_{SL}FE)}{(1 - 2\tilde{\delta}_L)^2} \quad \text{Eq. 2.23}$$

The friction factor for the liquid film, f_f , is evaluated from the single phase relationships at the film Reynolds number. The only additional quantities required are the interfacial friction factor, f_i , and the liquid fraction entrained, FE . To obtain appropriate correlations for these quantities, all the available annular-mist flow data were extracted from the Stanford Multiphase Flow Database (a total of 1,007 measurements) and the following procedure adopted.

By assuming that each experimental data point represented the desired pressure gradient and liquid volume fraction, a two-dimensional Newton-Raphson approximation was used to determine the values of f_i and FE that, when used with the model described herein, would produce these values. Some of the data were not able to converge to within the desired accuracy of 15% and were discarded. The remaining 742 observations were used to obtain the following correlations for FE and f_i :

$$\frac{FE}{1 - FE} = 3.523 \left(\frac{V_{SL}}{V_{SG} + V_{SL}} \right)^{0.15} N_D^{0.11} N_L^{0.03} N_B^{0.074} \quad \text{Eq. 2.24}$$

$$\frac{f_i}{f_c} = 5.91 \left(\frac{\sigma}{\rho_c V_c^2 D_c} \right)^{0.25} \left(\frac{V_c}{V_c - V_f} \right)^{2.79} \text{Re}_f^{0.103} \quad \text{Eq. 2.25}$$

The dimensionless quantities are defined as:

$$N_L = \mu_L \left[\frac{g_c}{\rho_L \sigma^3} \right]^{1/4}, \quad N_B = \frac{\mu_L^2 V_{SG}^2 \rho_G}{\sigma^2 \rho_L}, \quad N_D = D \sqrt{\frac{\rho_L g_c}{\sigma}} \quad \text{Eq. 2.26}$$

Barnea presents a model for the transition from annular flow based on two conditions. The first of these is based on the observation that the minimum interfacial shear stress is associated with a change in the direction of the velocity profile in the film. When the velocity profile becomes negative, stable annular flow cannot be maintained and the transition to intermittent flow occurs. The minimum shear stress condition may be determined from Eq. 2.18 to Eq. 2.20 by setting $\partial\tau_i/\partial\delta_L = 0$ and results in the following limit on Y :

$$Y_{\text{lim}} = \frac{f_f}{f_{SL}} (1 - FE)^2 \frac{(2 - \frac{3}{2} E_f)}{E_f^3 (1 - \frac{3}{2} E_f)} X^2 \quad \text{Eq. 2.27}$$

Note that this differs from the expression presented by Barnea which is based on the assumptions of no entrainment ($FE=0$) and smooth pipe friction factors based on the Blasius correlation.

The second mechanism proposed by Barnea for annular flow instability occurs when the supply of liquid in the film is sufficient to cause blockage of the gas core by bridging the pipe. This is said to take place when the in situ volume fraction of liquid exceeds one half of the value associated with the maximum volumetric packing density of gas bubbles (0.52). Hence, annular flow cannot exist when:

$$E_L \geq \frac{1}{2}(1 - 0.52) \text{ or } E_L \geq 0.24 \quad \text{Eq. 2.28}$$

The liquid volume fraction is calculated from:

$$E_L = 1 - (1 - 2\tilde{\delta}_L)^2 \frac{V_{SG}}{V_{SG} + FE V_{SL}} \quad \text{Eq. 2.29}$$

The pressure drop may be obtained directly from the momentum balance equations once the liquid film thickness is known.

2.2.3. Intermittent Flow

The intermittent flow model used here includes the slug and elongated bubble flow patterns. It is characterized by alternating slugs of liquid trailed by long bubbles of gas. The liquid slug may contain dispersed bubbles and the gas bubbles have a liquid film below them. It is assumed that the flow is incompressible and that the film thickness is uniform. A schematic representation of this model is shown in Figure 2.3.

Assuming that the flow is incompressible and a uniform depth for the liquid film, the liquid volume fraction may be determined by writing an overall liquid mass balance over a slug-bubble unit¹⁰:

$$E_L = \frac{E_{Ls}V_t + V_{Gdb}(1 - E_{Ls}) - V_{SG}}{V_t} \quad \text{Eq. 2.30}$$

where V_{Gdb} represents the velocity of the dispersed bubbles, V_t is the translational velocity of the slug, and E_{Ls} is the volume fraction liquid in the slug body. All of these quantities need to be determined based on empirical correlations.

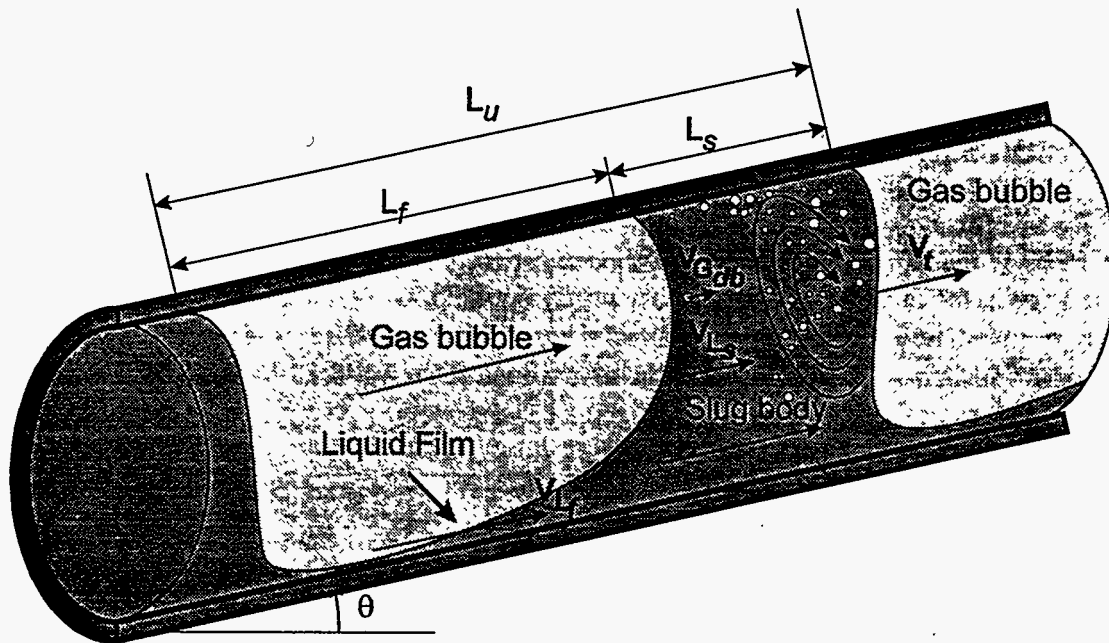


FIGURE 2.3 - INTERMITTENT FLOW MODEL

The liquid fraction in the slug E_{Ls} is calculated based on the Gregory¹¹ et al. correlation:

$$E_{Ls} = \frac{1}{1 + \left(\frac{V_m}{8.66}\right)^{1.39}} \quad \text{Eq. 2.31}$$

The translational velocity of the elongated bubbles is given by Bendiksen⁸ as:

$$V_t = C_0 V_m + V_b \quad \text{Eq. 2.32}$$

where the coefficient, C_0 is based on the Hughmark¹² correlation. It is approximately equal to 1.2 and approaches 2.0 as the flow becomes laminar. The bubble drift velocity, V_b , can be calculated from the Zuboski¹⁹ correlation:

$$V_b = f_m V_{b_{\infty}} \quad \text{Eq. 2.33}$$

where $f_m = 0.316\sqrt{\text{Re}_{\infty}}$ for $f_m < 1$, otherwise $f_m = 1$

$$\text{and } \text{Re}_{\infty} = \frac{\rho_L V_{b_{\infty}} D}{2\mu_L}$$

Bendiksen⁸ gives the bubble drift velocity at high Reynolds numbers as:

$$V_{b_{\infty}} = V_{bh_{\infty}} \cos \theta + V_{bv_{\infty}} \sin \theta \quad \text{Eq. 2.34}$$

The drift velocity of elongated bubbles in a horizontal system at high Reynolds numbers is given by Weber¹⁷ as:

$$V_{bh_{\infty}} = \left[0.54 - \frac{1.76}{\text{Bo}^{0.56}} \right] \sqrt{\frac{gD(\rho_L - \rho_G)}{\rho_L}} \quad \text{Eq. 2.35}$$

where the Bond Number, $\text{Bo} = \frac{(\rho_L - \rho_G) g D^2}{\sigma}$

Similarly, the drift velocity of elongated bubbles in a vertical system at high Reynolds numbers is given by Wallis¹⁶ as:

$$V_{bv_{\infty}} = 0.345 \left(1 - e^{(0.337 - 0.1\text{Bo})} \right) \sqrt{\frac{gD(\rho_L - \rho_G)}{\rho_L}} \quad \text{Eq. 2.36}$$

Finally, the velocity of the dispersed bubbles in the liquid slug is obtained from the correlation of Ansari²:

$$V_{Gdb} = C_0 V_m + V_b E_{Ls}^{0.1} \quad \text{Eq. 2.37}$$

$$V_b = 1.53 \left[\frac{g(\rho_L - \rho_G)\sigma}{\rho_L^2} \right]^{\frac{1}{4}} \sin \theta$$

The pressure drop may be obtained by writing the momentum balance over a slug-bubble unit:

$$-\left(\frac{dp}{dL} \right) = \rho_m \frac{g}{g_c} \sin \theta + \frac{1}{L_u} \left[L_s \left(\frac{\tau_{Ls} \pi D}{A} \right) + L_f \left(\frac{\tau_{L_f} S_{L_f} + \tau_{Gdb} S_{Gdb}}{A} \right) \right] \quad \text{Eq. 2.38}$$

where the mixture density, $\rho_m = E_L \rho_L + E_G \rho_G$

The frictional pressure gradient in the gas bubble is normally small compared to that in the liquid slug. Furthermore, no reliable method is available for estimating terms required in the above equation for calculating the frictional pressure gradient in the bubble region. Xiao et al. have modeled this part of intermittent flow by assuming it to be analogous to stratified flow. This treatment contradicts observations made in the laboratory. In view of these uncertainties, the following simple approach is selected:

$$-\left(\frac{dp}{dL} \right) = \rho_m \frac{g}{g_c} \sin \theta + [\eta(E_L - 1) + 1] \frac{2f_{Lm} \rho_L V_m^2}{g_c D} \quad \text{Eq. 2.39}$$

where $f_{Lm} = f(Re_{Lm}, \epsilon_k)$, $Re_{Lm} = \frac{D\rho_L V_m}{\mu_L}$, and the calibration factor, η , is normally taken as

1.0.

Barnea proposes that the transition from intermittent flow occurs when the liquid fraction in the slug exceeds the value associated with the maximum volumetric packing density of the dispersed bubbles (0.52). The same mechanism is adopted in this model with the exception that the liquid volume fraction in the slug is obtained from Eq. 2.31, as opposed to the correlation proposed by Barnea.

Although it is not treated as a separate flow pattern for the purposes of phase volume fractions and pressure drop determination, the elongated bubble flow regime is defined here as the portion of intermittent flow for which the liquid slug contains no dispersed bubbles of gas. This condition is represented in the model by the region where $E_{L_s} \geq 0.90$

This model is appropriate for slight downward inclinations, where $\theta \geq 15^\circ$, and for horizontal and uphill flow. For larger downward inclinations however, i.e. where $\theta \leq -15^\circ$, the intermittent flow pattern is less well understood and not often observed. There are therefore insufficient data to support a mechanistic approach. In the present model, the method adopted is to treat this region as a transition zone existing between dispersed bubble and annular-mist. If stable annular-mist flow cannot be attained and the liquid rate is not sufficient to achieve dispersed bubble flow, the flow pattern is described as "Froth II" and an interpolation is performed between the liquid rates at the dispersed bubble and the annular-mist transitions.

2.2.4. Dispersed Bubble Flow

A simple homogeneous model is used to calculate the in situ phase volume fractions and pressure drop for this flow pattern. Holdup is neglected and the pressure drop is evaluated based on Moody's chart using the gas-liquid mixture properties.

The dispersed bubble flow region is bounded by two criteria. The first is based on the previously mentioned transition to slug flow, i.e. $E_{L_s} > 0.48$. The other criterion involves the transition to froth flow when the maximum volumetric packing density of the gas bubbles is exceeded:

$$C_G = \frac{V_{SG}}{V_m} > 0.52 \quad \text{Eq. 2.40}$$

2.2.5. Bubble Flow

Bubble flow can exist if the flow is intermittent and both of the following conditions are satisfied:

- a) The Taylor bubble velocity exceeds the bubble velocity. This is satisfied in large diameter pipes (Taitel¹⁴ et al.) when:

$$D > 19 \left[\frac{(\rho_L - \rho_G)\sigma}{\rho_L^2 g} \right]^{1/2} \quad \text{Eq. 2.41}$$

- b) The angle of inclination is large enough to prevent migration of bubbles to the top wall of the pipe (Barnea⁷ et al.):

$$\cos\theta \leq \frac{3}{4\sqrt{2}} V_b^2 \left(\frac{C_l \gamma^2}{g d_b} \right) \quad \text{Eq. 2.42}$$

The lift coefficient, C_l ranges from 0.4 to 1.2, the bubble distortion (from spherical) coefficient γ ranges from 1.1 to 1.5 and a bubble size, d_b between 4 and 10 mm is recommended. For this model, C_l is taken as 0.8, γ as 1.3 and a bubble diameter of 7 mm is used.

When both of these conditions are satisfied, bubble flow is observed even at low liquid rates where turbulent forces do not cause bubble breakup. The transition to bubble flow from intermittent flow as suggested by Taitel¹⁴ et al. occurs when the gas void fraction (during slug flow) drops below the critical value of 0.25.

Unrealistic flow pattern transitions have been observed when the line represented by Eq. 2.42 falls within the slug flow region. For this reason, the present model checks for the existence of bubble flow only within the elongated bubble flow regime.

2.2.6. Froth Flow

Froth flow represents a transition zone between dispersed bubble flow and annular-mist flow and between slug flow and annular-mist. In this model the region is labelled "Froth I", to distinguish it from the transition region, Froth II, described above. The approach used in this model is to interpolate between the appropriate boundary regimes in order to determine the transition values of the in situ liquid volume fraction and pressure drop. This involves a number of iterative procedures in order to determine the superficial gas velocities at the dispersed bubble, annular-mist and slug transitions to froth. Once V_{SG} at each transition is known, the volume fraction and pressure drop values *at the transitions* are calculated and a linear interpolation between these values is made for each quantity.

2.3. Results

The evaluation of the model's performance has been performed using the following approaches.

The behavior of the model was examined over a wide range of flow rates and fluid properties using three-dimensional surface plots. This was done over the complete range of upward and downward pipe inclinations and both pressure gradient and volumetric liquid fraction were analyzed. The results indicate generally smooth transitions between flow regimes.

In addition, data were extracted from the Stanford Multiphase Flow Database for which pressure gradient, holdup and flow pattern observations were available. This resulted in a total of 5,951 measurements consisting of variations in fluid properties, pipe diameters and upward as well as downward inclinations. The model predictions for liquid volume fraction are plotted against the experimental measurements in Figure 2.4. Figure 2.5 shows a similar plot for the pressure gradient calculations. A summary of all these results is also given in Table 2.1.

It can be seen that the model was able to predict the in situ liquid volume fraction to within an accuracy of 25% in 3,972 of the 5,951 cases (67%). The pressure gradient was predicted to the same accuracy for 2,970 cases (50%). The flow pattern prediction capabilities of the model are presented in Table 2.2. The number of experimentally observed flow patterns are shown for each flow regime and these can be compared with the number predicted by the model.

The third column represents the number of instances where the predicted flow pattern matched the experimental observations and it can be seen that a total of 1,843 predictions matched the experiments. It should be noted however, that due to the difficulty in classifying flow patterns near the transition zone, a significant number of the 1,322 Froth I predictions might have been reported as either slug or annular-mist.

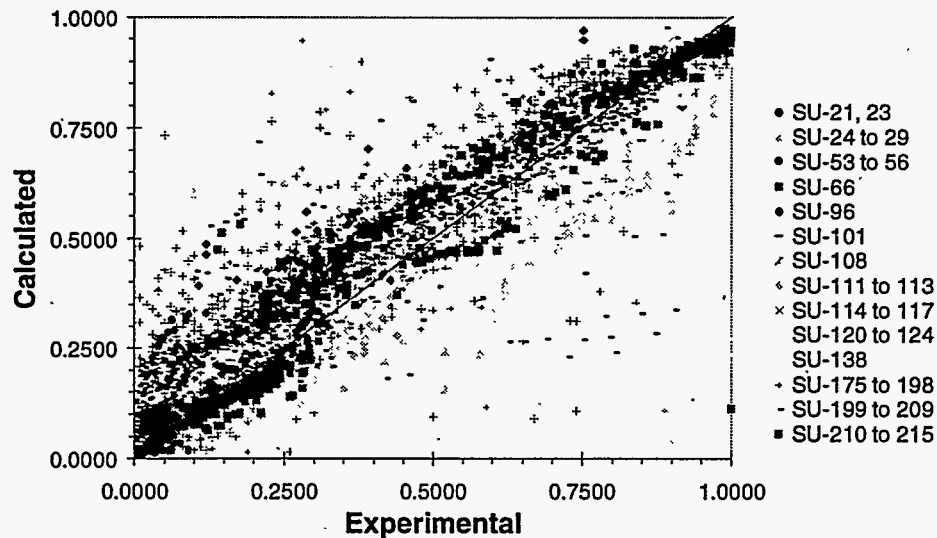


FIGURE 2.4 - COMPARISON OF CALCULATED LIQUID VOLUME FRACTION WITH EXPERIMENTAL DATA

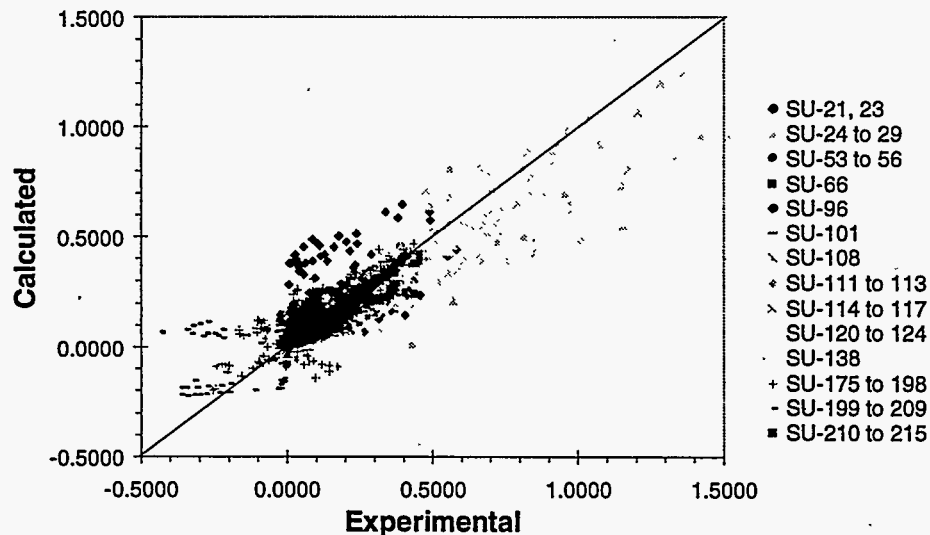


FIGURE 2.5 - COMPARISON OF CALCULATED PRESSURE GRADIENT WITH EXPERIMENTAL DATA.

TABLE 2.1 - COMPARISON WITH EXPERIMENTAL DATA

Error	ΔP	E_L	Cumulative			
	Count	Count	ΔP	E_L	Count	%
0-5%	1140	1633	1140	19%	1633	27%
5-10%	635	836	1775	30%	2469	41%
10-15%	469	643	2244	38%	3112	52%
15-20%	393	493	2637	44%	3605	61%
20-25%	333	367	2970	50%	3972	67%
25-30%	288	274	3258	55%	4246	71%
>30%	2693	1705				

TABLE 2.2 - FLOW PATTERN DISTRIBUTION IN EXPERIMENTAL DATA

Flow Pattern	Predicted	Measured	Matched
Elongated bubble	394	584	109
Bubble	43	426	0
Stratified smooth	148	449	99
Stratified wavy	670	563	163
Slug	1505	2103	627
Annular-Mist	1323	1007	656
Dispersed bubble	498	411	38
Froth I	1322	408	151
Froth II	48	0	0
	Total	5951	5951
			1843

2.4. Summary and Conclusions

A new mechanistic model has been presented which is applicable to all conditions commonly encountered in the petroleum industry. The model incorporates roughness effects as well as liquid entrainment, both of which are not accounted for by other models so far presented. The model has undergone extensive testing and has proven to be more robust than existing models and is applicable over a more extensive range of conditions.

While it is believed that significant improvements over existing models have been achieved, further research is needed to overcome problems associated with multiple roots and flow pattern transitions. Furthermore, empirical correlations necessary within the model can only be improved with accurate and consistent data over a wide range of conditions of commercial interest. Work in both of these areas is currently in progress.

Acknowledgements

The work described in this paper has been made possible through the support of the Reservoir Simulation Industrial Affiliates Program at Stanford University (SUPRI-B).

Nomenclature

A	Cross-sectional area
D	Pipe internal diameter
E	In situ volume fraction
FE	Liquid fraction entrained
g	Acceleration due to gravity
h_L	Height of liquid (Stratified flow)
L	Length
p	Pressure
Re	Reynolds number
S	Contact perimeter
V_{SG}	Superficial gas velocity
V_{SL}	Superficial liquid velocity
δ_L	Liquid film thickness (Annular-Mist)
ϵ_k	Pipe roughness
θ	Angle of inclination
μ	Viscosity
ρ	Density
σ	Interfacial (surface) tension
τ	Shear stress
\bar{x}	Dimensionless quantity, x

Subscripts

<i>b</i>	relating to the gas bubble
<i>c</i>	relating to the gas core
<i>f</i>	relating to the liquid film
<i>db</i>	relating to the dispersed bubbles
<i>G</i>	relating to the gas phase
<i>i</i>	relating to the interface
<i>L</i>	relating to the liquid phase
<i>m</i>	relating to the mixture
<i>SG</i>	based on superficial gas velocity
<i>s</i>	relating to the liquid slug
<i>SL</i>	based on superficial liquid velocity
<i>wL</i>	relating to the wall-liquid interface
<i>wG</i>	relating to the wall-gas interface

References

- 1) Andritsos, N., "Effect of Pipe Diameter and Liquid Viscosity on Horizontal Stratified Flow," Ph.D. Dissertation, U. of Illinois at Champaign-Urbana (1986)
- 2) Ansari, A. M. "A Comprehensive Mechanistic Model for Upward Two-Phase Flow," M. S. Thesis, The University of Tulsa, 1987
- 3) Ansari, A. M., Sylvester, A. D., Sarica, C., Shoham, O., and Brill, J. P., "A Comprehensive Mechanistic Model for Upward Two-Phase Flow in Wellbores," SPE Prod. & Facilities, pp. 143-152, May 1994
- 4) Aziz, K. and Petalas, N., "New PC-Based Software for Multiphase Flow Calculations," paper SPE 28249 presented at the SPE Petroleum Computer Conference, Dallas, 31 July-3 August, 1994
- 5) Baker, A., Nielsen, K. and Gabb A., "New Correlations - 1, Pressure Loss Liquid-Holdup Calculations Developed," Oil & Gas J., March 14, 1988, 55-59
- 6) Barnea, D. "A Unified Model for Predicting Flow-Pattern transitions for the Whole Range of Pipe Inclinations," Int. J. Multiphase Flow, 13, No. 1, 1-12 (1987)
- 7) Barnea, D., Shoham, O., Taitel, Y. and Dukler, A.E., "Gas-Liquid Flow in Inclined Tubes: Flow Pattern Transitions for Upward Flow," Chem. Eng. Sci., 40, 1 pp. 131-136 (1985)
- 8) Bendiksen, K. H. "An Experimental Investigation of the Motion of Long Bubbles in Inclined Pipes," Int. J. Multiphase Flow, 10, pp 1-12 (1984)
- 9) Colebrook, C. F., "Turbulent Flow in Pipes with Particular Reference to the Transition Region Between the Smooth and Rough-Pipe Laws," J. Inst. Civil Engrs., 11, 133 (1939)
- 10) Govier, G. W. and Aziz, K. "The Flow of Complex Mixtures in Pipes," Van Nostrand, Reinhold (1972), reprinted by Robert E. Kriger Publishing Co., Huntington, New York, 1977.
- 11) Gregory, G. A., Nicholson, M.K. and Aziz, K., "Correlation of the Liquid Volume Fraction in the Slug for Horizontal Gas-Liquid Slug Flow," Int. J. Multiphase Flow, 4, 1, pp. 33-39 (1978)
- 12) Hughmark, G. A., "Holdup and Heat Transfer in Horizontal Slug Gas Liquid Flow," Chem. Eng. Sci., 20, 1007-1010 (1965).
- 13) Oliemans, R. V. A., Pots, B. F., and Trope, N., "Modeling of Annular Dispersed Two-Phase Flow in Vertical Pipes," Int. J. Multiphase Flow, 12, No. 5, 711-732 (1986)
- 14) Taitel, Y., Barnea, D. and Dukler, A. E. "Modeling Flow Pattern Transitions for Steady Upward Gas-Liquid Flow in Vertical Tubes," AIChE Journal, 26, pp. 345-354 (1980)
- 15) Taitel, Y., and Dukler, A. E. "A Model for predicting Flow Regime Transitions in Horizontal and Near Horizontal Gas-Liquid Flow," AIChE Journal, 22, 47 (1976)
- 16) Wallis, G. B. "One-Dimensional two-Phase Flow," McGraw-Hill, New York, 1969
- 17) Weber, M. E., "Drift in Intermittent Two-Phase Flow in Horizontal Pipes," Canadian J. Chem. Engg., 59, pp. 398-399, June 1981
- 18) Xiao, J. J., Shoham, O., Brill, J. P., "A Comprehensive Mechanistic Model for Two-Phase Flow in Pipelines," paper SPE 20631, 65th ATC&E of SPE, New Orleans, September 23-26, 1990
- 19) Zukoski, E.E., "Influence of Viscosity, Surface Tension, and Inclination Angle on Motion of Long Bubbles in Closed Tubes," J. Fluid Mech., 25, pp. 821-837 (1966)

3. Well Indices for Horizontal Wells

by Pierre-David Maizeret, Sepehr Arbabi, and Khalid Aziz

Abstract

Horizontal Wells have proven to be very efficient in oil and gas production and many horizontal wells, some with complex profiles, are being drilled every year. However current reservoir engineering tools often fail to predict their performance. One of the contributing reasons could be the use of inappropriate well models in reservoir simulators: the horizontal well model used is essentially the same as that for vertical wells, which is only valid for an isolated well far from the boundaries. This study describes a semi-analytical method to obtain well indices to be used in simulation of wells of any profile.

3.1 Introduction

A reservoir simulator solves the flow equations numerically on grids defining a reservoir region. However, when a well is located in a grid-block, the block pressure is not equal to the well pressure. In order to join the well to the grid blocks in which the well is located, it is usual to use a single phase model to obtain the appropriate Well Index. The Well Index is based on the concept of an effective well radius at which the pressure of the block applies. This approach requires the flow in the area around the well to be radial. Peaceman [1] has proposed more general expressions for the effective radius, but all based on 2D flow.

As reservoirs are generally thin, a horizontal well cannot be far from the top or bottom boundary. In the case of multilateral wells, the situation is even worse, since the flow is perturbed not only by the boundaries but also by the other wells. Moreover, horizontal wells can be efficient in low permeability reservoirs, where the steady-state (or pseudo-steady-state) regime does not establish rapidly. This means that a single constant value for the well index cannot be used for all times.

The objective of this study is then to evaluate well indices for different configurations of horizontal wells. The well index will be computed for a homogeneous anisotropic single-phase flow and will then be reintroduced in the simulator for the full three-phase study.

The well index relates the pressure in the block to the pressure in the well for a given flow rate (see definition below). If these two pressures are known, the well index can be deduced easily. The block pressure can be evaluated by a simulator. The well pressure for a three-dimensional single-phase flow is not known analytically in general, but can be computed by the semi-analytical method described briefly below.

3.2 Well Pressure

3.2.1 Calculation

The method to evaluate the pressure in a three-dimensional, homogeneous, anisotropic single-phase flow has been described by Economides et al. [2]. The well is modeled as a line-source in a parallelepipedic reservoir. It need not be a straight line and in fact can take on any arbitrary shape. Instead of trying to compute the solution in one step using the method of images for instance, the problem is split into three parts. The idea is to consider the well as a series of point sources infinitely close to one another. Therefore, we need to compute the well-known instantaneous point source solution, then integrate it over time to obtain the continuous point source solution. The line source solution is the summation of these functions along the well path. The integrations requires a little care but can be implemented easily using a Fortran program (see Appendix).

The significant advantage of this method is that any profile can be considered. Moreover, using the superposition principle, it is also very easy to model more complicated well configurations, such as multilateral wells for instance.

3.2.2 Validation

The validity of the solution thus obtained has been checked in four different manners. For each case the reservoir dimensions and the well location are given in a small table and parameters therein are defined in the Nomenclature.

A) First, the objective was to reproduce the results obtained by Economides et al. [2]. We considered one of his examples: a 200 ft long horizontal well in a box.

Table 3.1: Geometric Parameters Used for Validation (A)

Reservoir dimensions (ft)	Well	
	from	to
$x_e=1000$	$x_0=400$	$x_1=600$
$y_e=1000$	$y_0=500$	$y_1=500$
$z_e=50$	$z_0=25$	$z_1=25$

The results look almost identical to those computed by Economides et al. [2] (see Figure 3.1).

B) The solution has also been tested against a 2D analytical solution based on the method of images. This time using a fully penetrating horizontal well in the same reservoir, the two results are identical (Figure 3.2).

C) Using the 2D solver we also compared the results in the case of two horizontal wells in the same reservoir, an injector and a producer, distance of 500 ft apart. Here again the results are identical (Figure 3.3).

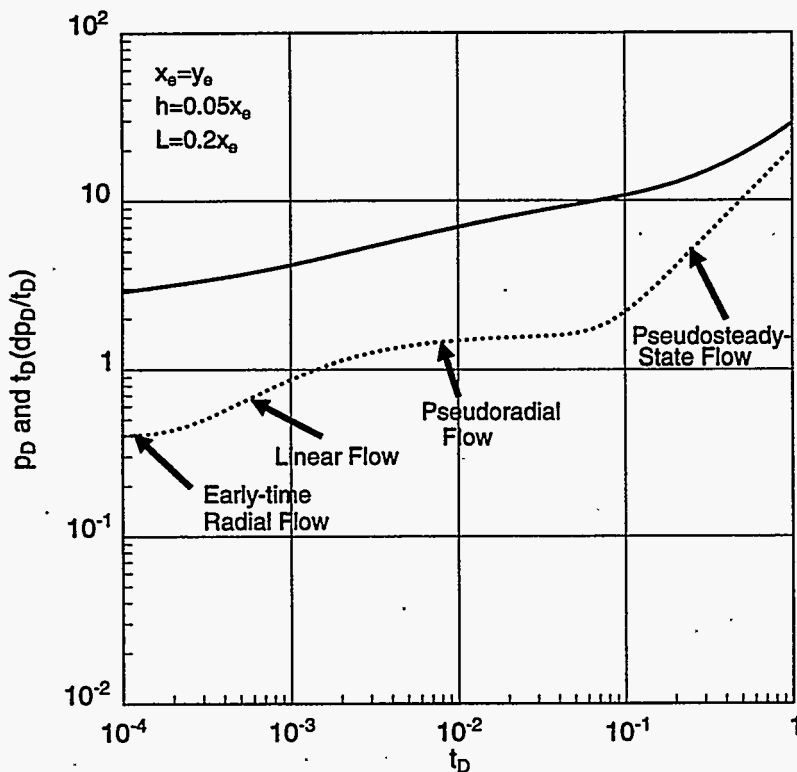


Figure 3.1: Flow regimes of a mildly laterally penetrating horizontal well

Table 3.2: Geometric Parameters Used for Validation (B)

Reservoir dimensions (ft)	Well	
	from	to
$x_e=1000$	$x_0=0$	$x_1=1000$
$y_e=1000$	$y_0=500$	$y_1=500$
$z_e=50$	$z_0=25$	$z_1=25$

D) Finally, we compared the results with a numerical simulator, Eclipse. We modeled an isolated well far from the boundaries, completed throughout the reservoir. The well is fully penetrating.

The results are shown in Figure 3.4, where we observe very good agreement.

All the validation tests were performed using the rock and fluid properties given in Table 3.5 below.

3.3 Well Index

3.3.1 Definition

To compute the bottomhole pressure from the well block pressure, a simulator uses a *well index* which only depends on the well block properties and on the well geometry.

For each phase p , the flow rate is proportional to the difference in pressure between

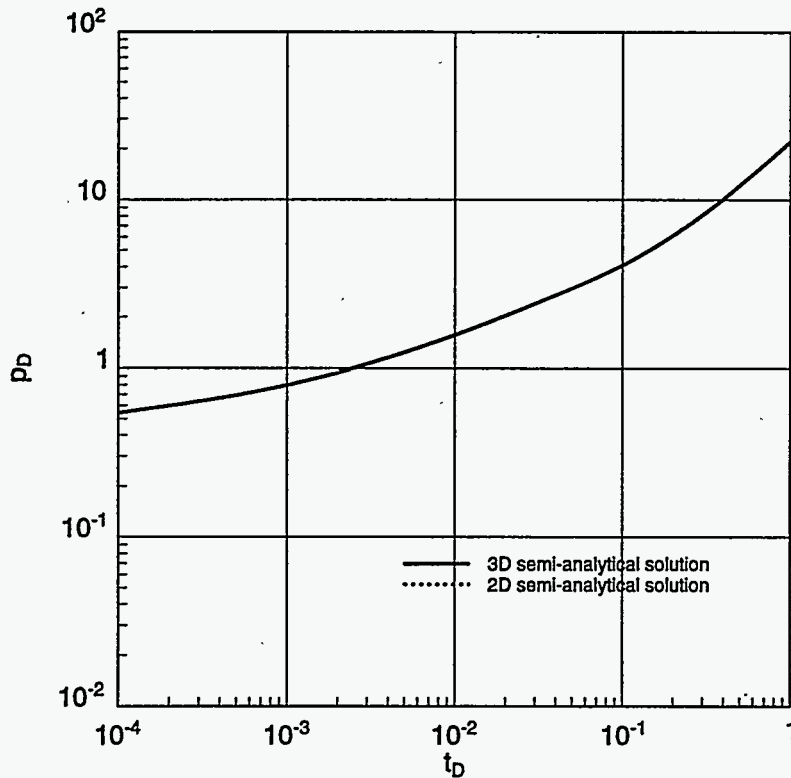


Figure 3.2: Comparison between a classical 2D solver and the 3D solution for one fully penetrating well (2D problem) in the middle of the reservoir

Table 3.3: Geometric Parameters Used for Validation (C)

Reservoir dimensions (ft)	Injector		Producer	
	from	to	from	to
$x_e=1000$	$x_0=0$	$x_1=1000$	$x_0=0$	$x_1=1000$
$y_e=1000$	$y_0=250$	$y_1=250$	$y_0=750$	$x_1=750$
$z_e=50$	$z_0=25$	$z_1=25$	$z_0=25$	$x_1=25$

the block and the well according to the relation:

$$q_p = WI \frac{k_{rp}}{\mu_p B_p} (P_{p,block} - P_{p,well})$$

Provided that the flow is approximately radial around the well, it is easy to show that there is an *effective radius*, r_0 such that:

$$WI = \theta kh / \ln \left(\frac{r_0}{r_w} \right)$$

where θ is the angle open to flow.

Peaceman [1] derived the following expression for r_0 (for a well parallel to the x-axis):

$$r_0 = 0.28 \frac{[(k_z/k_y)^{1/2} \Delta y^2 + (k_y/k_z)^{1/2} \Delta z^2]^{1/2}}{(k_z/k_y)^{1/4} + (k_y/k_z)^{1/4}}$$

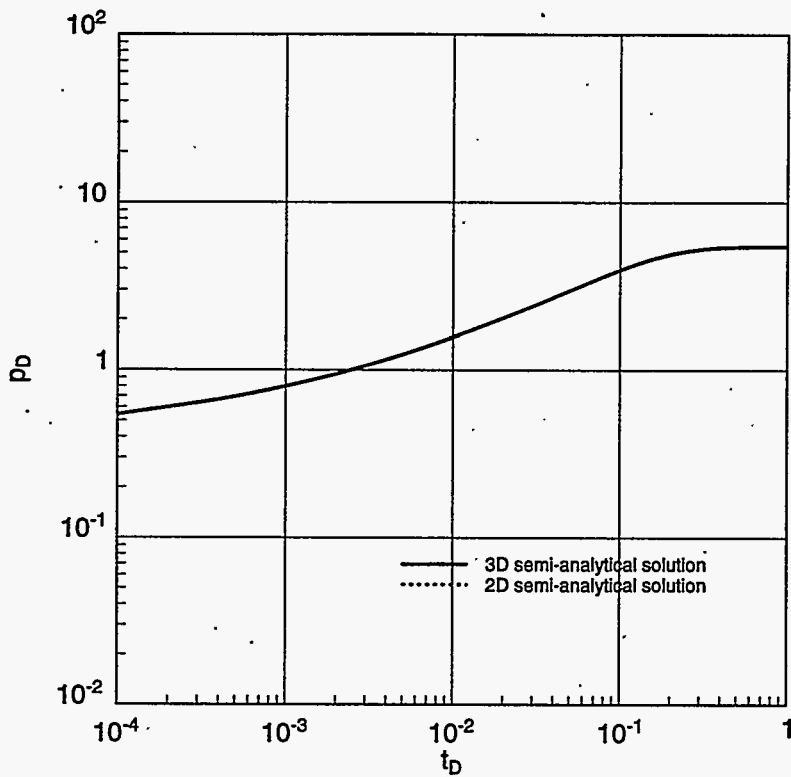


Figure 3.3: Comparison between a classical 2D solver and the 3D solution for an injector and a producer

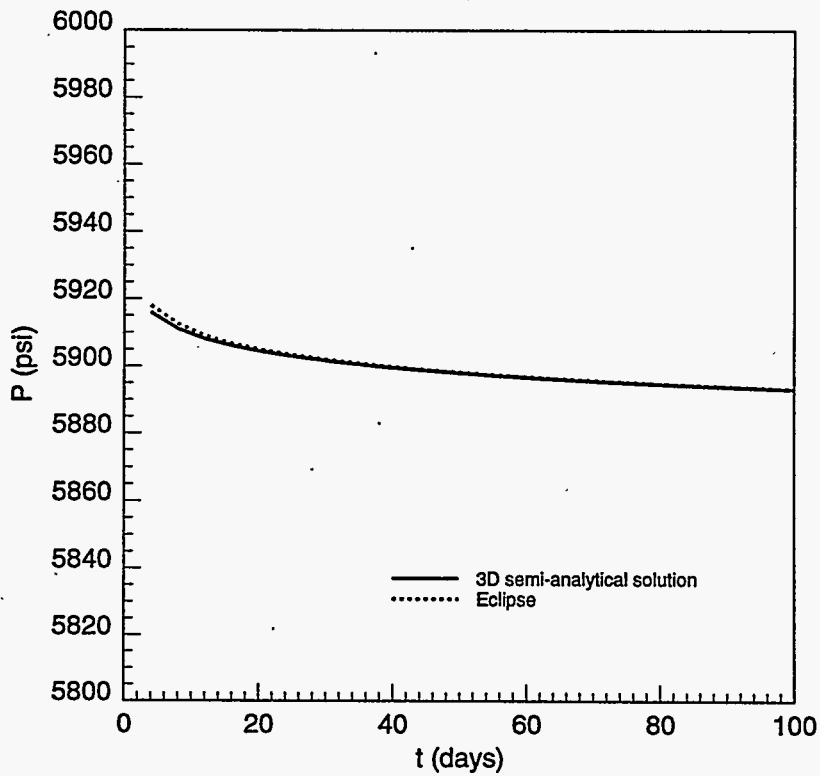


Figure 3.4: Comparison between Eclipse and the 3D solution for a single fully penetrating well

Table 3.4: Geometric Parameters Used for Validation (D)

Reservoir dimensions (ft)	Well	
	from	to
$x_e=1000$	$x_0=0$	$x_1=1000$
$y_e=9950$	$y_0=4975$	$y_1=4975$
$z_e=9950$	$z_0=4975$	$z_1=4975$

Table 3.5: Rock and Fluid Properties

$k = 10$ mD
$\Phi = 20$ %
$c_t = 7.7 \times 10^{-5}$ psi^{-1}
$q = 1000$ STB/d
$\mu = 1$ cp
$B = 1$ RB/STB
$P_{ini} = 6000$ psi

Most reservoir simulators use this expression to compute the well pressure. However its validity is based on the following assumptions:

- i) it is exact only for single phase flow,
- ii) the permeability must be uniform in the horizontal and vertical directions,
- iii) the well should be completed throughout the reservoir ("infinite" well length),
- iv) the grid must be uniform,
- v) the well must be isolated and far from the boundaries and other wells

3.3.2 New Model

Our analytical solution will not allow us to relax assumptions i) and ii), however the last three are not necessary any longer. For a given well geometry, both the analytical well pressure and the numerical well block pressure can be computed for a single phase flow case. The comparison of the two solutions leads to the evaluation of r_0 :

$$r_0 = r_w \exp\left(\frac{2\pi kL}{qB\mu}(P_{block} - P_{well})\right)$$

The Appendix outlines details of the analytical method to calculate P_{well} .

3.3.3 Applications

We investigate below the influence of the three geometric parameters on r_0 :

- well length,
- reservoir thickness,

- well location.

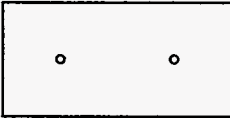



A) We first consider the steady-state case which is obtained by using an injector and a producer, flowing at the same rate. We have tried two different thicknesses, 495 ft and 55 ft, two different well lengths, 1000 ft (2D problem) and 200 ft (3D problem). The wells were first centered, then moved horizontally close to the boundaries and finally moved vertically close to the bottom boundary.

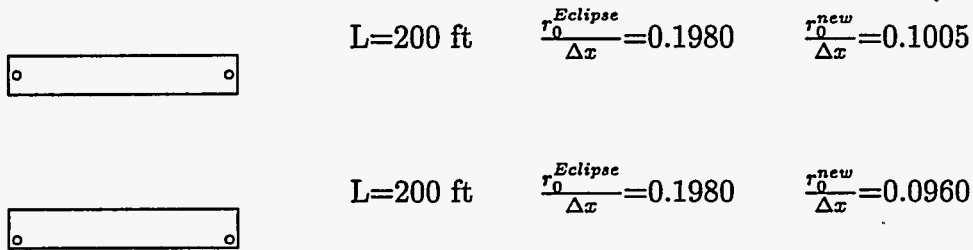
All the other parameters given in Table 3.6 below remain the same for the different cases:

Table 3.6: Parameters Used in the Application Examples

$x_e = 1000$ ft
$y_e = 990$ ft
$z_e = 495$ ft or 55 ft
$N_x = 1$ or 10
$N_y = 198$
$N_z = 99$ or 11
$\Delta x = 1000$ ft or 100 ft
$\Delta y = 5$ ft
$\Delta z = 5$ ft
$L = 1000$ ft or 200 ft
$q = 100$ bbl/d

The results are presented hereafter. We note that Eclipse is always using the same effective radius, $\frac{r_0}{\Delta x} \approx 0.1980$, which corresponds to Peaceman's formula.

	L=1000 ft	$\frac{r_0^{Eclipse}}{\Delta x} = 0.1981$	$\frac{r_0^{new}}{\Delta x} = 0.1983$
	L=1000 ft	$\frac{r_0^{Eclipse}}{\Delta x} = 0.1981$	$\frac{r_0^{new}}{\Delta x} = 0.1909$
	L=200 ft	$\frac{r_0^{Eclipse}}{\Delta x} = 0.1980$	$\frac{r_0^{new}}{\Delta x} = 0.1856$
	L=200 ft	$\frac{r_0^{Eclipse}}{\Delta x} = 0.1980$	$\frac{r_0^{new}}{\Delta x} = 0.1422$



We observe that when the conditions for evaluating the effective radius according to Peaceman's formula are not satisfied, the actual r_0 can be quite different from its default value, as shown particularly for the last three 3D cases above.

B) For a low permeability reservoir, the transient period can be quite long. Therefore the effective radius is not constant, but varies with time.

For the last 3D case for instance, the variations of r_0 with time are shown in Figure 3.5.

The steady-state regime is reached when t_D is approximately equal to 1.

Using the same rock and fluid properties as before, $t_D=1$ corresponds to $t=243$ days. For a permeability 10 times lower ($k=1$ mD), this would become 2433 days!

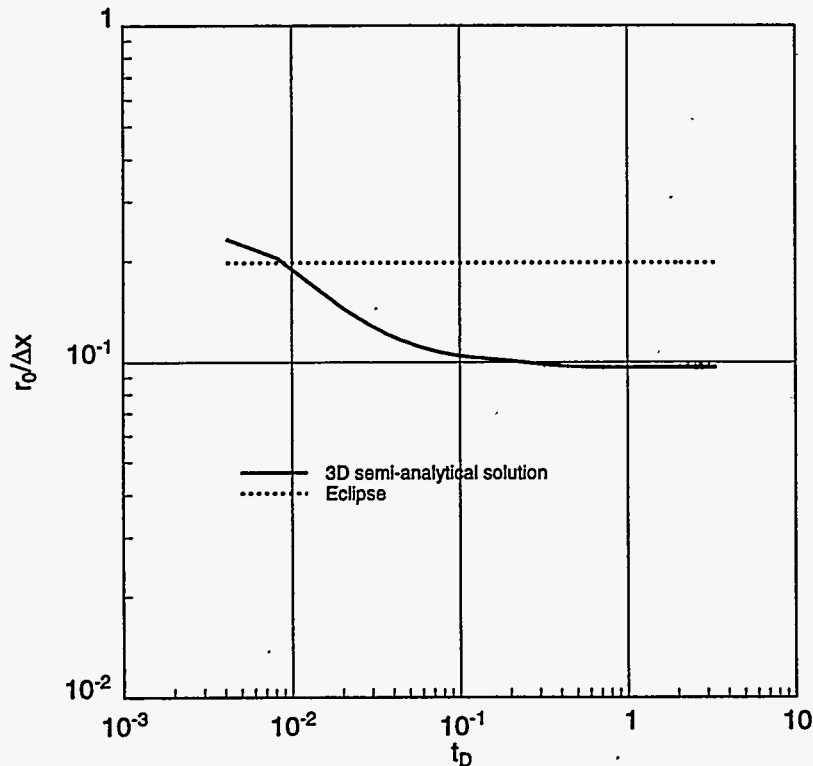


Figure 3.5: Variations of r_0 with time for Eclipse and for the new model for a 3D problem

3.4 Conclusions

When the well is close to the boundaries in a 3D case (partially penetrating well) the actual effective radius can differ from the one evaluated for an isolated well far from the boundaries.

The effective radius is constant only when the steady-state (or pseudosteady-state) regime is reached. During the transient period, the values used in the simulator should vary with time.

Moreover, the results shown here have been obtained for very simple cases where the well is a segment along the x-axis. For more realistic configurations, the differences could be much larger.

Nomenclature

B	Formation volume factor, resbbl/STB
c_{rock}	Rock compressibility, psi^{-1}
c	Total compressibility
k	Permeability, mD
k_x	Permeability in the x-direction, mD
k_y	Permeability in the y-direction, mD
k_z	Permeability in the z-direction, mD
L	Well length, ft
P	Pressure
P_{ini}	Initial pressure
q	Flow rate, STB/day
r_w	Wellbore radius, ft
r_0	Effective well radius, ft
t	Time, hrs
x_e	Extent of the reservoir in x-direction, ft
x_0	x location of heel of the horizontal well, ft
x_1	x location of toe of the horizontal well, ft
y_e	Extent of the reservoir in y-direction, ft
y_0	y location of heel of the horizontal well, ft
y_1	y location of toe of the horizontal well, ft
z_e	Extent of the reservoir in z-direction, ft
z_0	z location of heel of the horizontal well, ft
z_1	z location of toe of the horizontal well, ft
N_y	Number of simulation blocks in the y-direction
N_z	Number of simulation blocks in the z-direction
Δx	Simulation gridblock size in the x-direction
Δy	Simulation gridblock size in the y-direction
Δz	Simulation gridblock size in the z-direction
φ	Azimuth of well trajectory (relative to x-axis)
Φ	Porosity
Φ^0	Porosity at initial pressure
μ	Viscosity

Subscripts

D	Dimensionless
w	Well

References

- [1] Peaceman, D.W.: "Interpretation of Well-Block Pressures in Numerical Reservoir Simulation," *SPEJ* (June 1978) 183
- [2] Economides, M.J., Brand, C.W. and Frick, T.P.: "Well Configurations in Anisotropic Reservoirs", paper SPE 27980 presented at the University of Tulsa Petroleum Engineering Symposium, Tulsa, Aug. 29-31 (1994)
- [3] Besson, J.: "Performance of Slanted and Horizontal Wells on an anisotropic Medium", paper SPE 20965 presented at the European Petroleum Conference, The Hague, Neth., Oct. 21-24 (1990)
- [4] Carslaw, H.S. and Jaeger, J.C.: *Conduction of Heat in Solids*, Oxford University Press (1959)
- [5] Press, W.H., Teukolsky, S.A., Vetterling, W.T. and Flannery, B.P.: *Numerical Recipes in Fortran*, Cambridge University Press (1992)

3.5 Appendix: Outline of the 3D Semi-analytical method

3.5.1 Description of the Problem

The flow of an incompressible fluid in a closed box is described by the following equations:

$$\begin{cases} \underline{u} + \frac{k}{B\mu} \nabla P = 0 & (\text{Darcy's law}) \\ \nabla \cdot \underline{u} + \frac{\partial}{\partial t} \left(\frac{\Phi}{B} \right) = 0 & (\text{Mass Conservation}) \end{cases}$$

where the viscosity μ and the formation volume factor B are constant and porosity is a linear function of pressure:

$$\Phi = \Phi^0 [1 + c_{rock}(P - P_{ini})]$$

This can be rewritten as:

$$\nabla^2 P = \frac{\Phi^0 \mu c_{rock}}{k} \frac{\partial P}{\partial t}$$

The boundary conditions and the initial conditions are:

- no flow through the faces
- radial flow at the wellbore
- uniform initial pressure
- uniform pressure along the well

$$\begin{cases} \left(\frac{\partial P}{\partial x} \right)_0 = \left(\frac{\partial P}{\partial x} \right)_{x_e} = \left(\frac{\partial P}{\partial y} \right)_0 = \left(\frac{\partial P}{\partial y} \right)_{y_e} = \left(\frac{\partial P}{\partial z} \right)_0 = \left(\frac{\partial P}{\partial z} \right)_{z_e} = 0 \\ r \left(\frac{\partial P}{\partial r} \right)_{r_w} = -\frac{\mu q}{2\pi k L} \\ P(t=0) = P_{ini} \end{cases}$$

Defining dimensionless variables:

$$t_D = \frac{kt}{\Phi \mu c_{rock} x_e^2}, \quad q_D = \frac{Bq\mu}{x_e k P_i}, \quad p_D = \frac{P_i - P}{q_D P_i} = \frac{kx_e}{q\mu} (P_i - P)$$

The problem reduces to:

$$\nabla^2 p_D = \frac{\partial p_D}{\partial t_D}$$

with

$$\begin{cases} p_D(t_D = 0) = 0 \\ r_D \left(\frac{\partial p_D}{\partial t_D} \right)_{r_{Dw}} = \frac{1}{2\pi L_D} \\ \left(\frac{\partial p_D}{\partial x_D} \right)_0 = \left(\frac{\partial p_D}{\partial x_D} \right)_{x_{D_e}} = \left(\frac{\partial p_D}{\partial y_D} \right)_{y_{D_e}} = \left(\frac{\partial p_D}{\partial y_D} \right)_{y_{D_e}} = \left(\frac{\partial p_D}{\partial z_D} \right)_{z_{D_e}} = \left(\frac{\partial p_D}{\partial z_D} \right)_{z_{D_e}} = 0 \end{cases}$$

In the case where the permeabilities in the three directions are uniform but different from one another, the same equation can still be used provided we use the transformations introduced by Besson [3]:

- Transformation for the Well (if it is a straight line) are:

$$\begin{aligned} \text{Length} \quad L' &= L\alpha^{-1/3}\beta \\ \text{Wellbore Radius} \quad r'_w &= r_w \frac{\alpha^{2/3}}{2} \left(\frac{1}{\alpha\beta} + 1 \right) \end{aligned}$$

with

$$\alpha = \sqrt{\frac{(k_x k_y)^{1/2}}{k_z}}$$

and

$$\beta = \left(\sqrt{\frac{k_y}{k_x}} \cos^2 \varphi + \sqrt{\frac{k_x}{k_y}} \sin^2 \varphi \right)^{1/2}$$

- Transformation for the Reservoir Dimensions are:

$$\begin{aligned} x' &= x \frac{\sqrt{k_y k_z}}{k} \\ y' &= y \frac{\sqrt{k_x k_z}}{k} \\ z' &= z \frac{\sqrt{k_x k_y}}{k} \\ \bar{k} &= \sqrt[3]{k_x k_y k_z} \end{aligned}$$

3.5.2 Description of the Solution

The solution is evaluated in three steps.

We first need to obtain a solution of an instantaneous point source with a unit strength, located inside the box at $M_w (x_{Dw}, y_{Dw}, z_{Dw})$. This function is called **ipsrc**.

Two representations of the analytical solution have been given by Carslaw and Jaeger [4]. They involve infinite sums, but they converge rapidly.

The solution of a continuous point source with a unit strength, **cpsrc**, is then the result of the integration of **ipsrc** over time. This requires an adaptive method. We used an adaptive stepsize control in the Runge-Kutta method [5].

$$cpsrc(M_D, M_w, t_D) = \int_0^{t_D} ipsrc(M_D, M_w, \xi) d\xi$$

Finally, the solution to a continuous line source, **clsrc**, is the result of the integration of **cpsrc** along the line.

However, close to the line (i.e. at a distance equal to a well radius) the solution is almost singular. Indeed close to a point source, the flow is spherical and the pressure varies with the inverse of the distance. The pressure is the solution to:

$$r_D^2 \frac{\partial p_D}{\partial r_D} = \frac{1}{4\pi}$$

Therefore the trick is to subtract a term $\frac{1}{4\pi r_D}$ from **cpsrc** to compute the integral:

$$clsrc(M_D, M_0, M_1, t_D) = \int_{M_0}^{M_1} \left(cpsrc(M_D, M_w, t_D) - \frac{1}{4\pi r_D} \right) dM_w + \int_{M_0}^{M_1} \frac{1}{4\pi r_D} dM_w$$

This last integral can be calculated numerically. If the well is represented by a segment $[M_0, M_1]$, and the contribution of the integral is evaluated at the position M, denoting the angle $(\vec{M_0M_1}, \vec{M_0M})$ as β and the length $|M_0M|$ as X:

$$\begin{aligned}
 I &= \int_{M_0}^{M_1} \frac{1}{4\pi r_D} dM_w \\
 &= \frac{1}{4\pi L} \ln \left[\frac{1 - \frac{X}{L} \cos\beta + \sqrt{\frac{X^2}{L^2} - \frac{2X}{L^2} \cos\beta + 1}}{\frac{X}{L}(1 - \cos\beta)} \right]
 \end{aligned}$$

If the well is not a straight line, it is possible to either compute this same integral for a different configuration, or break the curve into segments.

4. Analytical Reservoir/Wellbore Coupling

by Raju Penmatcha, Sepehr Arbabi, and Khalid Aziz

Abstract

As the length of a horizontal well is increased, its contact with the reservoir increases. But at the same time, the resistance to the flow in the well also increases which has a direct negative effect on the productivity of the well. The overall performance of horizontal wells depends on the balance of these two opposing factors. No reliable tools are currently available that account for both these factors in the evaluation of horizontal well performance. An analytical well-model is developed which can quantify the effects of both single phase oil and two-phase oil/gas flow pressure loss in the well on the overall well performance. A methodology is developed to calculate the optimum horizontal well length. A sensitivity study is conducted on the effect of various reservoir, fluid and well parameters on well performance.

4.1 Previous Work

Previous work can be categorized into three types:

Type 1: Infinitely Conductive Well

An infinitely conductive well can be evaluated using either a numerical simulator or an appropriate analytical equation, if available. Analytical equations are available only for simple homogeneous reservoirs. Based on the nature of flow, any of the available equations can be used for a quick performance evaluation of a horizontal well in a single phase oil reservoir. Because of the infinite conductivity assumption in all these analytical treatments, their predictions are accurate only when the pressure drop in the wellbore is insignificant. A numerical simulator, on the other hand, can be used for a thorough analysis of any complex reservoir. Unfortunately, at the present time, none of the commercial simulators rigorously account for the wellbore pressure drop.

Type 2: Wellbore Coupled to an Analytically Approximated Reservoir

Realizing the importance of wellbore pressure drop, a few groups have recently developed some simple techniques to evaluate the wellbore frictional effects. This section outlines the available methods that couple the wellbore to an analytically approximated reservoir. The behavior of many homogeneous, single phase reservoirs can be approximated analytically. Many reservoirs are in reality more complex and cannot be represented analytically (heterogeneous, multiphase flow, etc). None of the approaches presented in the literature take into account multiphase flow, or radial inflow effects in the wellbore.

Stone *et al.* [1] used the model of Chow & Ransom [2] for wellbore pressure drop calculations. The flow from the reservoir to the wellbore was calculated using the productivity

index (PI) concept and the PI was assumed to be constant along the well. The equations developed were solved using the Yale sparse matrix package.

Dikken [3] presented an analytical model that couples the wellbore to the reservoir with turbulent flow in the wellbore. By using single phase flow frictional pressure drop calculations in the wellbore, the wellbore was linked to the reservoir using a material balance relationship. Both laminar and turbulent flows in the reservoir were considered. For turbulent flow, Blasius' formula was used to compute the friction factor. Dikken solved this problem analytically for an infinite horizontal well and numerically for a finite horizontal well. He assumed that the productivity index is constant along the well, which is placed in a reservoir with constant pressure boundaries. End effects and hence the spherical flow at the ends of the finite acting horizontal well were ignored and no transient flow was considered.

Islam *et al.* [4] developed a model for radial influx into the wellbore by numerical analysis. They suggested that bubbles created at the perforations due to radial influx and jet-like flow through the perforations induce additional turbulence in the wellbore. They didn't show how the well was linked to the reservoir, although they stated that hybrid grids were used in the simulator near the well.

Novy [5] coupled the reservoir to the wellbore in a manner similar to Dikken's model. Volume balance of fluids leaving the reservoir and entering the wellbore was used to accomplish this coupling. The problem was formulated as a boundary value problem and was solved using a finite-difference scheme. While Dikken's model cannot be applied to gas recovery (only oil recovery), the model by Novy can be applied to single phase gas or oil flow. Novy suggested that if the pressure drop in the wellbore is more than 10% of the drawdown, then it is important and should be considered. He showed that for laminar oil flow, friction reduces production rate by at least 10% when the wellbore pressure drop is more than 15% of the drawdown. He provided graphs that show that 1/3 of all oil wells and 3/4 of all gas wells as of 1992 in the world were not affected by friction in the wellbore. This is either due to low flow rates or large well diameters.

Ozkan *et al.* [6] did a similar kind of analytical coupling as Dikken except that they used the solution based on Green's function to describe the flow in the reservoir, while Dikken used a PI relationship. Ozkan *et al.* used only the infinite acting line source model to describe the flow in the reservoir. The model was presented in terms of dimensionless variables.

Landman [7] improved Dikken's model by allowing PI to vary along the well length. PI can vary along the well due to variation in perforation density, formation permeability or flow characteristics (radial, spherical, etc). Spherical flow at the end of the well was taken into account by using the approximate specific PI of a partially penetrating well in his original equations.

Type 3: Wellbore Coupled to a Numerically Approximated Reservoir

In the following papers, a wellbore pipe flow model was linked to a numerical simulator.

Folefac *et al.* [8] concluded that well length, well diameter and perforated interval have the most significant effect on the magnitude of pressure drop in the wellbore. They used a drift flux model in the wellbore and allowed for inter-phase mass transfer in the wellbore using an equation of state. They state that production logging shows variation of flow rate along the well, which could be due to pressure drop in the wellbore.

Brekke *et al.* [9] developed a network wellbore simulator, called HOSIM, which can calculate pressure drop with up to three phases in the wellbore. Their approach is modular and any new developments can be easily implemented. However, the network model, representing the wellbore, has to be built on a PC before it can be coupled to the reservoir. Any of the three existing multi-phase flow models built in the code can be chosen. Eclipse is used for reservoir simulation. The reservoir(Eclipse) and wellbore(HOSIM) were connected using the PI approach. PI is allowed to vary with time and location along the well length. It can be calculated from Eclipse runs by slightly disturbing the flow rate and then internally calculating dQ/dP during every iteration.

4.2 Modeling

In this section, a brief description of our general method of modeling is presented. Consider a simple case with a horizontal well located in the center of a cylindrical reservoir. The flow is assumed to be at steady-state both in the reservoir and in the wellbore. The simple reservoir model can be easily replaced by a more comprehensive model, such as the one discussed in the last chapter. We first define production loss in terms of wellbore pressure drop and drawdown as follows:

(I) Production Loss vs. Pressure Drop Ratio

The following parameters are used:

1. PI = productivity index of the well in rbbl/day/psi
2. Q = total flow rate from the well in rbbl/day
3. $J_s = PI/L$ = productivity index per unit length of the well (assumed constant)
4. $p_{w,0} = p_{w,x=0}$ = pressure at the heel of the well in psia
5. p_e = pressure at the reservoir boundary in psia

If $q_s(x)$ is the flow in the reservoir per unit length of the wellbore, then

$$q_s(x) = J_s[p_e - p_w(x)] \quad (4.1)$$

Integrating the above equation gives the total flow rate from the well as,

$$Q_{w,fric} = \int_{x=0}^L q_w(x)dx = \int_0^L J_s[p_e - p_w(x)] = J_s p_e L - J_s \int_0^L p_w(x)dx \quad (4.2)$$

When there is no pressure drop in the wellbore, then

$$Q_{w,nof} = \int_{x=0}^L q_w(x)dx = \int_0^L J_s[p_e - p_{w,0}] = J_s L [p_e - p_{w,0}] \quad (4.3)$$

Production Loss, P.L., is defined by:

$$\begin{aligned}
 P.L. &= \frac{Q_{w,nof} - Q_{w,fric}}{Q_{w,nof}} = \frac{J_s L(p_e - p_{w,0}) - J_s p_e L + J_s \int_0^L p_w(x) dx}{J_s L(p_e - p_{w,0})} \\
 &= \frac{\frac{1}{L} \int_0^L p_w(x) dx - p_{w,0}}{(p_e - p_{w,0})} = \frac{\frac{1}{L} \int_0^L [p_w(x) - p_{w,0}] dx}{[p_e - p_{w,0}]} \quad (4.4)
 \end{aligned}$$

Hence, P.L. = $\frac{\text{average wellbore pressure drop}}{\text{drawdown}}$

(II) Flowrate vs. Length

(A) CONSTANT J_s ALONG THE WELL LENGTH AND CONSTANT p_e :

The formulation is at first developed for the case with constant productivity index and constant pressure at the boundary for the entire horizontal well length. That is, J_s and p_e are constant and are independent of well length L . We have already assumed that the flow in the reservoir can be represented by Eq. (4.1). Mass balance gives the following equation for the flow in the wellbore:

$$\frac{d}{dx} q_w(x) = -q_s(x) \quad (4.5)$$

where $q_w(x)$ is the flow rate in the wellbore and it varies along the length of the well. Combining Equations (1) and (5), we have

$$\frac{d}{dx} q_w(x) = -J_s [p_e - p_w(x)] \quad (4.6)$$

Differentiating Eq. (4.6), under constant J_s and p_e assumptions, results in

$$\frac{d^2 q_w(x)}{dx^2} = J_s \frac{dp_w(x)}{dx} \quad (4.7)$$

Multiplying both sides by $\frac{dq_w(x)}{dx}$, we get

$$\frac{dq_w(x)}{dx} \frac{d}{dx} \left[\frac{dq_w(x)}{dx} \right] = J_s \frac{dp_w(x)}{dx} \frac{dq_w(x)}{dx} \quad (4.8)$$

$$\frac{1}{2} \frac{d}{dx} \left[\frac{dq_w}{dx} \frac{dq_w}{dx} \right] = J_s \frac{dp_w(x)}{dx} \frac{dq_w(x)}{dx} \quad (4.9)$$

$$d \left[\left(\frac{dq_w}{dx} \right)^2 \right] = 2J_s \frac{dp_w(x)}{dx} dq_w(x) \quad (4.10)$$

Integrating the above equation, we obtain

$$\int_{q_w=Q}^{q_w=q_w} d \left[\left(\frac{dq_w}{dx} \right)^2 \right] = 2J_s \int_{q_w=Q}^{q_w=q_w} \frac{dp_w(x)}{dx} dq_w(x) \quad (4.11)$$

$$\left[\frac{dq_w}{dx} \right]_{q_w}^2 - \left[\frac{dq_w}{dx} \right]_{q_w=Q}^2 = 2J_s \int_Q^{q_w} \frac{dp_w(x)}{dx} dq_w(x) \quad (4.12)$$

Using boundary condition I, defined as:

$$\left[\frac{dq_w}{dx}\right]_{x=0} = \left[\frac{dq_w}{dx}\right]_{q_w=Q} = -J_s[p_e - p_{w,0}] = -J_s\Delta p_0 \quad (4.13)$$

Equation (4.12) becomes

$$\left[\frac{dq_w}{dx}\right]^2 - [-J_s\Delta p_0]^2 = 2J_s \int_Q^{q_w} \frac{dp_w(x)}{dx} dq_w(x) \quad (4.14)$$

$$\frac{dq_w}{dx} = -\sqrt{2J_s \int_Q^{q_w} \frac{dp_w(x)}{dx} dq_w(x) + [J_s\Delta p_0]^2} \quad (4.15)$$

The choice of negative for the square root in the above equation comes from the fact that q_w increases as x decreases. Using boundary condition II, defined as

$$q_{w,x=L} = 0 \quad (4.16)$$

we get,

$$\int_{x=x}^{x=L} dx = - \int_{q_w=q_w}^{q_w=0} \frac{dq_w(x)}{\sqrt{2J_s \int_Q^{q_w} \left[\frac{dp_w}{dx}\right] dq_w(x) + [J_s\Delta p_0]^2}} \quad (4.17)$$

$$L - x = \int_0^{q_w(x)} \frac{dq_w(x)}{\sqrt{2J_s \int_Q^{q_w} \left[\frac{dp_w}{dx}\right] dq_w(x) + [J_s\Delta p_0]^2}} \quad (4.18)$$

Since at the heel, $q_w(x=0) = Q$, the above equation can be expressed as,

$$L = \int_0^Q \frac{dq_w(x)}{\sqrt{2J_s \int_Q^{q_w} \left[\frac{dp_w}{dx}\right] dq_w(x) + [J_s\Delta p_0]^2}} \quad (4.19)$$

Using Eq.(4.19), we can calculate the required length L for a horizontal well, to produce a flow rate Q with a drawdown of (Δp_0) at the heel. Using Eq.(4.18), for a well with a given length L and drawdown Δp_0 , the flow along the well $q_w(x)$ can be calculated. Also, based on this information, the variation of pressure along the well length, $p_w(x)$, can be calculated and substituted in Eq.(4.4) to obtain the P.L.

Equation (4.19) is independent of the method of calculating $\frac{dp_w(x)}{dx}$. As long as $\frac{dp_w(x)}{dx}$ can be written as a function of the variable of integration in Eq(4.19), q_w , the above equation poses no problem. For single phase oil flow, we can write:

$$\frac{dp_w(x)}{dx} = f \left[\frac{\rho U^2}{2D} \right] = f q_w^2 \left[\frac{8\rho}{\pi^2 D^5} \right] \quad (4.20)$$

"f" in the above equation is the Moody friction factor and is a function of pipe roughness and flow rate q_w .

Table 4.1: Parameters Used in Example Problems

Horizontal Permeability	3000 mD
Vertical Permeability	300 mD
Reservoir Thickness	50 ft
Outer Boundary Pressure	5000 psia
Oil Formation Volume Factor	1.18
Gas Formation Volume Factor	0.0045
Oil Viscosity	1.0 cp
Gas Viscosity	0.02 cp
Oil Density	40.0 lbm/cu.ft
Gas Density	2.0e-04 lbm/cu.ft
Drainage Area	650 acres
Well Radius	3.0 inch
Skin	0.0
Wellbore Absolute Roughness	0.0 ft

4.3 Example Problem

Using the parameters in Table 4.1 and the equations developed so far, the effects of friction are illustrated below. It is also shown how the presence of two phases aggravates the frictional problems in the wellbore.

All the cases described below are run for steady state flow with single phase oil flowing in the reservoir. The steady state equations developed by Economides *et al.* [10] are used for describing the flow in the reservoir. The productivity index per unit length (J_s) is obtained by dividing the productivity index of the horizontal well with its length. J_s is then assumed constant along the entire horizontal well length.

Figure 4.1 shows the case when there is single phase oil flowing both in the reservoir and the wellbore. The dark lines in the plot show the variation of oil production rate with well length for three different drawdowns. The concave shape of the dark line, for example, for 5 psi drawdown shows that flow rates of 8000 STB/day or higher can never be reached with these drawdowns with any length of the horizontal well. If friction were neglected in the wellbore, then we could have estimated unrealistically that well productivity can always be increased to the desired value by increasing the length of the horizontal well.

The dashed lines in the plot show the percentage of production loss due to friction in the wellbore. As shown, for a given rate the production loss is higher for a lower drawdown than it is for a larger drawdown. Also noticeable is that the productivity losses at a given length increase as the flow rate is increased.

The frictional effects in the wellbore worsen when there are two-phases flowing in the wellbore. The two-phase flow effects are illustrated below by looking at a case where the GOR is 1000 SCF/STB. It was assumed that the pressure drop in the reservoir due to the gas flow is insignificant. In other words, the pressure drop due to gas in the reservoir is neglected for the sake of simplicity but it is accounted for in the wellbore. The GOR is assumed to be constant throughout the entire length of the horizontal well.

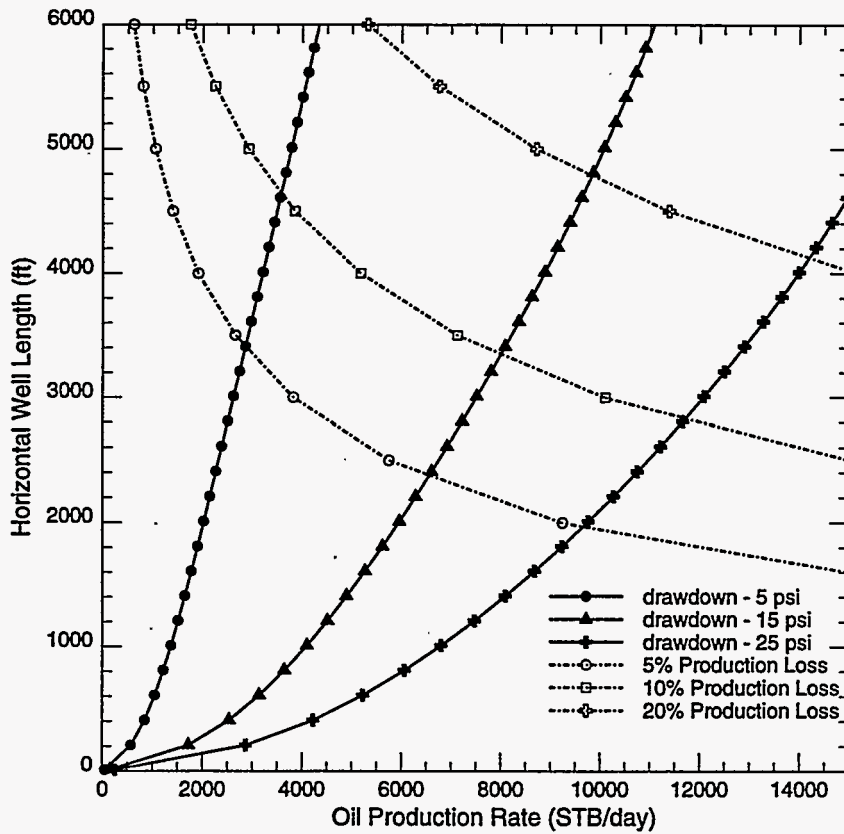


Figure 4.1: Flow Rate vs. Well Length: Single Phase Oil

In Figure 4.2, the two-phase pressure drop in the wellbore is calculated using the homogeneous flow model used in the Eclipse reservoir simulator. And in Figure 4.3, the pressure drop in the wellbore is calculated using the Beggs & Brill [11] correlation for two-phase flow pressure drop in the wellbore.

Figure 4.4 shows a comparison of four different cases with a 15 psi drawdown in the reservoir. The four cases considered include: a) single phase oil flowing in the wellbore, b) two-phase flow in the wellbore and homogeneous model used for pressure drop calculations, c) two-phase flow in the wellbore with Beggs & Brill model used for pressure drop calculations and d) friction neglected in the wellbore. Let us look, for example, when oil rate is 8000 STB/day. If friction is not considered in the wellbore, then the calculation shows that a horizontal well of length 3000 ft is sufficient to produce this flowrate under 15 psi drawdown conditions. But when frictional effects are considered a 3500 ft long well is required. Since friction is inevitable in reality, a 3000 ft well drilled would produce only 7500 STB/day. As the graph suggests, frictional effects get worse when there are two phases flowing in the wellbore. The plot also shows that the productivity loss was more when the Beggs & Brill correlation was used as compared to the homogeneous flow assumptions for the pressure drop calculations in the wellbore.

(B) J_s AND/OR p_e VARIABLE:

In reality, we observe that J_s can vary along the well length and so does p_e . Let us divide the horizontal well section into three parts as shown in Figure 4.5. The productivity index per unit length for these three parts are $J_{s,I}$, $J_{s,II}$ and $J_{s,III}$, respectively. Within each

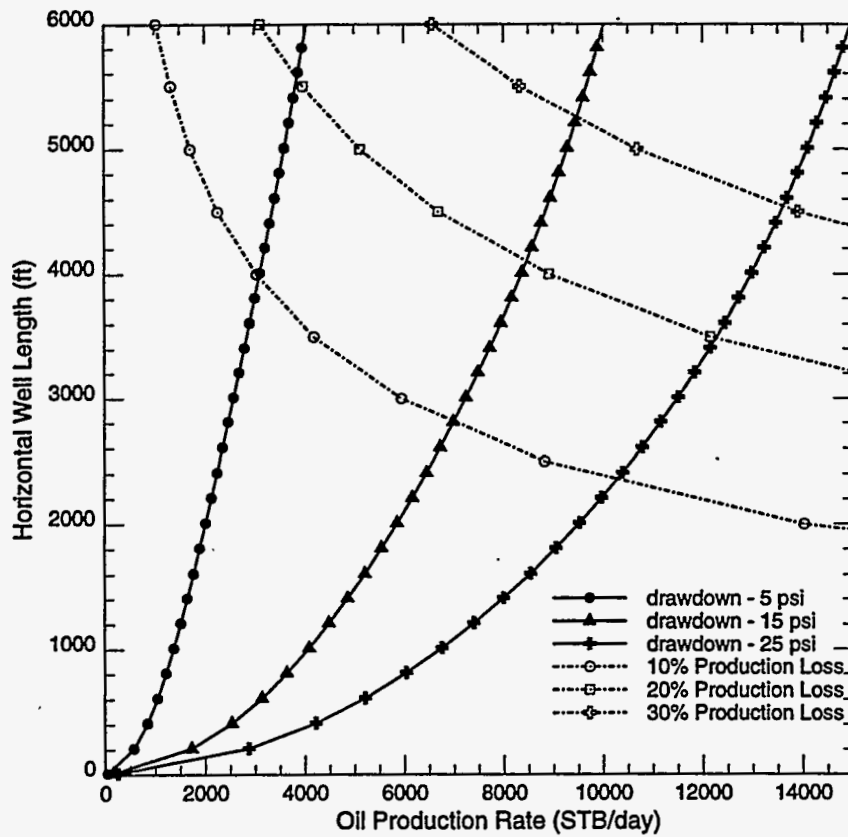


Figure 4.2: Flow Rate vs. Well Length: Two-Phase Flow, GOR=1000 SCF/STB, Homogeneous Flow Model Used

section, J_s is assumed to be constant. If this well is represented in a simulator, then each section represents one reservoir block in which the well is completed. Let the steady state block pressures be \bar{p}_I , \bar{p}_{II} and \bar{p}_{III} respectively. The pressure at the heel $p_{w,0}$ and the length of the well L are known.

Since within each section, J_s is constant, Eq. (4.19) can be used within each section. For section I,

$$L_I = \int_0^{Q_a} \frac{dq_w(x)}{\sqrt{2J_{s,I} \int_{Q_a}^{q_w} \left[\frac{dp_w}{dx} \right] dq_w(x) + [J_{s,I}(\bar{p}_I - p_a)]^2}} \quad (4.21)$$

For section II,

$$L_{II} = \int_{Q_a}^{Q_b} \frac{dq_w(x)}{\sqrt{2J_{s,II} \int_{Q_b}^{q_w} \left[\frac{dp_w}{dx} \right] dq_w(x) + [J_{s,II}(\bar{p}_{II} - p_b)]^2}} \quad (4.22)$$

and for section III,

$$L_{III} = \int_{Q_b}^Q \frac{dq_w(x)}{\sqrt{2J_{s,III} \int_Q^{q_w} \left[\frac{dp_w}{dx} \right] dq_w(x) + [J_{s,III}(\bar{p}_{III} - p_{w,0})]^2}} \quad (4.23)$$

p_a and p_b in the above equations are pressures at the end of sections I and II respectively. Equating Eq. (4.15) and Eq. (4.6) yields,

$$-J_s[p_e - p_w(x)] = -\sqrt{2J_s \int_Q^{q_w} \frac{dp_w(x)}{dx} dq_w(x) + [J_s \Delta p_o]^2} \quad (4.24)$$

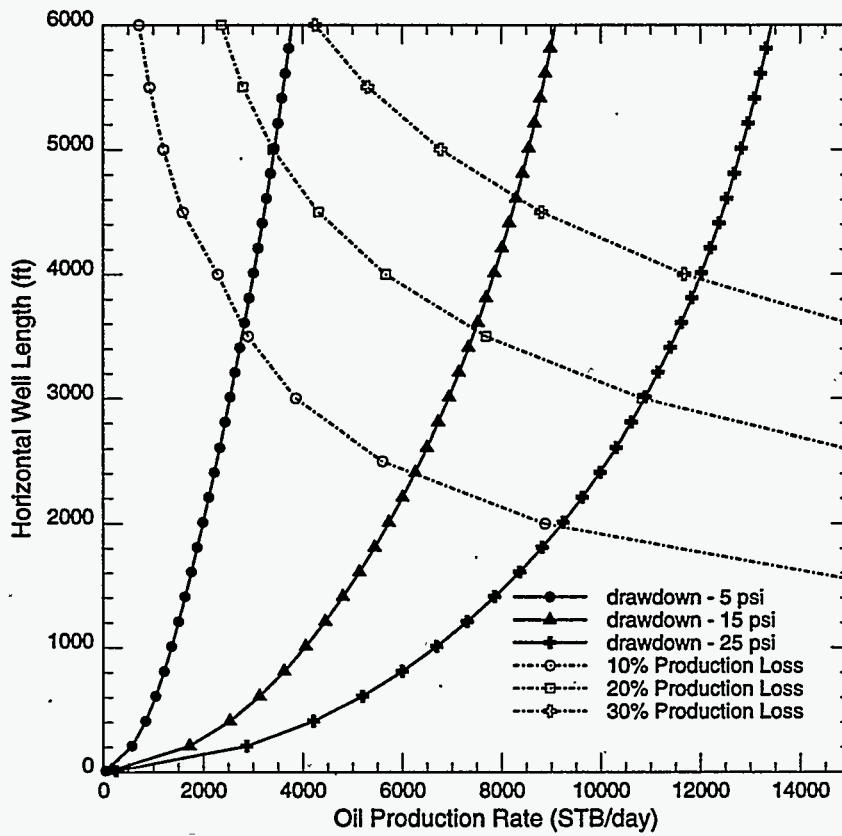


Figure 4.3: Flow Rate vs. Well Length: Two-Phase Flow, GOR=1000 SCF/STB, Beggs & Brill Correlation Used

When $x = L$,

$$p_w(L) = p_e - \sqrt{\frac{2}{J_s} \int_Q^{q_w} \frac{dp_w(x)}{dx} dq_w(x) + [\Delta p_o]^2} \quad (4.25)$$

Using the above equation, for section II,

$$p_a = \bar{p}_{II} - \sqrt{\frac{2}{J_{s,II}} \int_{Q_b}^{q_w} \frac{dp_w(x)}{dx} dq_w(x) + [\bar{p}_{II} - p_b]^2} \quad (4.26)$$

and similarly for section III,

$$p_b = \bar{p}_{III} - \sqrt{\frac{2}{J_{s,III}} \int_Q^{q_w} \frac{dp_w(x)}{dx} dq_w(x) + [\bar{p}_{III} - p_w,0]^2} \quad (4.27)$$

In the above formulation, there are five unknowns, Q_a , Q_b , Q , p_a and p_b and five equations. So the system can be solved, and unique solutions can be found. The methodology presented above can be generalized easily to the case where the horizontal well is divided into "n" sections.

4.4 Optimum Well Length

Optimum well length is defined here as the length of the horizontal well that gives maximum revenues in a given reservoir after considering friction in the wellbore. In its

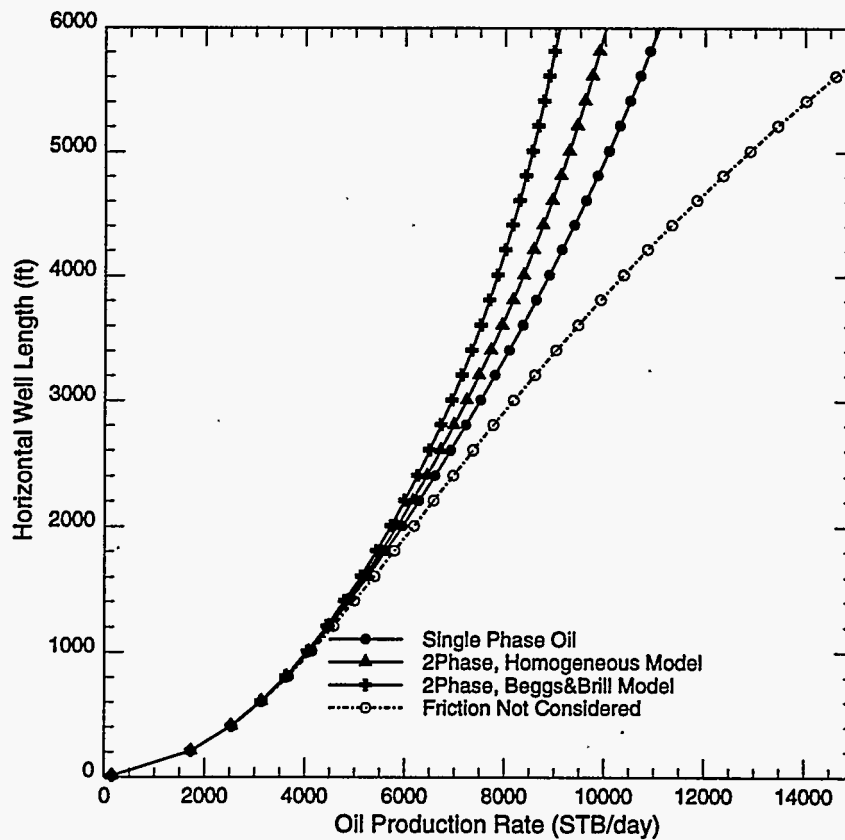


Figure 4.4: Comparison Plot With Different Models For Wellbore Pressure Drop (Fixed Drawdown of 15 psi)

formulation, the following parameters are used:

1. C_F = Fixed cost for drilling & completion of the vertical part of the well in \$
2. C_H = Cost per unit length for drilling & completion of the horizontal part of the well in \$/ft
3. C_M = Operating cost per day of production in \$/day
4. $Q_{w,fric}$ = Actual production rate from the well at steady state, STB/day, defined in Eq.(4.2)
5. $Q_{w,nof}$ = Production rate from the well when friction is zero at steady state, STB/day, defined in Eq. (4.3)
6. t = Total production time in days
7. P_{oil} = Oil price in \$/STB
8. I = Annual interest rate
9. PF = Productivity factor = $\frac{Q_{w,fric}}{Q_{w,nof}} = 1 - P.L.$

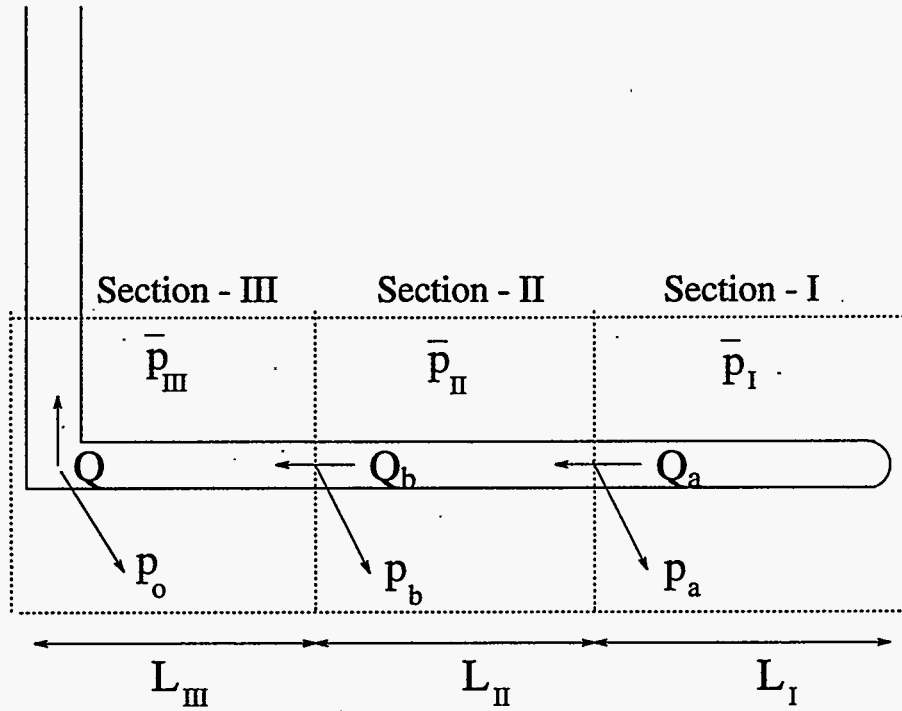


Figure 4.5: Horizontal Well Divided Into Three Sections

Net Revenue $R = \text{Total Income} - \text{Total Expenses}$

$$\text{Total Income} = \sum_{i=1}^t \frac{P_{oil}^i Q_{w,fric}^i}{(1+I)^i} \quad (4.28)$$

$Q_{w,fric}$ is constant because of the steady state assumption. Also assuming that P_{oil} is constant with time, we get

$$\text{Total Income} = P_{oil} Q_{w,fric} F(t, I) \quad (4.29)$$

where

$$F(t, I) = \sum_{i=1}^t \frac{1}{(1+I)^i} \quad (4.30)$$

$$\text{Total Expenses} = C_F + C_H L + C_M t \quad (4.31)$$

The expression for net revenue then becomes,

$$R = P_{oil} Q_{w,fric} F(t, I) - C_F - C_H L - C_M t \quad (4.32)$$

For a given reservoir and well, productivity factor PF is a function of well length L . As the well length increases, PF decreases. (In the special case, when the frictional effects are negligibly small, PF is equal to 1 for all well lengths.)

$$Q_{w,fric} = (PF) Q_{w,nof} = (PF) J_s L \Delta p_o \quad (4.33)$$

Optimum length is obtained by setting the derivative of R w.r.t. L to zero.

$$\frac{dR}{dL} = 0 \quad (4.34)$$

Whether or not an analytical expression can be obtained for the optimum length depends on whether or not we can obtain simple enough analytical expression for PF.

(I) Laminar Flow

An analytical expression can be obtained for PF when there is just laminar flow in the wellbore. From Dikken [3], for the case of laminar flow in the wellbore,

$$Q_{w,fric} = \sqrt{\frac{J_s}{R_w}} \tanh(L\sqrt{J_s R_w}) \Delta p_o \quad (4.35)$$

Therefore,

$$PF = \frac{Q_{w,fric}}{Q_{w,nof}} = \frac{1}{L\sqrt{J_s R_w}} \tanh(L\sqrt{J_s R_w}) = \frac{1}{LB} \tanh(LB) \quad (4.36)$$

where,

$$B = \sqrt{J_s R_w} \quad (4.37)$$

Using Eqs. (4.32) and (4.33),

$$R = P_{oil}(PF)J_s L \Delta p_o F(t, I) - C_F - C_H L - C_M t \quad (4.38)$$

$$\frac{dR}{dL} = P_{oil} J_s \Delta p_o F(t, I) \frac{1}{B} \frac{d}{dL} [\tanh[LB]] - C_H = 0 \quad (4.39)$$

$$P_{oil} J_s \Delta p_o F(t, I) \operatorname{sech}^2(LB) - C_H = 0 \quad (4.40)$$

$$\operatorname{sech}^2(LB) = \frac{C_H}{P_{oil} J_s \Delta p_o F(t, I)} \quad (4.41)$$

Solving the above equation for L gives the optimum length as,

$$L_{opt} = \frac{1}{\sqrt{J_s R_w}} \cosh^{-1} \left(\sqrt{\frac{P_{oil} J_s \Delta p_o F(t, I)}{C_H}} \right) \quad (4.42)$$

(II) Turbulent Flow

When there is turbulent flow in the well, an analytical expression cannot be obtained for the PF. In such a case, the optimum well length has to be determined numerically.

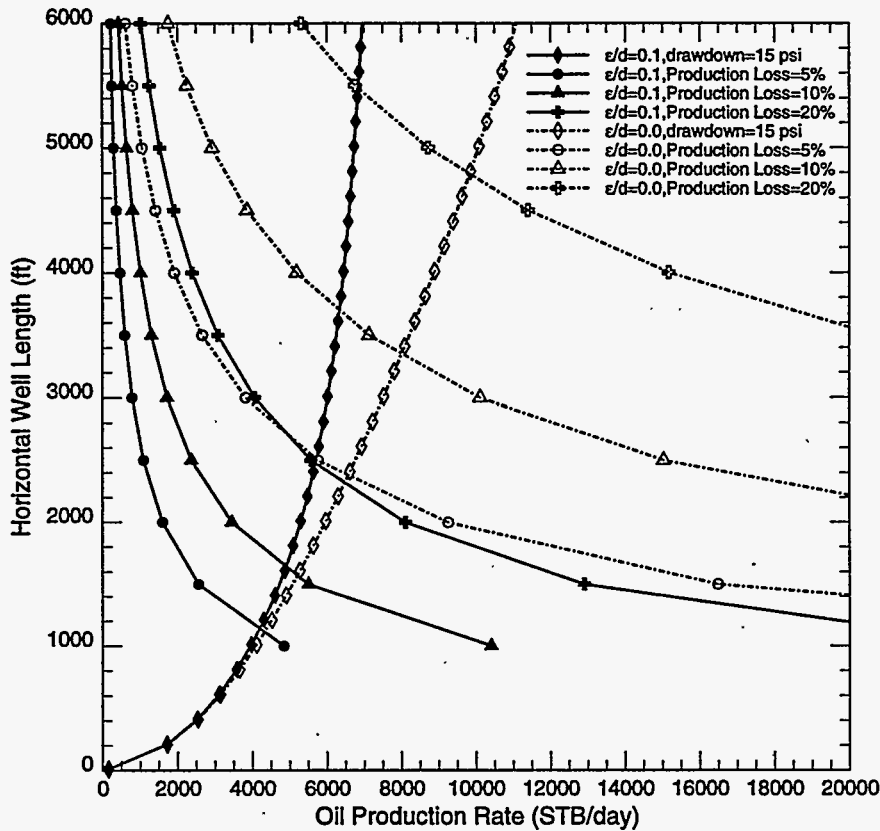


Figure 4.6: Effect of Wellbore Roughness With 15 psi Drawdown

4.5 Production Loss vs. Pressure Drop Ratio

As shown in Eq.(4.4), the production loss increases as the pressure drop ratio increases. Using this relationship, we can perform some interesting sensitivity analyses. For all these cases, the productivity index of the well (PI) is assumed to be constant along the well length.

(A) Effect of Well Length L

As shown in Figure 4.1, for a given drawdown in the reservoir, as the well length increases, pressure drop in the wellbore also increases, due to the increase in the flow rate. Hence, the longer the well, the larger the ratio of pressure drops and the productivity losses from Eq. (4.4) are higher. This result suggests that the required flow rate should be produced with the maximum possible drawdown (or shortest well length), so that the productivity loss will be kept to a minimum. This fact is also apparent in Figure 4.1. The lesser the productivity loss the more uniform is the flow into the horizontal well. Uniform flow into the wellbore becomes desirable when cresting needs to be controlled. But by drilling a shorter horizontal well, we will be nullifying the extra advantage of a horizontal well. So the decision on the well length has to be made by taking these two factors into consideration.

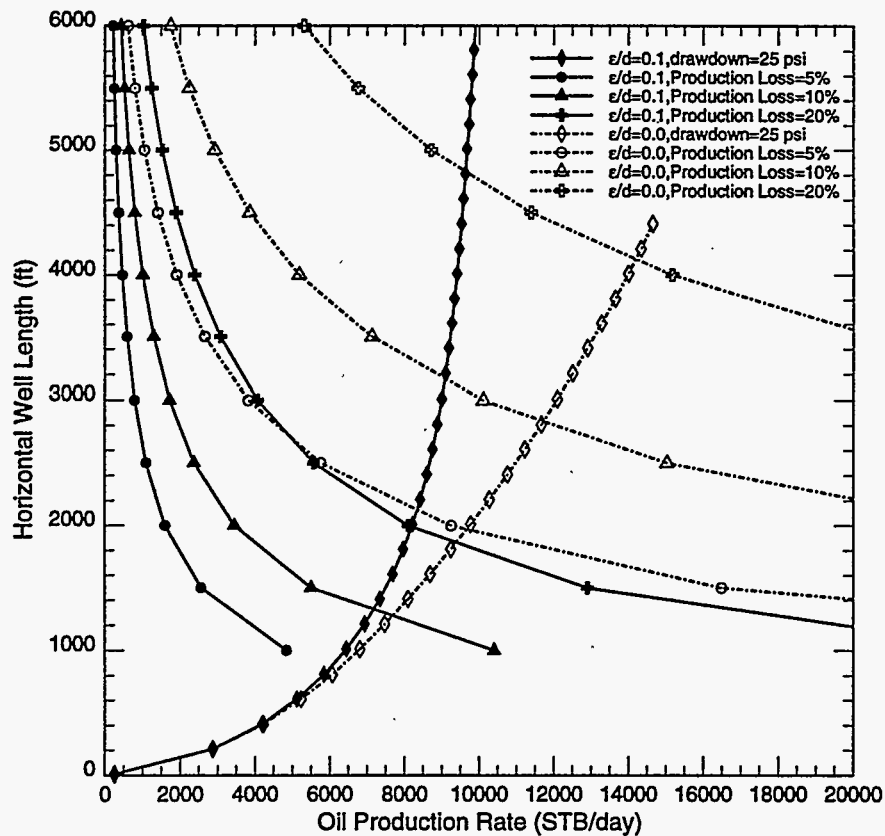


Figure 4.7: Effect of Wellbore Roughness With 25 psi Drawdown

(B) Effect of Flow Rate Q

When the flowrate is increased, the pressure drop in the reservoir increases linearly due to laminar flow. But, the pressure drop in the wellbore can increase at a much higher rate due to turbulence in the wellbore. Hence higher flow rates give larger pressure drop ratios and cause higher productivity losses.

This result can be illustrated by using Figure 4.1 once again. Let us assume that the well length is fixed at 3000 ft. The flow rate from this well can be increased by increasing the drawdown. When the drawdown is 5 psi, the flow rate is around 2600 STB/day and the production loss is below 5%. By increasing the drawdown to 15 psi, the flow rate can be increased to 7500 STB/day. But the production loss has also increased and it now lies between 5% and 10%. The production loss goes above 10% when the drawdown is increased to 25 psi. So when the well length is fixed, decision about the well production rate has to be made by taking these results into consideration.

(C) Effect of Wellbore Roughness ϵ

The effects of wellbore roughness are shown in Figure 4.6 and Figure 4.7. The dashed lines in both of these figures are plotted using the parameters in Table 4.1 for single phase oil flowing both in the reservoir and the wellbore. The bold lines in both of these figures are

drawn for the case when the wellbore relative roughness is increased from 0.0 to 0.1 and keeping everything else the same as in Table 4.1. Figure 4.6 illustrates the effects of wellbore roughness when the drawdown is 15 psi while Figure 4.7 illustrates the same effects when the drawdown is 25 psi.

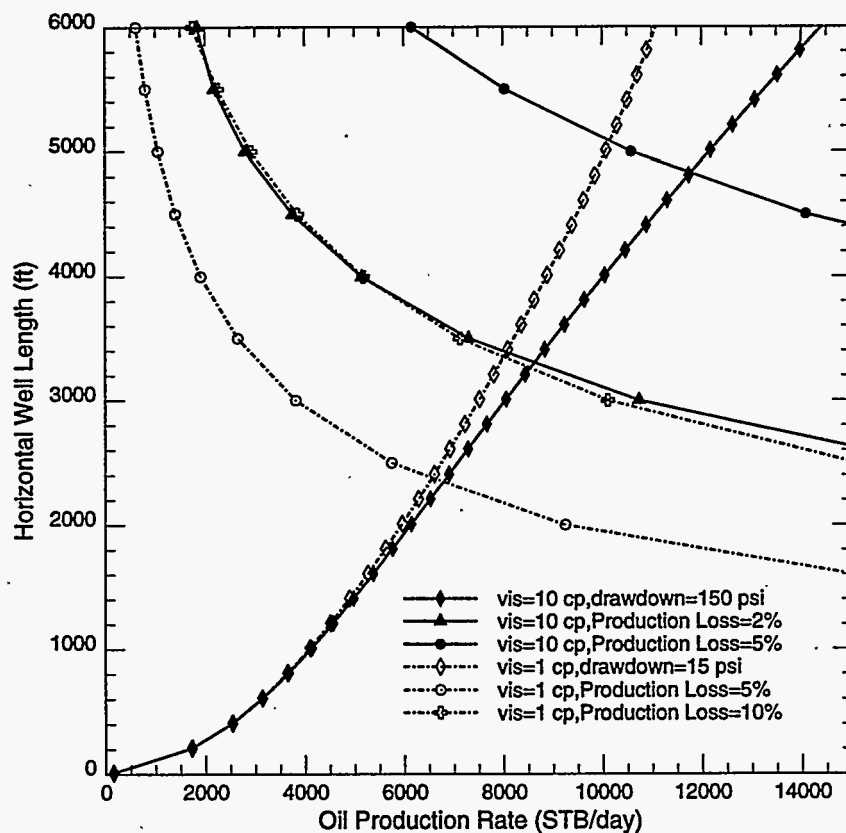


Figure 4.8: Effect of Viscosity

For a well of length 3000 ft, Figure 4.6 shows that increasing the wellbore roughness does two things. It decreases the production rate and increases the production loss. The production loss increase in this case is from approximately 8% to approximately 25%. It can also be observed from these figures that for a fixed production rate, the required well length increases with the increase of wellbore friction. Figure 4.7 shows that some of these effects due to increased wellbore roughness can be reduced by increasing the drawdown. Radial influx into the wellbore can be one of the factors that can increase the effective wellbore roughness.

(D) Effect of Viscosity μ

The flow in the reservoir is always considered to be laminar (except for high rate gas wells), while in the wellbore the flow can be turbulent. Because of this, an increase in

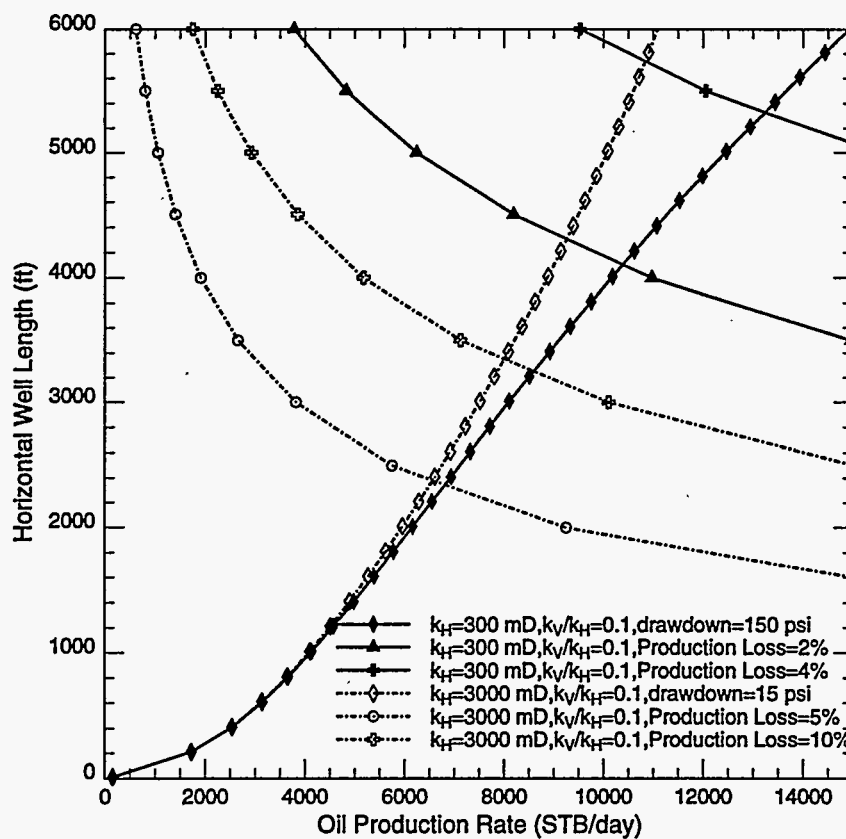


Figure 4.9: Effect of Permeability

viscosity causes the pressure drop in the wellbore to increase less than the increase in the pressure drop in the reservoir. This gives the surprising result that the productivity loss can be lower for higher viscosity oils. These effects are illustrated in Figure 4.8. The dashed lines are drawn using the parameters in Table 4.1 with 15 psi drawdown for single phase oil flow. The bold lines are drawn by increasing the viscosity in Table 4.1 to 10 cp and drawdown to 150 psi. As shown in Figure 4.8, for producing 8000 STB/day, the required horizontal well lengths for the two cases shown are not very different. But the production loss for the case with 10 cp viscosity is less than 2% while that for the case with 1 cp viscosity is much higher at 10%.

(E) Effect of Absolute Permeability k

The effects of reservoir permeability are shown using Figure 4.9. The dashed lines, once again, are drawn using the parameters in Table 4.1 for single phase oil with 15 psi drawdown. The bold lines in the figure are drawn by decreasing the horizontal permeability from 3000 mD to 300 mD and increasing the drawdown to 150 psi. The anisotropic ratio k_V/k_H is kept constant at 0.1 in both of these cases. The Figure clearly indicates that the production losses increase with increasing reservoir permeability.

4.6 Conclusions

Analytical equations are developed that can couple the wellbore to the reservoir both for single phase oil flow and two-phase oil/gas flow.

Based on the calculation of production loss due to friction, an optimum well length can be found for a given reservoir that gives the maximum net revenue.

The production loss due to frictional effects in the horizontal well is proportional to the ratio of the pressure drop in the wellbore to the drawdown at the heel of the well.

An increase in the well length, production rate, wellbore roughness, or reservoir permeability tend to increase the production losses, while an increase in the fluid viscosity tends to decrease these losses.

References

- [1] Stone, T.W. and Kristoff, B.J.: "A Comprehensive Wellbore/Reservoir Simulator," paper SPE 18419 presented at the SPE Symposium on Reservoir Simulation, Houston, Feb. 6-8 (1989)
- [2] Chow, H. and Ransom, V.H.: "A Simple Interphase Drag Model For Numerical Two-Fluid Modeling of Two-Phase Flow Systems", presented at the Second Nuclear Thermohydraulics Meeting of the A.N.S., (1984)
- [3] Dikken, B.J.: "Pressure Drop in Horizontal Wells and its Effects on Production Performance," *JPT*, 1426-1433, (Nov. 1990)
- [4] Islam, M.R. and Chakma, A.: "Comprehensive Physical and Numerical Modeling of a Horizontal Well," paper SPE 20627 presented at 65th Annu. Tech. Conf. SPE, New Orleans, La, (1990)
- [5] Novy, R.A.: "Pressure Drop in Horizontal Wells: When Can They Be Ignored?," paper SPE 24941 presented at the 67th Annu. Tech. Conf. SPE, Washington, DC, (1992).
- [6] Ozkan, E., Sarica, C., and Hacıislamoglu, M.: "Effect of Conductivity on Horizontal Well Pressure Behavior," paper SPE 24683 presented at the 67th Annu. Tech. Conf. SPE, Washington, DC, (1992)
- [7] Landman, M.J.: "Analytical Modeling of Selectively Perforated Horizontal Wells," *Journal of Petroleum Science & Engineering*, 10, 179-188, (1994)
- [8] Folefac, A.N., Archer, J.S., and Issa, R.I.: "Effect of Pressure Drop Along Horizontal Wellbores on Well Performance," paper SPE 23094 presented at the Offshore Europe Conf., Aberdeen, (1991)
- [9] Brekke, K., Johansen, T.E., and Olufsen, R.: "A New Modular Approach to Comprehensive Simulation of Horizontal Wells," paper SPE 26518 presented at the 68th Annu. Tech. Conf. SPE, Houston, TX, (1993)

- [10] Economides, M.J., Hill, A.D., and Economides, C.E.: *Petroleum Production Systems*, PTR Prentice Hall, (1994)
- [11] Beggs, H. D. and Brill, J. P.: "A Study of Two-Phase Flow in Inclined Pipes," *JPT*, 607-617, (May, 1973)

Nomenclature

- B Parameter Used For Simplification of Algebra (defined in Eq.(4.37))
- C_F Fixed Cost for the Drilling & Completion of the Vertical Part of the Well, \$
- C_H Cost per Unit Length for Drilling & Completion of the Horizontal Part of the Well, \$/ft
- C_M Operating Cost per Day of Production, \$/day
- D Diameter of Wellbore, ft
- f Moody Friction Factor
- F A Specified Function
- I Annual Interest Rate
- J_S Productivity Index per Unit Length of the Well, rbbl/day/psi/ft
- k Reservoir Permeability, mD
- L Horizontal Well Length, ft
- p Pressure, psi
- PF Productivity Factor
- $P.L.$ Production Loss
- P_{oil} Oil Price, \$/STB
- q_s Flow in the Reservoir per Unit Length of the Wellbore, rbbl/day/ft
- Q Production Rate, rbbl/day
- q_w Flow Along the Wellbore, rbbl/day
- R Net Revenue, \$
- R_w Resistance in the Wellbore, (day)(psi)/rbbl/ft
- t Total Production Time, day
- U Superficial Oil Flow Rate in Wellbore, ft^3/sec
- x Distance on the Wellbore Coordinate, ft

Greek Letters

- ρ Oil Density, lbm/ft^3
- Δp_o Drawdown at the Heel of the Well, psi

Subscripts

- H Horizontal
- V Vertical
- w Well
- e External Boundary
- s Specific
- $fric$ Frictional Effects Considered
- nof Frictional Effects Not Considered
- opt Optimum

Superscripts

- Reservoir Block

5. Correlations for Cresting Behavior in Horizontal Wells

by Antonio Souza, Sepehr Arbabi, and Khalid Aziz

Abstract

Water and gas cresting behavior in horizontal wells are important phenomena in reservoirs that have an aquifer and/or a gas-cap. In practical situations, many reservoirs are produced under super-critical rates and a breakthrough of the displacing phase becomes inevitable. At the beginning of a reservoir simulation study, it is a common procedure to make an estimate of the breakthrough time and the post-breakthrough behavior, and to make grid sensitivity runs to obtain the best grid block sizes to use. In this work we are developing correlations for breakthrough time, water-oil ratio (gas-oil ratio) and optimum grid as a function of the relevant parameters involved in a study. A thorough literature review is presented, together with the more common correlations and parameters used. A set of dimensionless variables is defined, transforming the flow equations to a system of coordinates where the important parameters can be easily visualized. An extensive number of runs are made to find the more important effects of the variations in grid block size dimensions or parameters. Correlations of breakthrough time with each important parameter are presented along with post-breakthrough behavior.

5.1 Introduction

Petroleum reservoirs often have a gas cap and/or an aquifer. In these situations they are subjected to rapid gas and/or water movement towards the well, created by a sharp pressure gradient in the well direction. The interface between the fluids, that is, gas-oil contact (GOC) or water-oil contact (WOC), deforms from its initial plane shape to a cone or crest as the production begins. When a field is developed by vertical wells, the shape of the deformation is called a cone, but when it is developed by horizontal wells, this deformation is better described as a crest. Moreover, the term cusp is also used in literature to describe the shape of the GOC near horizontal wells.

During the time when a reservoir is infinite acting, a transient cone is formed which approaches the well. If there is a constant potential boundary support, (created by a line of injection wells, for instance) the cone ultimately reaches a steady-state condition, provided that the well rate is not greater than the so-called critical rate, above which the cone becomes unstable and the gas or water phase reaches the well and its production begins.

Several analytical solutions for coning behavior for vertical wells and more recently for horizontal wells have been reported in the literature. Most of those solutions were developed for the steady-state condition reached by the cone with a constant potential boundary condition, specially to calculate the critical rate, for which several different approaches have been used. These solutions are useful when there is some injection pattern in the reservoir, creating a constant potential boundary between production and injection wells.

There are also analytical solutions available for infinite acting reservoirs and for closed-boundary reservoirs, the later being especially useful when there are several production wells in a line, creating a no-flow boundary. In those situations, what becomes more important is not the critical rate, but the breakthrough time of the displacing phase (gas or water) and the post-breakthrough behavior for super-critical rates.

Analytical solutions are useful for several cases shown in the literature, since they can give a good estimate of the solution for the physical system being studied, are easy to apply and, more importantly, they do work for some field situations. For these reasons, despite their limitations, they are still being developed, and used at least during the early stages of a study.

The assumptions used to derive analytical solutions limit their applicability. Analytical solutions are accurate when the assumptions made are valid, but they are not general. These limitations have led to the use of numerical simulators to study coning and cresting behavior. Simulators solve the complete set of equations and along with the correct boundary conditions, they can handle important reservoir complexities and their use has become a standard practice in reservoir engineering.

However, simulators have their own limitations. The numerical diffusion created by the approximations made during the discretization of time and spatial terms leads to the requirement of using a large number of blocks to get accurate results. The number of blocks are limited by computer storage and time consumption which are ultimately limited by hardware and economical constraints.

For these reasons, some important questions that arise when a reservoir simulation study starts are:

- 1 - What is the optimum grid (OG) to start the simulation?
- 2 - What is the expected breakthrough time (BT) of the displacing phase?
- 3 - What is the maximum production rate for a given BT?
- 4 - What will be the post-breakthrough behavior of water-oil ratio (WOR) or gas-oil ratio(GOR)?
- 4 - How can the performance of a coarse grid model be improved?

These and other questions can only be answered after extensive grid sensitivity studies and with the help of analytical correlations for BT and WOR.

Based on a thorough literature survey, we can make the following conclusions:

1 - Correlations for BT and WOR(GOR) derived from analytical solutions use a large number of assumptions (resulting in a small number of parameters) which limit their general use.

2 - Correlations derived for BT and WOR based on results from numerical models use a larger number of parameters but normally use specific sets of PVT and rock-fluid data, which still limit their applicability.

3 - Grid sensitivity studies are normally made for specific situations and can't be generalized.

In this work, we are developing correlations for breakthrough time, water-oil ratio and optimum grids for the study of cresting behavior in horizontal wells. We first present the mathematical model used for coning problems, with the common assumptions and boundary conditions in Section 5.2. In Section 5.3 we present a literature review, with the most important solutions found in literature. In Section 5.4 we give the development of equations

and assumptions made in this work. Finally, in Section 5.5 we show the development of the new correlations.

5.2 Mathematical Model

In this section we describe the general mathematical framework used for studying coning behavior. The common assumptions and boundary conditions (BC), dimensionless variables (DV) and parameters used to derive the correlations are discussed.

Refer to the Nomenclature for the definition of the terms used in this section and throughout this report.

5.2.1 General Equations

The general problem of coning is that of multiphase flow in a porous medium and therefore it obeys the classical laws of mechanics and thermodynamics. The reservoir is assumed to be isothermal, local thermodynamics equilibrium applies and Darcy's law substitutes the classical Navier-Stokes momentum equation for Newtonian fluids. Applying material balance for an elementary control volume, we can get the traditional continuity equation for each component c flowing in n_l phases [1, 2] :

$$-\sum_{l=1}^{n_l} \nabla \cdot (\rho_l \zeta_{c,l} \vec{u}_l) - \rho_l \zeta_{c,l} \tilde{q}_c = \sum_{l=1}^{n_l} \frac{\partial}{\partial t} (\phi \rho_l \zeta_{c,l} S_l) \quad (5.1)$$

For immiscible flow it is reduced to:

$$-\nabla \cdot (\rho_l \vec{u}_l) - \rho_l \tilde{q}_l = \frac{\partial}{\partial t} (\phi \rho_l S_l) \quad (5.2)$$

Darcy's law is given by:

$$\vec{u}_l = -\frac{k k_{rl}}{\mu} \nabla \Phi_l \quad (5.3)$$

where:

$$\Phi = p - \gamma z \quad (5.4)$$

Substituting into 5.2

$$\nabla \cdot \left[\rho_l \frac{k k_{rl}}{\mu_l} \nabla \Phi_l \right] - \rho_l \tilde{q}_l = \frac{\partial}{\partial t} (\phi \rho_l S_l) \quad (5.5)$$

Alternatively, this equation can be written using the definition of formation volume factor (FVF) as following: :

$$B_l = \frac{V_{lres}}{V_{lstd}} = \frac{\rho_{lstd}}{\rho_{lres}} \quad (5.6)$$

Which gives:

$$\nabla \cdot \left[\frac{kk_{rl}}{\mu_l B_l} \nabla \Phi_l \right] - \tilde{q}_l = \frac{\partial}{\partial t} \left(\frac{\phi S_l}{B_l} \right) \quad (5.7)$$

which can also be written using the potential definition 5.4 as:

$$\nabla \cdot \left[\frac{kk_{rl}}{\mu_l B_l} (\nabla p_l - \gamma_l \nabla z) \right] - \tilde{q}_l = \frac{\partial}{\partial t} \left(\frac{\phi S_l}{B_l} \right) \quad (5.8)$$

This is the general equation for three-dimensional multiphase flow of immiscible phases in porous media. Together with the capillary pressure and relative permeability relations, saturation constraints and appropriate boundary conditions, they give the basic equations for many reservoir engineering problems. Since it is a nonlinear partial differential equation, an analytical solution is only possible under some limiting assumptions, which leaves the numerical simulation as the only tool to solve it without any further simplifications.

5.2.2 Assumptions

The assumptions commonly used to develop solutions for coning studies are the following:

- 1 - Homogeneous medium (constant permeability in each direction).
- 2 - Non-deformable formation ($c_r = 0$) and constant porosity.
- 3 - Isotropic medium (same permeability for all directions).
- 4 - Constant viscosity for each phase.
- 5 - Absence of capillary pressures.
- 6 - Incompressible flow.
- 7 - Two-dimensional flow : For vertical wells, it implies radial flow and the problem is solved in r-z coordinates. For horizontal wells, it implies a cross-sectional model, with the well penetrating the entire formation. In this situation, the pressure drop in the well is also neglected.
- 8 - One-dimensional flow (in each streamtube).
- 9 - Vertical equilibrium or hydrostatic pressure distribution.
- 10 - Undersaturated reservoir ($p > p_b$).
- 11 - Constant production rate.
- 12 - Dead oil ($R_s = 0$).
- 13 - Piston-like displacement.
- 14 - Segregated phase flow.
- 15 - Complete displacement $S_{or} = 0$.
- 16 - Well at the top or bottom of the formation.
- 17 - Steady-state flow.
- 18 - Two-phase flow.
- 19 - Unity mobility ratio ($M = 1$).
- 20 - Symmetry for the well position : Assume that the lateral boundary size is the same for both sides of the well.
- 21 - Specific set of rock-fluid and PVT data.

The previous works found in the literature use several of the assumptions stated above, which in most cases reduces the basic flow equations to simple forms such as Laplace, Poisson or Boussinesq equations and hence making it possible to find an analytical solution.

5.2.3 Boundary Conditions

The boundary conditions(BC) normally used are the following:

A - On the lateral edges:

a - Dirichlet or BC of the first kind: Gives a steady-state solution. It can occur in a reservoir with a line drive, creating a constant potential boundary between the injection and production wells.

b - Neumann or BC of the second kind: Important for the case where the reservoir is closed or is developed with production wells in a pattern, creating no-flow boundaries between wells.

c - Infinite acting reservoir: In this case there is always transient behavior. In many cases this occurs only for a short period of time. This behavior becomes more important when there is only one well in a reservoir.

B - On the top and/or bottom of the reservoir: The top and bottom boundaries of the reservoir are normally considered impermeable (no-flow boundary).

C - At the WOC or GOC:

a - Constant potential: This ignores the viscous forces in the gas cap/aquifer.

b - Inactive aquifer/gas-cap with a constant interface elevation: In this approach, the shape of the cone is not taken into account. Static equilibrium at the interface is assumed.

c - Inactive aquifer or gas cap free interface.

d - Active aquifer or gas cap with free interface.

e - Active aquifer or gas cap with constant pressure interface.

D - At the well : The well can be included in the equations as a source/sink term or as a boundary condition. In both cases, all solutions assume constant production rate in the well.

5.2.4 Dimensionless Variables

There are several sets of dimensionless variables for coning studies reported in the literature. The most common are:

1 - Lateral dimension:

a - Isotropic case:

$$x_D = \frac{x}{h_o} \quad (5.9)$$

b - Anisotropic case:

$$x_D = \frac{x}{h_o} \sqrt{\left(\frac{k_v}{k_h}\right)} \quad (5.10)$$

2 - Longitudinal dimension:

$$y_D = \frac{y}{L} \quad (5.11)$$

3 - Vertical dimension:

$$z_D = \frac{z}{h_o} \quad (5.12)$$

4 - Radial dimension:

$$r_D = \frac{r}{h_o} \sqrt{\left(\frac{k_v}{k_h}\right)} \quad (5.13)$$

5 - Time:

a - Isotropic case:

$$t_D = \frac{\Delta \rho g k_o t}{\phi_{ef} \mu_o h_o} \quad (5.14)$$

Where ϕ_{ef} is the effective porosity given by:

$$\phi_{ef} = \phi(1 - S_{wc} - S_{or}) \quad (5.15)$$

b - Anisotropic case based on porosity:

$$t_D = \frac{\Delta \rho g k_v t}{\phi \mu_o h_o} \quad (5.16)$$

c - Anisotropic case based on effective porosity:

$$t_D = \frac{\Delta \rho g k_v t}{\phi_{ef} \mu_o h_o} \quad (5.17)$$

d - Anisotropic case based on dynamic pressure:

$$t_D = \frac{\Delta p k_v t}{\phi_{ef} \mu_o h_o^2} \quad (5.18)$$

6 - Rate:

a - Isotropic case:

$$q_D = \frac{\mu_o q_o}{\Delta \rho g k_o L h_o} \quad (5.19)$$

b - Anisotropic case based on linear flow:

$$q_D = \frac{\mu_o q_o B_o}{\Delta \rho g \sqrt{k_v k_h} L h_o} \quad (5.20)$$

c - Anisotropic case based on radial flow and formation height:

$$q_D = \frac{\mu_o q_o B_o}{2\pi \Delta \rho g k_r h_o^2} \quad (5.21)$$

d - Anisotropic case based on radial flow and well dimension:

$$q_D = \frac{\mu_o q_o B_o}{2\pi \Delta \rho g \sqrt{k_v k_h} L h_o} \quad (5.22)$$

e - Anisotropic case based on linear flow and mobility:

$$q_D = \frac{q_o}{\Delta \gamma \lambda_o \sqrt{k_v k_h} L h_o} \quad (5.23)$$

With:

$$\lambda_o = \frac{k_{r ocw}}{\mu_o} \quad (5.24)$$

f - Anisotropic case based on well drainage area:

$$q_D = \frac{\mu_o q_o B_o}{\Delta \gamma \sqrt{k_v k_h} A} \quad (5.25)$$

7 - Potential:

a - Based on hydrostatic pressure:

$$\Phi_D = \frac{\Phi}{\Delta \rho g h_o} \quad (5.26)$$

b - Based on dynamic pressure:

$$\Phi_D = \frac{p + \Delta \rho g h_o}{\Delta p} \quad (5.27)$$

5.2.5 Parameters

The parameters normally used in the literature to derive correlations are the following:

- 1 - Dimensionless rate (q_D) : Given by one of the expressions in the last section.
- 1 - Well drainage radius : Given by expression 5.10, with $x = x_e$, so that $x_D = x_{eD}$.
- 2 - Well drainage radius: Given by expression 5.13, $r = r_e$ so that $r_D = r_{eD}$.
- 3 - Horizontal well dimension:
 - a - Isotropic case:

$$L_D = \frac{L}{h} \quad (5.28)$$

b - Anisotropic case:

$$L_D = \frac{L}{h} \sqrt{\left(\frac{k_v}{k_h}\right)} \quad (5.29)$$

4 - Well height:

$$h_{wD} = \frac{h_w}{h_o} \quad (5.30)$$

5 - Mobility :

$$M = \frac{k_{rwo}\mu_o}{k_{rocw}\mu_w} \quad (5.31)$$

6 - Anisotropy: Normally included in x_D and q_D , it is also used as a separate parameter defined as:

$$k_D = \frac{k_h}{k_v} \quad (5.32)$$

5.3 Literature Review

In this section we review the related important solutions found in the literature.

Except where pointed out, all the equations used throughout this work are in a consistent system of units, normally SI (International System). Refer to the Appendix to get the conversion factors for other systems of units used in the literature.

The works on coning and cresting problems can be divided in two main groups: Steady-state solutions and transient solutions. The first group looks for solutions for the critical rate and the latter for correlations for BT and WOR(GOR).

5.3.1 Steady-State Solutions

Steady-state solutions normally seek the critical oil rate, which is defined as the maximum production rate without any gas or water production. This is only possible when the potential at the lateral boundary is constant, creating a steady-state flow condition.

Here we will mention just the more important solutions. A more extended study of those solutions can be found in Arbabi and Fayers [3]. Refer to Table 5.1 at the end of the section for the assumptions and BC used by various authors.

A fundamental equation for steady-state solutions is Darcy's law derived for the flow along the streamtubes that are created in the direction of the well. The total rate can be written as:

$$Q = -kwh \frac{d\Phi}{ds} = -kwh \frac{dh}{ds} \quad (5.33)$$

The first attempt to analytically solve a gravity-drainage problem was done by Dupuit [4] when studying an unconfined ground water flow problem. He derived a discharge equation for water through a dam, assuming the flow along the streamlines as essentially horizontal, that is, assuming vertical equilibrium. For this situation, we can write $dx = ds$ in Equation 5.33. His solution can be extended for the gas/water-cone case, giving the familiar expression for the critical rate as :

$$Q_c = \frac{k_o \pi (\rho_o - \rho_g) g (h_e^2 - h_p^2)}{\mu_o \ln(\frac{r_e}{r_w})} \quad (5.34)$$

Forchheimer [5] used Dupuit's assumption to derive a continuity equation for the water potential, giving :

$$\frac{\partial}{\partial x}(kh \frac{\partial h}{\partial x}) = 0 \quad (5.35)$$

Muskat [6] studied the applicability of partially penetrated vertical wells theory for single-phase flow to water coning problems for vertical wells. He derived an iterative process to calculate the critical rate neglecting the shape of the cone. He also studied the presence of a shale lens to suppress the cone.

Meyer and Garder [7] extended the Dupuit-Forchheimer solution for the three-phase case, when both water and gas cones are present. They also gave an expression for the critical rate when a shale lens was present between the well and the fluids contact.

Efros [8] and Giger [9] solved Equation 5.33 without Dupuit's assumption, using a hodograph method.

In another article [10], Giger presented a solution for the no-flow B.C. in the lateral edge with an active aquifer. In this situation the critical rate is defined as the rate below which there is no water production for a particular time [11].

Chaperon [12] extended Muskat's approach for horizontal wells for either isotropic or anisotropic permeabilities. She compared the critical rates between horizontal and vertical wells, concluding that horizontal wells generally have higher critical rates than vertical wells, but this advantage is reduced with an increase in anisotropy. She also extended her solution to the pseudo-steady-state behavior, with no-flow on lateral edge boundaries, using a different drainage radius for horizontal and vertical wells.

Joshi [13] used the Dupuit-Forchheimer solution for vertical wells to derive an expression for the critical rate for horizontal wells using an effective wellbore radius concept. He concluded that for any situation, $Q_{ch} > Q_{cv}$.

Wheatley [14] used a theory based on a combination of line and point sources to develop a new approach to calculate critical rates and the water-oil cone profile for vertical wells. He used Muskat's approach, but did not neglect the effect of the cone itself in his calculations.

Guo and Lee [15] developed a solution for critical rates for horizontal wells based on the hodograph method, using conformal mapping.

Fayers et al. [16] summarized the main methods to calculate critical rates for horizontal wells during steady-state behavior. They found factors of 4 to 24 between the solutions for the same problems by different methods.

Arbabi and Fayers [3] used concepts from Wheatley's theory and developed a new semi-analytic solution for horizontal wells at any depth. They also compared their solution and others' with simulation results, concluding that, besides theirs, Efros [8] and Giger [9] solutions were the most reliable, but the latter two are only applicable for well at the top or boundary of the formation.

A summary of the assumptions and boundary conditions used by each author to derive their solutions throughout this section is shown in Table 5.1 The number or letter associated with each assumption or BC are given in sections 5.2.2 and 5.2.3 Assumptions 1-2,4-6,10-14,17,19-20 and boundary conditions B and D are not given in the Table, since they were used in all derivations. Assumption 18 is used by all authors except Meyer and

Reference	Assumptions and Boundary conditions						
	3	7	8	9	16	A	C
[3]		x				a	c
[4]	x		x	x	x	a	a
[5]	x		x	x	x	a	a
[6]	x		x		x	a	b
[7]	x		x	x	x	a	a
[8]	x		x		x	a	c
[9]	x		x		x	a	c
[10]	x		x		x	a	e
[12]		x			x	a	b
[13]	x		x	x		a	a
[14]		x				a	c
[15]		x				a	c

Table 5.1: Assumptions and BC used to get steady-state solutions. Refer to sections 5.2.2 and 5.2.3

Garder [7] who also gave an expression for 3-phase flow. Assumptions 15 and 21 were not used by any author in this section. Whenever any assumption was not clearly evident from the publication, it was not included in the Table.

5.3.2 Transient Solutions

Transient solutions normally look for correlations for BT and post-BT behavior. Here we only summarize the most important solutions found in the literature. Refer to Tables 5.2, 5.3 and 5.4 for the assumptions, BC, DV and parameters used by each author whose work is reviewed here.

A fundamental equation for transient solutions is the Boussinesq [17] equation, which is the extension of Forchheimer equation for transient flow. It is given by:

$$\frac{\partial}{\partial x} \left(kh \frac{\partial h}{\partial x} \right) = \frac{\phi \mu \partial h}{k \partial t} \quad (5.36)$$

Which is also known as Dupuit-Forchheimer Equation.

Chappelear and Hirasaki [18] developed an expression for the water-cut assuming vertical equilibrium and a sequence of steady-state conditions for cone development in vertical wells. They installed their expression in a two-dimensional areal simulator, using it to calculate the post-breakthrough water-cut. The oil thickness was calculated from the grid block saturation of the previous time-step.

Addington [19] developed correlations using a radial grid for gas coning in the Prudhoe Bay field. He developed correlations to calculate the average oil column height above the perforations at BT and gas-liquid rate (GLR) after BT.

For the average oil height above the perforations he gives, in field units:

$$\bar{h}_{obt} - h_t = 137.9 \frac{[q(\frac{K_v}{K_h})^{0.1} \mu_o F_1 F_2]^{0.429}}{[k_h \sqrt{h_p}]^{0.429}} \quad (5.37)$$

where the factor F_1 is related to the thickness ratio and F_2 to the well spacing.
For GLR:

$$\log(GLR) = m(\bar{h}_o - \bar{h}_{obt}) + \log(Rs) \quad (5.38)$$

where m is taken from a graphical correlation.

He implemented these correlations in a coarse grid model. He also simulated a heterogeneous case, varying the number and the height of small shales between the well and the gas-oil interface.

Nolen [20] discusses some problems associated with the implementation of Addington's approach in his simulator, giving some hints on how to install the GLR correlation after breakthrough.

Konieczek [21] solved Bousinesq's Equation for horizontal wells using both numerical and semi-analytical procedures. His results were presented in a set of dimensionless decline type-curves for various well spacings and well elevations. He found a simple correlation for BT as:

$$t_{btD} = \frac{C}{q_D^2} \quad (5.39)$$

Where the constant C can be approximated by the following regression polynomial:

$$C = a_1(1 - h_{wD}) + a_2(1 - h_{wD})^2 + a_3(1 - h_{wD})^3 \quad (5.40)$$

With h_{wD} given by 5.30 and $a_1 = -0.0183$, $a_2 = 2.6377$ and $a_3 = -1.7363$.

Papatzacos et al. [22] developed correlations for BT for horizontal wells for both single-cone and two-cone cases in an infinite acting reservoir. They solved numerically Equation 5.8 for oil phase using movable boundary conditions for the fluids interfaces. For the single-cone case, assuming gravity equilibrium in the cone, they found the following correlation for BT:

$$t_{btD} = -1.7179 - 1.1633(\ln q_D) + 0.16308(\ln q_D)^2 - 0.046508(\ln q_D)^3 \quad (5.41)$$

For $q_D > 0.4$, it can be reduced to:

$$t_{btD} = 1 - (3q_D - 1) \ln \left[\frac{3q_D}{3q_D - 1} \right] \quad (5.42)$$

Another solution assuming constant pressure on the moving boundary is given as:

$$t_{btD} = \frac{1}{6q_D} \quad (5.43)$$

For the two-cone case, they defined a parameter β for the location of the well (h_{wD} , as defined by Equation 5.30) and developed correlations for BT and for the optimum well

placement β_{opt} , defined as the position where both water and gas cones have the same BT. Their correlation is expressed as a polynomial of the form:

$$Y = c_0 + c_1X + c_2X^2 + c_3X^3 \quad (5.44)$$

Where Y is either β_{opt} or $\ln(t_{btD})$, X is $\ln(q_D)$ and the constants c_j are tabulated as function of the density difference ratio, given by:

$$\psi = \frac{\rho_w - \rho_o}{\rho_o - \rho_g} \quad (5.45)$$

They compared their correlations with numerical simulations. In order to obtain more accurate simulations, they performed a grid block sensitivity study. For most of the cases simulated, they needed to use very refined grids, specially between the well and GOC, to get reliable solutions.

Ozkan and Raghavan [23] developed a similar approach to that used by Papatzacos et al, using constant pressure in the active aquifer. They reduced Equation 5.8 to Laplace's Equation and solved it using Green's function. The solution was then integrated to find a BT correlation for both vertical and horizontal wells, the latter is given by:

$$t_{btD} = \frac{L_D}{2.47q_D} \quad (5.46)$$

Tiefenthal [24] extended Konieczek's work for the anisotropic case, but still assuming vertical equilibrium. He gave correlations for single-cone and two-cone cases for either critical and super-critical conditions. Beginning from Equation 5.8, he derived Bousinesq's Equation and found the following expression for the dimensionless oil rate after breakthrough:

$$q_{oD} = \sqrt{\frac{C}{2t_D - t_{btD}}} \quad (5.47)$$

He applied his results to the simulation of a real field.

Yang and Wattenbarger [25] derived correlations for water coning from refined grid models for both vertical and horizontal wells. They used the same definitions as Addington [19] and found correlations for BT, WOR and critical rate for a particular time. For HW, their expressions are given by:

$$\left(\frac{h - h_{ap}}{h_{wb}}\right)^2 = 1 + 4.7921 \times 10^{-4} x_e^{0.32} \left[\frac{1}{x_{eD}}\right]^{0.65} \frac{1}{q_D} \frac{1}{1 + M^{0.4}} \quad (5.48)$$

and:

$$\log(WOR + 0.25) = m(h_{bp} - h_{wb}) + \log(0.25) \quad (5.49)$$

With m given by:

$$m = 0.004 \left[1 + 2.7496 \frac{x_e^{0.18}}{h_o} \left(\frac{1}{x_{eD}}\right)^{0.4} \left(\frac{1}{q_D}\right)^{0.5} (1 + M^{0.25})(1 - h_{wD})^{0.3} \right] \quad (5.50)$$

Mohammed and Hatzignatiou [26] derived correlation from refined grid models for gas and water coning for VW and HW. They followed the conclusions of Papatzacos et al [22]

Reference	Assumptions and Boundary conditions												
	4	6	8/9	10	12	13	14	17	18	19	21	A	C
[3]		x		x	x			x		x		a	c
[12]		x		x	x	x	x				x	b	d
[19]				x	x						x	b	d
[21]	x	x	x	x		x	x			x		c	d
[22]	x	x		x	x	x	x			x		c	d
[23]	x	x		x	x	x	x			x		c	e
[24]	x	x	x	x	x	x	x		x			b	d
[25]									x		x	b	d
[26]									x		x	b	d

Table 5.2: Assumptions and BC used to get transient solutions. Refer to sections 5.2.2 and 5.2.3

to build their grid block dimensions and studied the effect of the numerical diffusion using a Buckley-Leverett model. They attributed a difference of 6% in BT to numerical diffusion. For HW, their expression for BT for water coning is given by:

$$t_{bt} = \frac{172.8Ah\phi(1 - S_{wc} - S_{or}) h_D^{1.2} L_D^{0.455} K_D^{0.4}}{qB_o q_D^{0.04} M^{0.5}} \quad (5.51)$$

and for gas coning by:

$$t_{bt} = \frac{227.4Ah\phi(1 - S_{wc} - S_{or}) h_D^{0.973} L_D^{0.452} K_D^{0.337} m^{0.1124}}{qB_o q_D^{0.715} M^{0.1124}} \quad (5.52)$$

with m defined as the gas-liquid ratio slope.

Arbabi and Fayers [3] used numerical simulations to derive a correlation for BT for the constant potential lateral boundary case. They found that the arithmetic mean between expressions 5.42 and 5.43 gave good results.

A summary of the assumptions and boundary conditions used by various authors to derive their solutions throughout this section are shown in Table 5.2. The number or letter associated with each assumption or BC are given in sections 5.2.2 and 5.2.3. Assumptions 1,2,5,11,20 and boundary conditions B and D are not given in the Table, since they were used in all derivations. Assumption 3 was used only by Konieczek [21]. Assumption 7 was not used only by Mohammed and Hatzignatiou [26] who also included the well length in their correlations. Assumption 15 was used only by Papatzacos et al [22]. Assumption 16 was used only by Ozkan and Raghavan [23]. Again, as in section 5.3.1, any assumption not clearly expressed by the author or evident in his publication has not included in the Table.

A summary of the DV and parameters used by each author in this section are given in Tables 5.3 and 5.4. Refer to sections 5.2.4 and 5.2.5 and Nomenclature for the definitions.

Reference	Dimensionless variables				
	x_D	z_D	r_D	t_D	q_D
[3]	1b	2a		5b	6d
[12]					
[19]					
[21]	1a	2a		5a	6a
[22]	1b	2a		5b	6d
[23]		2a	4a	5c	6c
[24]	1b	2a		5d	6b
[25]	1b	2a			6e
[26]		2a			6f

Table 5.3: Dimensionless variables used to get transient solutions. Refer to section 5.2.4

Reference	Parameters				
	q_D	x_{eD}	L_D	h_{wD}	M
[3]	x			x	
[12]				x	x
[19]		x		x	x
[21]	x			x	
[22]	x				
[23]	x		x		
[24]	x	x		x	x
[25]	x	x		x	x
[26]	x	x	x	x	x

Table 5.4: Parameters used to develop BT and WOR correlations. Refer to section 5.2.5

5.4 Development of Equations

In this section we provide a general mathematical development for this study, giving the assumptions and boundary conditions used in this work. Starting with Equation 5.8, let us use assumptions 1,2,4,5,7,10, 11,18 and 20 from section 5.2.2. In this situation, the basic flow equations for oil and water components can be written as:

Oil:

$$\frac{\partial}{\partial x} \left[\frac{k_h k_{ro}}{B_o} \frac{\partial \Phi_o}{\partial x} \right] + \frac{\partial}{\partial z} \left[\frac{k_v k_{ro}}{B_o} \frac{\partial \Phi_o}{\partial z} \right] - \frac{\tilde{q}_o}{B_o} = \mu_o \phi \frac{\partial}{\partial t} \left(\frac{S_o}{B_o} \right) \quad (5.53)$$

Water:

$$\frac{\partial}{\partial x} \left[\frac{k_h k_{rw}}{B_w} \frac{\partial \Phi_w}{\partial x} \right] + \frac{\partial}{\partial z} \left[\frac{k_v k_{rw}}{B_w} \frac{\partial \Phi_w}{\partial z} \right] - \frac{\tilde{q}_w}{B_w} = \mu_w \phi \frac{\partial}{\partial t} \left(\frac{S_w}{B_w} \right) \quad (5.54)$$

Let us use a set of dimensionless variables defined by Equations 5.10, 5.11, 5.12, 5.26 and:

$$t_D = \frac{\Delta \rho g \lambda_o k_v t}{\phi_{ef} h_o} \quad (5.55)$$

where $\Delta \rho$ is the initial density difference at WOC.

$$q_D = \frac{q_o B_o}{2\pi \Delta \rho g \lambda_o \sqrt{k_v k_h} L h_o} \quad (5.56)$$

$$N_{pD} = \frac{N_p \sqrt{\frac{k_v}{k_h}}}{2\pi \phi_{ef} L h_o^2} \quad (5.57)$$

$$p_D = \frac{p - p_{STD}}{\Delta \rho g h_o} \quad (5.58)$$

$$c_{lD} = c_l \Delta \rho g h_o, l = o, w \quad (5.59)$$

Let us also assume FVF as straight line functions of pressure, with a value of unity at standard conditions, so that:

$$B_l = 1 - c_{lD} p_D, l = o, w \quad (5.60)$$

Normalized saturations are:

$$S_w^* = \frac{S_w - S_{wc}}{1 - S_{wc} - S_{or}} \quad (5.61)$$

$$S_o^* = \frac{S_o - S_{or}}{1 - S_{wc} - S_{or}} \quad (5.62)$$

so that:

$$S_o^* + S_w^* = 1 \quad (5.63)$$

Relative permeabilities can be written as:

$$k_{rw} = k_{rwo}k_{rw}^* \quad (5.64)$$

$$k_{ro} = k_{rocw}k_{ro}^* \quad (5.65)$$

with normalized relative permeabilities given by exponential functions of saturations as:

$$k_{rw}^* = (S_w^*)^{n_w} \quad (5.66)$$

$$k_{ro}^* = (S_o^*)^{n_o} \quad (5.67)$$

Using this set of DV in Equations 5.53 and 5.54 together with parameter M defined by 5.31 we get:

Oil:

$$\frac{\partial}{\partial x_D} \left[\frac{k_{ro}^*}{B_o} \frac{\partial \Phi_{oD}}{\partial x_D} \right] + \frac{\partial}{\partial z_D} \left[\frac{k_{ro}^*}{B_o} \frac{\partial \Phi_{oD}}{\partial z_D} \right] - 2\pi q_{oD} = \frac{\partial}{\partial t_D} \left(\frac{S_o^*}{B_o} \right) \quad (5.68)$$

Water:

$$\frac{\partial}{\partial x_D} \left[\frac{k_{rw}^*}{B_w} \frac{\partial \Phi_{wD}}{\partial x_D} \right] + \frac{\partial}{\partial z_D} \left[\frac{k_{rw}^*}{B_w} \frac{\partial \Phi_{wD}}{\partial z_D} \right] - 2\pi q_{wD} = \frac{1}{M} \frac{\partial}{\partial t_D} \left(\frac{S_w^*}{B_w} \right) \quad (5.69)$$

where:

$$q_{lD} = \frac{q_D k_{rl}^*}{k_{ro}^* + M k_{rw}^*}, l = o, w \quad (5.70)$$

With these equations, we can derive correlations for breakthrough time, water-oil ratio and optimum grid as a function of q_D , M , x_{eD} , h_{wD} , c_{oD} and the exponents of relative permeabilities n_o and n_w . Water is considered incompressible for these derivations.

We will also consider the effect of Rs (constant for undersaturated oil) in the simulations. The boundary conditions will be no-flow on the lateral edge and on the top of the reservoir. A large aquifer to give pressure support will be placed at the bottom of the reservoir.

5.5 Water Cresting Correlations

In this section we describe the procedure to get correlations for breakthrough time, water-oil ratio and optimum grid for the water cresting problem. Equations 5.68 and 5.69 can be solved using a commercial simulator with the appropriate input data. A basic data set for the ECLIPSE simulator was developed using some of the common assumptions shown in Table 5.5.

With those data we initially varied the vertical and horizontal grid block sizes, the lateral boundary size, the aquifer size, the well block dimensions, oil compressibility and Rs. Variations in density difference and permeabilities were not considered here, since they are already implicit in the DV. After several runs, we could make the following initial conclusions:

1 - The vertical block size dimension affects numerical diffusion more than the horizontal one.

The optimum grid is defined here as the dimension of the grid blocks that gives the minimum number of blocks for the simulation with a small variation in BT, N_{pD} and WOR behavior when compared with a refined grid block.

2 - A vertical dimension of $\Delta z_D = 0.01$ is a refined grid block size for most of the situations run. A refined grid block is defined here as the dimension of the grid blocks that gives no noticeable variation in BT or WOR behavior when its performance is compared with smaller grid block sizes. Any grid block sizes larger than those are considered here as coarse grid blocks.

3 - A good horizontal block size distribution is obtained by starting with the vertical block size dimension, then doubling it 8 to 16 times, then using this dimension for the next 10 blocks and, after that, continue doubling. This gives better results than the approaches normally used, that is, the use of a number of blocks of the same dimension close to the well and then start doubling (or just double from the well block) [22].

4 - The well block dimensions do not affect either BT or WOR behavior if a square block with dimensions equal to those used between the well and WOC is also used for the well block. What is more important for this situation is to maintain the same well position.

5 - There was no variation in BT or WOR for different values of R_s , once the same initial densities at WOC were maintained.

6 - The reservoir behaves as infinite for $x_{eD} > 20$, since there was no noticeable variation in either BT or WOR for these situations. In fact, there was no noticeable variation in BT for $x_{eD} > 10$.

7 - An aquifer size of 200 times the reservoir size must be used to maintain the reservoir pressure without any injection. Smaller aquifers result in rapid decline of reservoir pressure, which normally results in changing the well control from constant production rate to specified bottom hole pressure (BHP). This changes completely the BT, since the assumption of constant production rate is no longer valid.

8 - A large aquifer, however, can also be modeled using a line of injectors at the bottom of the aquifer with total injection matching total production, for an aquifer size of 20 times the reservoir size. This line of injectors was simulated here using a HW injector in the lateral direction.

9 - Smaller aquifers with injectors give different BT depending on the position of the injectors and aquifer size, with no reasonable variation that could be correlated with a parameter that included the aquifer size. For such reasons, the correlations developed here will assume a large aquifer giving pressure support for the reservoir.

10 - There was no noticeable variation in BT or WOR for $c_{oD} < 10^{-5}$, which can be considered to be the incompressible oil flow case.

12 - Only for very small mobilities the parameter n_w gave a noticeable variation in BT and WOR. Even in this situation, the variation is about 10%. For this reason, this parameter will not be included in the correlations.

With these initial conclusions, we can define the form of the correlations as:

$$U = f(q_D, M, x_{eD}, h_{wD}, c_{oD}, n_o) \quad (5.71)$$

Oil column, h	100 m
Horizontal permeability, k_h	1 D
Vertical permeability, k_v	1 D
Porosity, ϕ	0.1
Oil density, ρ_o (standard)	1000 kg/m^3
Water density, ρ_w (standard)	900 kg/m^3
Gas density, ρ_g (standard)	1 kg/m^3
Gas-oil solubility ratio R_s	0
Oil viscosity, μ_o	1 cp
Water viscosity, μ_w	1 cp
Oil compressibility, c_o	1e-5 bar^{-1}
Water compressibility, c_w	1e-5 bar^{-1}
Rock compressibility, c_r	0.0
Connate water saturation, S_{wc}	0
Residual oil saturation, S_{or}	0
Oil relative permeability exponent, n_o	1
Water relative permeability exponent, n_w	1
Oil relative permeability at S_{wc} , k_{rocv}	1
Water relative permeability at S_{or} , k_{rwro}	1
Production rate, $q(q_D = 0.1)$	5428.74 m^3/day

Table 5.5: Basic data set for simulation runs

where U is either t_{btD} , WOR or Δz_D .

The reference case for the runs is based on :

- $q_D = 0.1$
- $M = 1$
- $x_{eD} = 20$
- $n_o = 1$
- $h_{wD} = 1$
- $c_{oD} = 10^{-5}$

With this basic data, we then started varying each of the parameters for the practical cases found in real field examples. The dimensionless range of parameters is given in Table 5.6. They cover the most common range used in practical situations. For instance, q ranges from 1000 m^3/day to 50000 m^3/day .

5.5.1 Breakthrough Time

Since a refined grid was used, the values of BT were recorded as the first appearance of water in the well. For this situation, large variations in BT are not expected for more refined grids, which was confirmed by several runs.

The reported values of BT using this procedure are shown in Table 5.6 In order to fit the BT values with each parameter, a set of basic equations for linear regression was used,

q_D	M	x_{eD}	h_{wD}	n_o	t_{btD}	C	m	Ermax(%)	C(m=0.5)	Ermax(%)
0.1	1	20	1	1	4.362	0.499	0.497	5.2	0.494	4.4
0.15					2.379	0.667	0.501	5.6	0.668	5.6
0.2					1.577	0.798	0.508	5.4	0.809	6.1
0.3					0.895	1.039	0.496	7.7	1.031	6.4
0.5					0.431	1.342	0.519	9.6	1.418	12.1
0.7					0.254	1.577	0.535	18.8	1.747	18.0
1.0					0.133	1.978	0.518	22.0	2.034	19.4
0.07					7.715	0.392	0.491	7.5	0.318	5.5
0.05					13.669	0.300	0.492	9.0	0.290	7.4
0.03					34.021	0.185	0.507	10.5	0.191	11.4
	2				3.688	0.568	0.498	9.7	0.566	9.4
	5				3.125	0.620	0.506	14.3	0.632	15.4
	10				3.058	0.669	0.499	17.1	0.668	16.9
	50				2.697	0.684	0.507	22.3	0.699	23.5
	100				2.260	0.651	0.522	25.8	0.694	30.3
	0.5				5.557	0.455	0.474	3.9	0.424	2.4
	0.1				12.044	0.305	0.461	3.4	0.265	7.8
		10			4.330	0.497	0.507	5.9	0.508	6.9
		5			4.155	0.369	0.671	4.9	0.601	24.0
		3			3.775	0.141	1.178	31.6	*	*
		2			3.236	0.109	1.520	34.0	*	*
		1			2.135	0.057	2.675	56.3	*	*
			0.9		4.073	0.524	0.481	4.4	0.498	2.2
			0.8		3.526	0.566	0.456	1.7	0.502	6.2
			0.7		2.863	0.625	0.419	2.0	0.512	12.8
			0.6		2.173	0.700	0.400	3.7	0.529	21.4
			0.5		1.522	0.791	0.374	6.6	0.554	30.96
				2	4.140	0.514	0.489	4.5	0.499	2.9
				3	3.685	0.542	0.477	2.8	0.508	2.7
				4	3.264	0.572	0.469	1.7	0.524	4.6
				5	2.927	0.599	0.466	0.85	0.542	6.3

Table 5.6: Dimensionless BT and parameters C and m of Equation 5.73 for each simulated data. A blank entry indicates that parameter has same value of reference case (first row)

* No reasonable correlation for m=0.5

Parameter	f(x)	f(y)	a	b	c	d
q_D	ln x	ln y	-1.9983	-1.7789	-0.2323	-0.0501
M	lnx	ln y	1.4701	-0.2613	0.0627	-0.0077
x_{eD}	lnx	y	2.1253	1.9515	-0.4307	0.0
h_{wD}	lnx	y	4.4306	4.2689	0.0	0.0
n_o	x	y	4.7994	-0.3746	0.0	0.0

Table 5.7: Correlations for BT using equation 5.72 with each parameter for the reference case.

given by:

$$f(y) = a + bf(x) + cf(x)^2 + df(x)^3 \quad (5.72)$$

With $f(x) = x$ or $\ln(x)$ and $f(y) = y$ or $\ln(y)$. x represents any of the parameters of Equation 5.71 and y is t_{btD} .

With this procedure we have four linear functions (with $c = d = 0$), four quadratic functions (with $d = 0$) and four cubic functions to fit the BT variation with each of the parameters, giving 12 functions to match the simulation results. The criteria to find the best match between the functions was a maximum error of 5% in the simplest possible function, since in several cases there is not much improvement from a linear to a quadratic or to a cubic regression.

The best matches for each case are shown in Table 5.7. The match for t_{btD} with q_D is shown in Fig. 5.1.

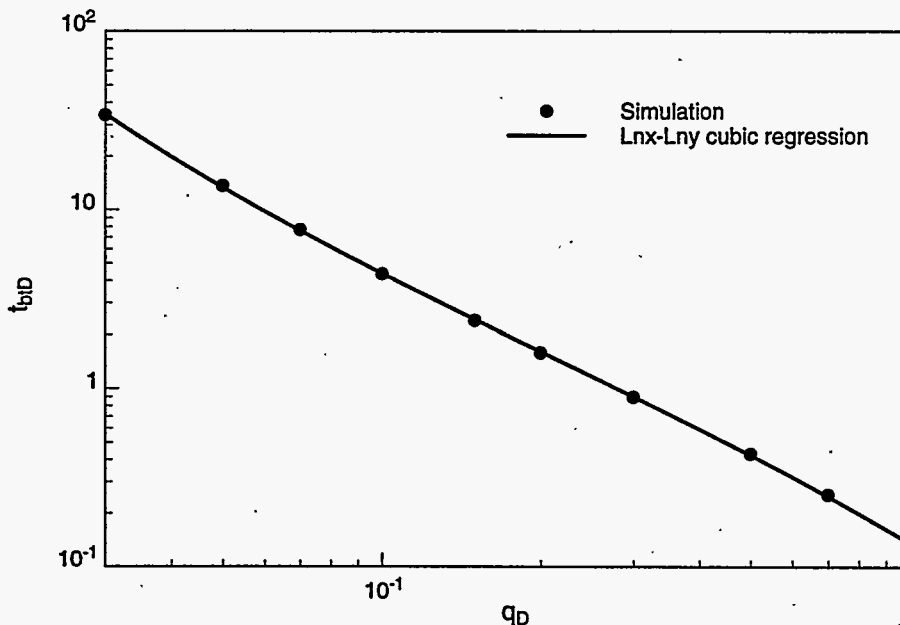


Figure 5.1: Comparison of breakthrough time correlation and simulation results

Figure 5.2 shows the correlation for t_{btD} with q_D compared with several correlations

found in literature described in Section 5.3. It can be noted that the correlations based on vertical equilibrium tend to overestimate BT while those based on constant pressure boundary at the aquifer tend to underestimate BT.

The next step is to include the parameter c_{oD} in the correlations and develop a general correlation for BT as a function of all the parameters.

5.5.2 Water-Oil Ratio

Figures 5.3 through 5.7 show the variation of WOR with each of the parameters studied in this work.

The correlations for WOR were derived using the result by Tiefertal [24] given by Equation 5.47, that can be written for WOR as:

$$1 + WOR = C(h_{wD})q_D(2t_D - t_{btD})^m \quad (5.73)$$

where $m = 0.5$.

As mentioned earlier, this equation is derived assuming vertical equilibrium. The runs demonstrated that the constant C is not only a function of h_{wD} , but also of all other parameters considered in this work. The exponent m can be assumed equal to 0.5 with a rather small error for all the parameters except x_{eD} .

Table 5.6 shows the values of C and m obtained by non-linear regression using the Gauss-Newton method, with the maximum relative error found for each case. It also shows the values of C assuming $m=0.5$.

Figure 5.8 shows the match for $q_D = 0.7$, the case where $m=0.535$, the largest difference from $m=0.5$ for rate variation. A good fit is obtained except in the beginning of the water production, which is normally responsible for the largest errors in all matches. Those differences, however, do not affect the general shape of the WOR curve, which can be seen in Fig. 5.9, which also shows the small difference for the match when $m=0.5$ is used.

The next step is to derive a correlation for C as a function of all the parameters and a correlation for m as a function of x_{eD} .

5.5.3 Optimum Grid.

The optimum grid is defined here as the dimension of the grid blocks that gives the minimum number of blocks for the simulation with a small variation in BT, N_{pD} and WOR behavior when compared with a refined grid block. From what is reported in literature and the experience with several runs, we can define the criteria for the optimum grid as:

- 1 - Maximum variation of 5% in BT for a refined grid block.
- 2 - Maximum variation of 3% in N_{pD} at $t_D = 3t_{btD}$ for a refined grid block.
- 3 - Visual inspection for WOR variation, that normally loses its smooth behavior for coarse grids.

Here we just need to find the variation of the vertical block dimension Δz_D , since the horizontal dimension Δx_D can be specified, as described at the beginning of this section, as a function of Δz_D .

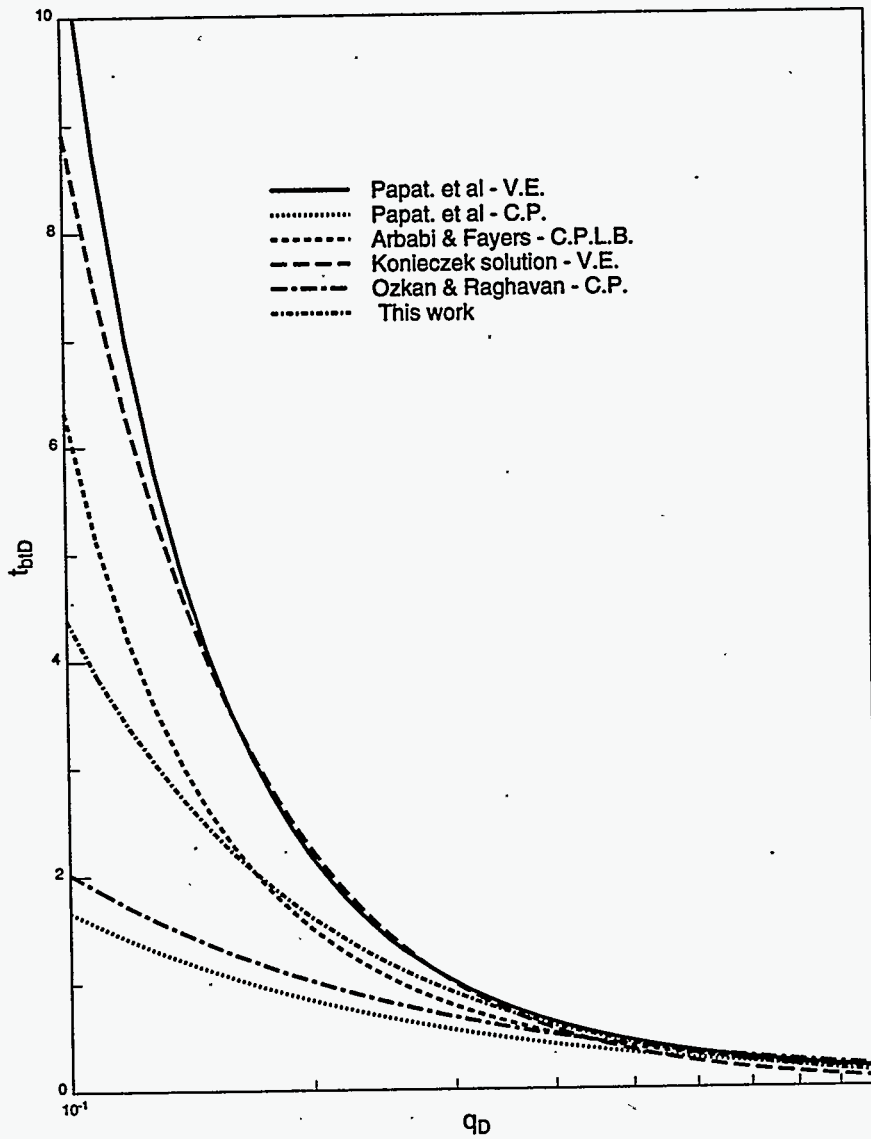


Figure 5.2: Comparison of various correlations for breakthrough time

Δz_D	t_{btD}	Var(%)	N_{pD}	Var(%)
0.01	4.362	-	0.9501	-
0.02	4.301	1.4	0.9485	0.2
0.03	4.258	2.4	0.9482	0.2
0.04	4.180	4.2	0.9396	1.1
0.05	4.160	4.6	0.9355	1.5
0.08	4.015	7.9	0.9125	3.9
0.1	3.898	10.6	0.8927	6.0
0.2	3.388	22.3	0.8085	14.9

Table 5.8: Variations in BT and N_{pd} with grid size for the reference case.

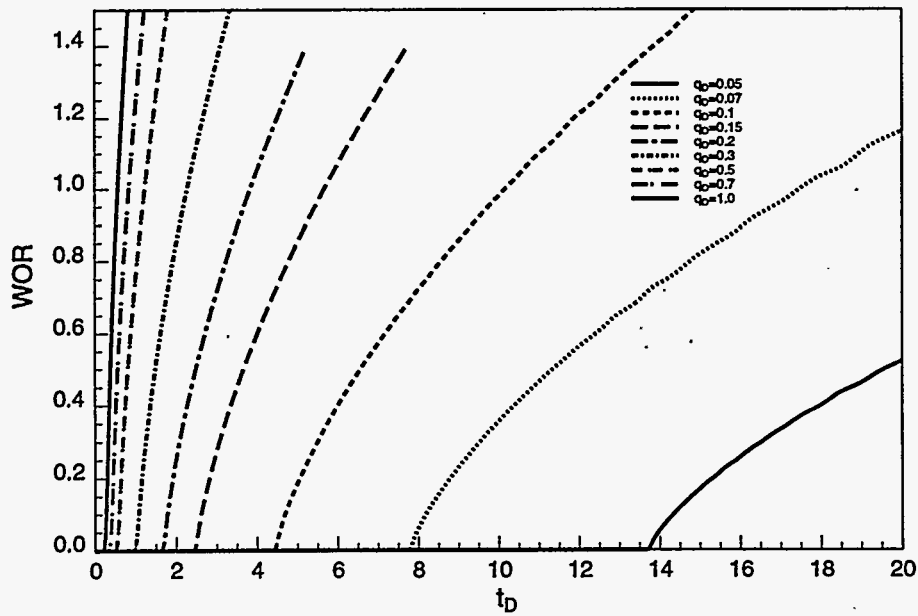


Figure 5.3: Effect of production rate in WOR as a function of time

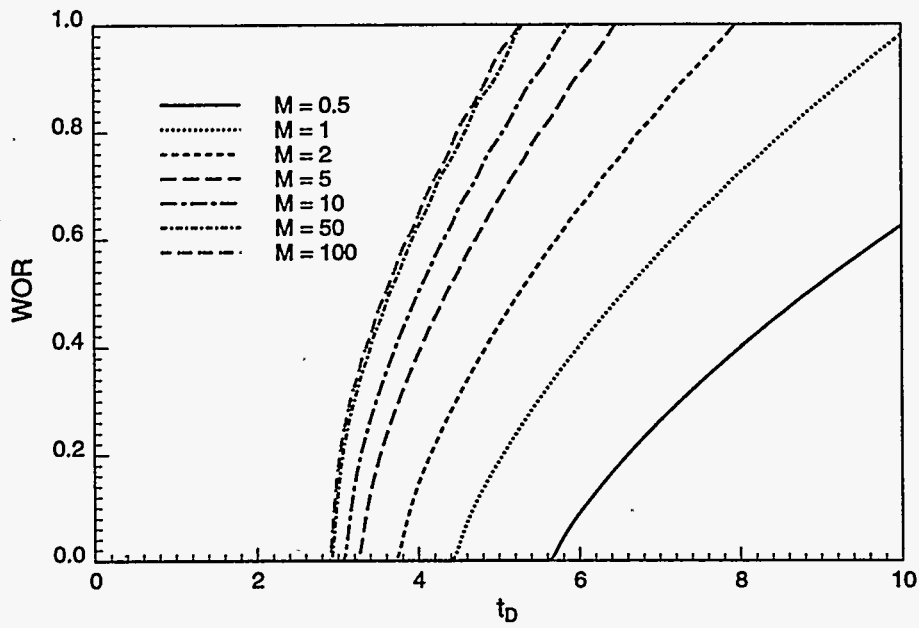


Figure 5.4: Effect of mobility ratio in WOR as a function of time

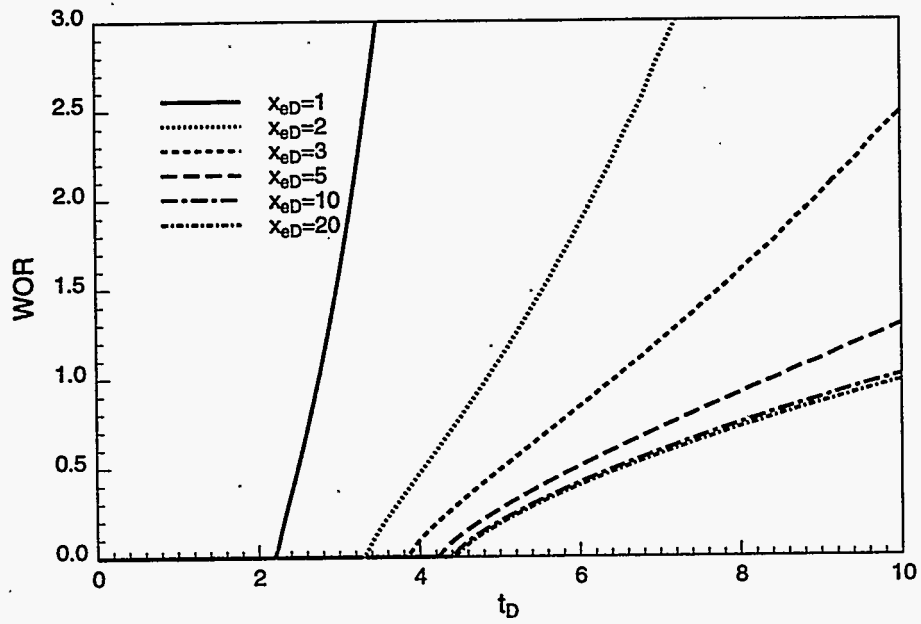


Figure 5.5: Effect of lateral reservoir size in WOR as a function of time

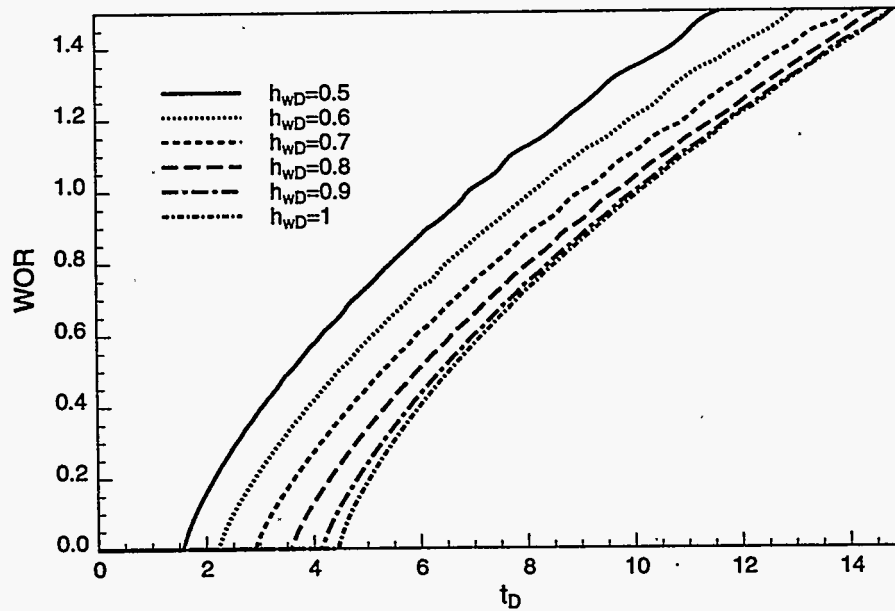


Figure 5.6: Effect of well height in WOR as a function of time

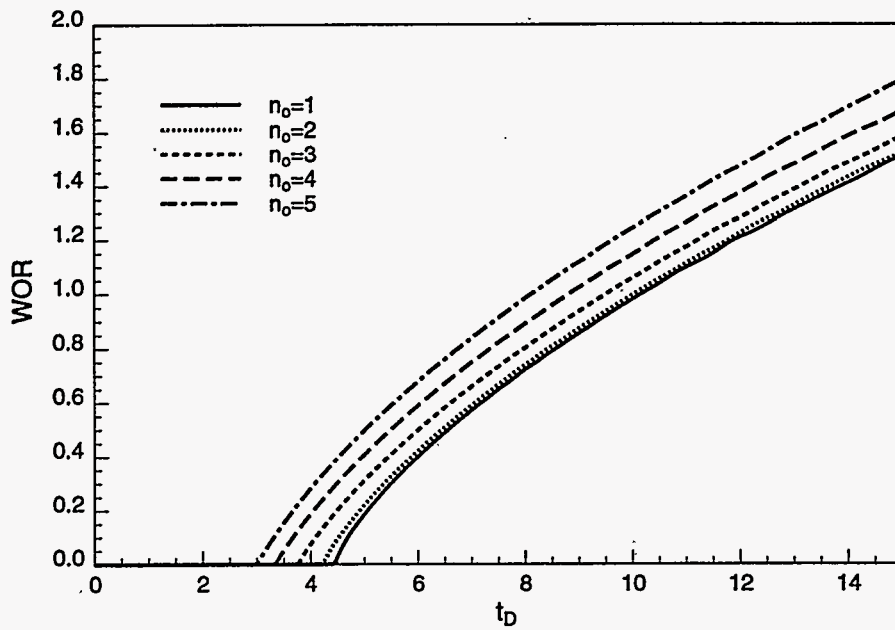


Figure 5.7: Effect of oil relative permeability exponent in WOR as a function of time

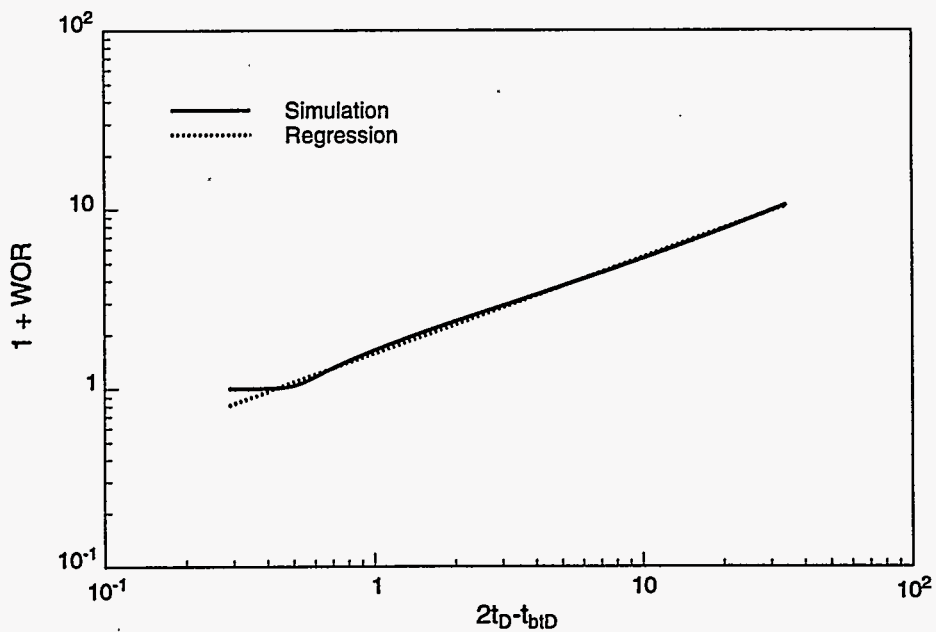


Figure 5.8: Comparison of WOR correlation and simulation results for a dimensionless rate of 0.7

Table 5.8 shows the variation of BT and N_{pD} for the reference case for several Δz_D , which are plotted in Fig. 5.10. Using the criteria defined above, we can give the optimum grid for the reference case as $\Delta z_D = 0.05$.

The next step here is to find the optimum grid for each case and then develop a correlation as a function of all the parameters.

5.6 Conclusions

We can give the following conclusions for this work:

Water and gas cresting behavior are important reservoir phenomena for which several analytical solutions and correlations have been developed throughout the petroleum history.

A thorough literature review of steady-state and transient solutions for cresting behavior was presented, showing the assumptions and parameters used by each author in their derivations.

A set of dimensionless variables was defined, leading the flow equations to a system of coordinates where the important parameters for a reservoir study can be easily visualized.

A new set of correlations for breakthrough time, water-oil ratio and optimum grid are being developed. They use the relevant parameters given by the flow equations and can be used at the beginning of a reservoir study to estimate breakthrough time, post breakthrough behavior and give an initial approach for the grid block sizes to use in the simulation runs.

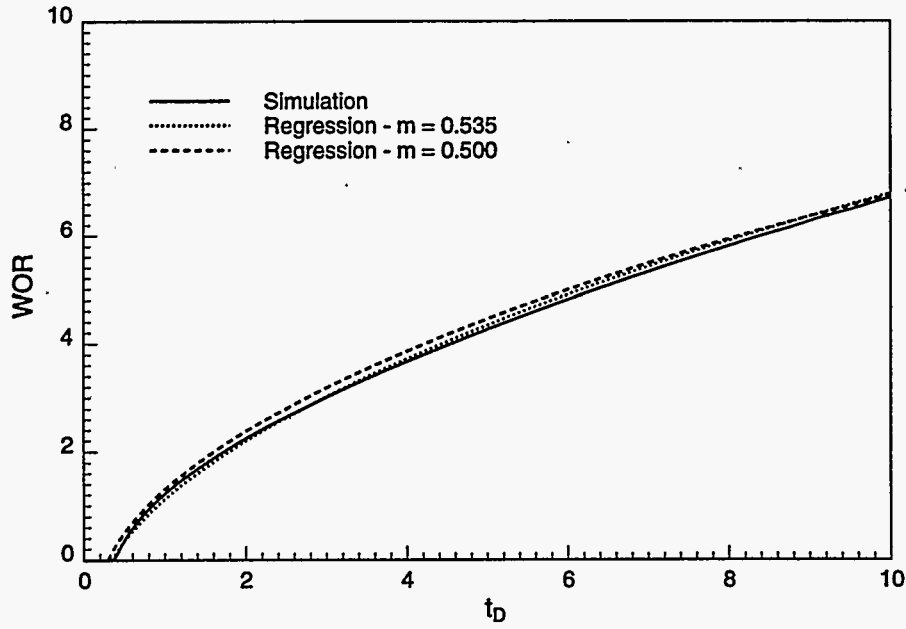


Figure 5.9: Comparison of WOR correlations and simulation results for a dimensionless rate of 0.7

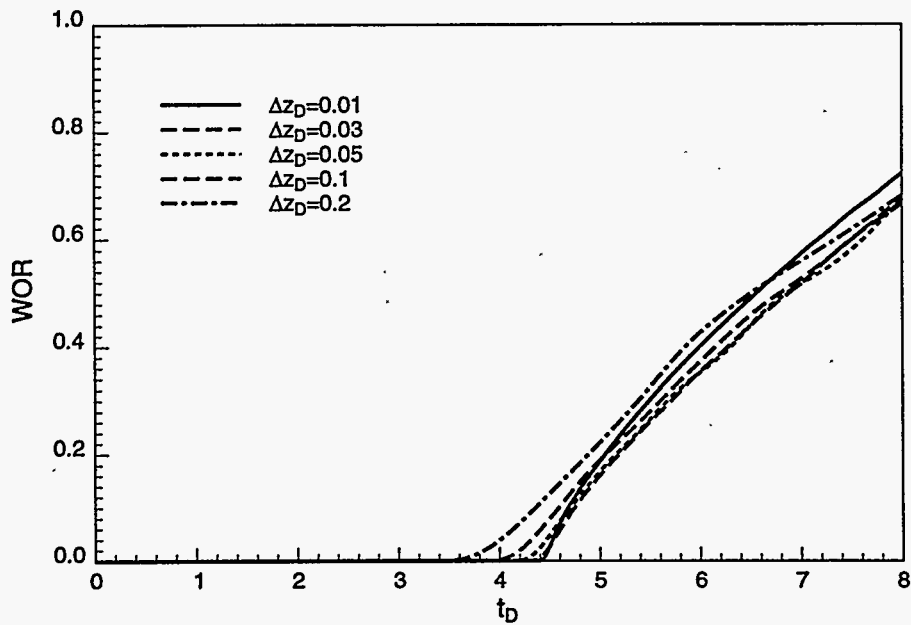


Figure 5.10: Effect of vertical block dimension in WOR as a function of time

Nomenclature

<i>B</i>	formation volume factor , m^3/m^3
<i>BC</i>	Boundary conditions
<i>BT</i>	Breakthrough time
<i>c</i>	compressibility, Pa^{-1}
<i>CP</i>	Constant pressure
<i>CPLB</i>	Constant potential in the lateral boundary
<i>D</i>	depth, distance from the surface, m
<i>DV</i>	Dimensionless variables
<i>f_w</i>	fractional water flow
<i>FVF</i>	formation volume factor, m^3/m^3
<i>g</i>	gravity acceleration = $9.81m/s^2$
<i>GLR</i>	Gas-liquid ratio
<i>GOC</i>	Gas-oil contact
<i>GOR</i>	Gas-oil ratio
<i>h</i>	height, distance from the bottom of the reservoir, m
<i>HW</i>	Horizontal well
<i>k</i>	permeability , m^2
<i>l</i>	phase
<i>L</i>	well length, m
<i>OG</i>	Optimum grid
<i>p</i>	pressure , Pa
<i>q</i>	rate at reservoir conditions, m^3/s
<i>Q</i>	rate at standard conditions, m^3/s
<i>Rs</i>	solubility ratio, m^3/m^3
<i>r</i>	radial direction, m
<i>s</i>	length in the streamline direction, m
<i>S</i>	saturation
<i>t</i>	time, s
<i>u</i>	velocity, m/s^2
<i>V</i>	volume , m^3
<i>VE</i>	vertical equilibrium
<i>VW</i>	vertical well
<i>x</i>	main horizontal direction, with the origin in the well, m
<i>w</i>	width (y direction), m^3
<i>WOC</i>	Water-oil contact
<i>WOR</i>	Water-oil rate
<i>WCT</i>	Water-cut
<i>y</i>	horizontal y direction, m
<i>z</i>	vertical direction, with the origin at the top of the reservoir, m

Greek

α	hydraulic diffusivity, m^2/s
γ	hydrostatic gradient = ρg , Pa/m
μ	viscosity $Pa.s$
ρ	density, kg/m^3
ϕ	porosity
Φ	potential, Pa
θ	angle
ζ	molar fraction of each component

Subscripts

b	barrier
bt	breakthrough
c	critical
cp	component
D	dimensionless
e	external (lateral edge)
ef	effective
g	gas
h	horizontal direction
i	grid block discretization index
l	phase
o	oil
or	oil residual
p	perforation
r	relative
res	reservoir
std	standard conditions
t	top of the perforations
v	vertical direction
w	water
wc	connate water
ω	well

Superscripts

-	average
~	per unit volume
n	time discretization level

Conversion Factors

$$\text{day} \times 8.64 \times 10^4 = \text{s}$$

$$\text{ft} \times 3.048 \times 10^{-1} = \text{m}$$

$$\text{bbl} \times 1.58987 \times 10^{-1} = \text{m}^3$$

$$\text{lbm} \times 4.53592 \times 10^{-1} = \text{kg}$$

$$\text{dyn} \times 1.0 \times 10^{-5} = \text{N}$$

$$\text{psi} \times 6.89476 \times 10^3 = \text{Pa}$$

$$\text{atm} \times 1.01325 \times 10^5 = \text{Pa}$$

$$\text{Bar} \times 1.0 \times 10^5 = \text{Pa}$$

$$\text{g/cm}^3 \times 1.0 \times 10^3 = \text{kg/m}^3$$

$$\text{lb/ft}^3 \times 1.60184 \times 10^1 = \text{kg/m}^3$$

$$\text{cp} \times 1.0 \times 10^{-3} = \text{Pa}\cdot\text{s}$$

$$\text{md} \times 9.86923 \times 10^{-4} = \mu\text{m}^2$$

$$\text{bbl/day} \times 1.84013 \times 10^{-6} = \text{m}^3/\text{s}$$

$$\text{psi/ft} \times 2.29158 \times 10^4 = \text{Pa/m}$$

* Conversion factor is exact

References

- [1] K. Aziz and A. Settari. *Petroleum Reservoir Simulation*. Elsevier Applied Science, New York, 1979.
- [2] K. Aziz. *Notes for Petroleum Reservoir Simulation*. Stanford University, 1994.
- [3] S. Arbabi and F. J. Fayers. Comparative aspects of coning behavior in horizontal and vertical wells. In *8th European Symposium on Improved Oil Recovery*, Vienna, Austria, May 1995.
- [4] J. Dupuit. *Etudes théoriques et pratiques sur le mouvement des eaux*. Dunod, Paris, Paris, 1863. In french.
- [5] P. Forchheimer. *Hydraulik Encyclopädie der Mathematischen Wissenschaften*. B.G. Teubner, Leipzig, 1901. In German.
- [6] M. Muskat. *The Flow of Homogeneous Fluids Through Porous Media*. Reprinted by I.H.R.D.C., Boston, 1982.
- [7] H. I. Meyer and A. O. Garder. Mechanics of two immiscible fluids in porous media. *Journal of Applied Physics*, 25(11):1400–1406, November 1954.
- [8] D. A. Efros. *Study of multiphase flow in porous media*. Gastoptexizdat, Leningrad, 1963. in Russian.
- [9] F. M. Giger. Evaluation théorique de l'effett d'arête d'eau sur la production par puits horizontaux. *Revue de l'institut Francais du Petrole*, 38(3), May 1983. In french.
- [10] F. M. Giger. Analytic 2-d models of water cresting before breakthrough for horizontal wells. *S.P.E.R.E.*, pages 409–416, November 1989.
- [11] B. J. Karcher, F. M. Giger, and J. Combe. Some practical formulas to predict horizontal well behavior. In *SPE 61st Annual Technical Conference and Exhibition*, New Orleans, Loisiaana, October 1986.
- [12] I. Chaperon. Theoretical study of coning toward horizontal and vertical wells in anisotropic formations: Subcritical and critical rates. In *SPE 61st Annual Technical Conference and Exhibition*, New Orleans, Loisiaana, October 1986.
- [13] S. D. Joshi. Augmentation of well productivity with slant and horizontal wells. *J.P.T.*, pages 729–739, June 1988.
- [14] M. J. Wheatley. An approximate theory of oil/water coning. In *SPE 60st Annual Technical Conference and Exhibition*, Las Vegas, September 1985.
- [15] B. Guo and R. L. Lee. An exact solution to critical oil rate of horizontal wells with water-oil interface cresting. In *Lerkendal Petroleum Engineering Workshop*, Trondheim, February 1992.

- [16] S. Fayers, F. J. and Arbabi and K. Aziz. Opportunities for horizontal wells and problems in predicting their performance. Technical report, Stanford University, 1993.
- [17] J. Boussinesq. Recherches theoriques sur l'ecoulement des nappes d'eau infiltrées dans le sol et sur debit de sources. *C.R.H. Acad. Sci. J. Math. Pures Appl.*, (10):5-78, June 1903. In french.
- [18] J. E. Chappellear and G. J. Hirasaki. A model of oil-water coning for 2-d areal reservoir simulation. *S. P. E. J.*, pages 65-74, April 1976.
- [19] D. V. Addington. An approach to gas-coning correlations for a large grid cell reservoir simulator. *J. P. T.*, pages 2267-2274, November 1981.
- [20] J. S. Nolen. Treatment of wells in reservoir simulation. In *3rd International Forum on Reservoir Simulation*, Baden, Austria, July 1990.
- [21] J. Konieczek. The concept of critical rate in gas coning and its use in production forecasting. In *SPE 65th Annual Technical Conference and Exhibition*, New Orleans, Louisiana, September 1990.
- [22] R. U. Papatzacos, T. R. Herring, R. Martinsen, and S. M. Skjaeveland. Cone breakthrough time for horizontal wells. *S.P.E.R.E.*, pages 311-318, August 1991.
- [23] E. Ozkan and R. Raghavan. A breakthrough time correlation for coning toward horizontal wells. In *SPE European Offshore Petroleum Conference*, The Hague, Netherlands, October 1990. Paper SPE 20964.
- [24] S. A. Tiefenthal. Supercritical production from horizontal wells in oil-rim reservoirs. *S.P.E.R.E.*, pages 272-277, November 1994.
- [25] W. Yang and R. A. Wattenberger. Water coning calculations for vertical and horizontal wells. In *SPE 66th Annual Technical Conference and Exhibition*, Dallas, October 1991.
- [26] F. Mohammed and D. G. Hatzignatiou. Water and gas coning in horizontal and vertical wells. In *45th Annual C.I.M. Petroleum Society et al Technical Meeting*, Calgary, Canada, June 1994.

6. Critical Rates for Simultaneous Gas and Water Cresting in Horizontal Wells

by Sepehr Arbabi and F. John Fayers

Abstract

We have extended our earlier semi-analytical method for determining critical cresting rates in horizontal wells [1] to the case of both water and gas cresting. The method and the procedure will be briefly described below. We also show the application of the method to an example problem and compare the results with direct numerical simulation.

6.1 Introduction

In the case of vertical wells, Piper and Gonzalez [2] devised a method for the double interface problem (simultaneous gas and water coning) based on Wheatley's method [3]. Figure 6.1 shows a schematic of the problem they have considered. For a vertical well partially completed in the pay zone, their method divides the oil column into two regions, one is referred to as the "gas region" and the other as the "water region". The division is based on locating a no flow boundary positioned somewhere in the completion interval. The location of this no flow boundary is determined when a dimensionless oil potential, defined as the ratio of the oil potential on the fluid contact to that on the well radius, is the same in both gas and water regions.

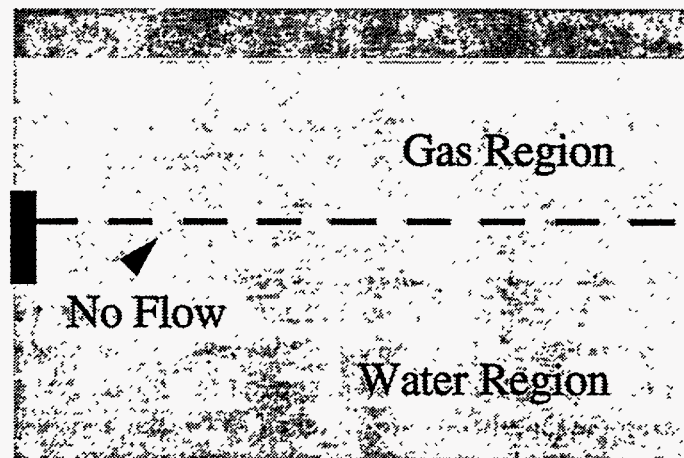


Figure 6.1: Schematic of the Water and Gas Coning Problem in Vertical Wells as Considered by Piper and Gonzalez [2]

It is found that the no flow boundary always falls in the well completion interval provided that the interval is not too close to either water or gas interface. Once the no flow boundary is located, the "gas region" and the "water region" have been identified. Next the critical rate for each region is

determined independently using Wheatley's method. The critical coning rate of the double interface problem is then given by the minimum of the two critical rates.

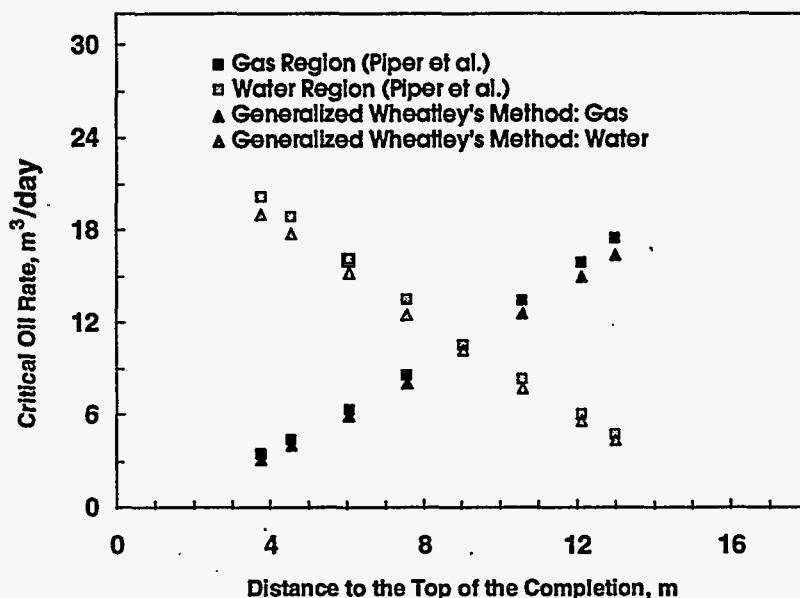


Figure 6.2: Variation of Critical Oil Rate versus Distance to the Top of the Completion for Vertical Wells

6.2 Considerations for Horizontal Wells

The use of a similar approach in extending our method to the double interface problem is not feasible as the horizontal well is modeled as a point sink in 2D and thus there is no completion interval where a no flow boundary might fall. Instead an alternative approach based on another method for vertical wells is utilized. In this second method referred to as the "generalized Wheatley's method," the restriction in Wheatley's method where the completion interval must extend to the upper or lower boundaries has been removed. Therefore, we can find critical rates for a vertical well partially completed in the oil zone for the *single* interface problem (either water or gas coning). These two approaches have been applied to an example problem involving both gas and water coning (example parameters are all taken to be the same as those used in Ref. [1], the only additional new parameter is $\rho_{ow} = 0.52$ gm/cc). Figure 6.2 above displays the results where we have plotted critical oil rate against the distance to the top of the completion. We observe two critical rates one associated with gas and the other with water in both methods. When these two rates become equal, such as when the completion interval is 9.15 m below the top of the reservoir in this example, the well is said to be positioned at its optimum location. The critical rate for any well located below the optimum well placement is governed by the encroachment of the water cone and similarly by the gas cone for wells located above the optimum location. Focusing on the Piper and Gonzalez solution in Fig. 6.2, we recall that the critical rate of the problem is given by the minimum of the two critical rates observed below and above the optimum well location. Figure 6.2 also demonstrates a very good agreement between

the Piper and Gonzalez solution and those from the generalized Wheatley's method (which are based on single interface problem) especially when the well is far away from a coning interface. In other words, when the well is moved away from a boundary with different boundary conditions related to the two and single interface problems, the influence of that boundary on the flow becomes similar in the two cases. That is why the two methods predict very close critical coning rates.

6.2.1 Procedure for Calculating Critical Cresting Rates

Based on the above result and discussion and the fact that the horizontal well could be at any depth in our method, we can devise a procedure using our single interface method to calculate critical cresting rates Q_c for cases with simultaneous water and gas cresting. A brief outline of the procedure is presented below:

1. Determine Optimum Well Location:

- Solve for Q_c with only gas present (one interface problem) Q_c (gas)
- Solve for Q_c with only water present (one interface problem) Q_c (water)
- Move the horizontal well until Q_c (gas) = Q_c (water) at h_{w0} . This locates the optimum well position and defines the "gas region" and the "water region".

2. Determine Critical Cresting Rate:

- for a horizontal well in the "gas region" ($h_w < h_{w0}$) $Q_c \sim Q_c$ (gas)
- for a horizontal well in the "water region" ($h_w > h_{w0}$) $Q_c \sim Q_c$ (water)

6.3 Example Problem

We have applied this procedure to an example problem involving water and gas cresting for both isotropic and anisotropic cases with the horizontal well located above and below the optimum well location (same parameters as in Fig. 6.2). Simulations were also performed to estimate critical cresting rates for the same example problem. Results are summarized in Table 6.1 for a horizontal well of length 500 m with a well spacing of about 400 m. The optimum well location is at 11.5 m below the top and the corresponding critical rate is 26 m³/day. Table 6.1 shows very good agreement between the method and the simulation results. We note the weak dependence of the critical rate for horizontal wells when the anisotropy ratio is reduced from 1 to 0.1. It is also counterintuitive to observe that Q_c decreases with a decrease in vertical permeability as predicted by the method and verified by the simulation results. This trend has also been documented by others [4-5] and is opposite to that observed in vertical wells. Finally, we give a direct comparison between the method and the simulation in regard to the shape of the interface. Figure 6.3 shows the shapes of the gas and water interfaces from the method and the simulation for case 2 in Table 6.1, which had the largest relative percentage difference of 5.5%. First of all, we see excellent agreement between the shape of the interface from the potential and stream

functions for both gas and water. Secondly, very good agreement is observed between the shape of the gas crest from the simulation and the new method while the agreement for the water interface is only reasonable. We note that the critical rate for this case is determined by the movement of the gas crest as the horizontal well is located above h_{wo} .

Table 6.1: Comparison of Critical Rates from the Method and the Simulation

Case	h_w, m	$Q_c, m^3/day$ Simulation	$Q_c, m^3/day$ New Method	% Difference
1 $K_v/K_h=1$	8.33	18.8	19.6	+4.3
2 $K_v/K_h=0.1$	8.33	16.4	17.3	+5.5
3 $K_v/K_h=1$	12.11	25.5	24.7	-3.1
4 $K_v/K_h=0.1$	12.11	23.7	22.4	-5.4

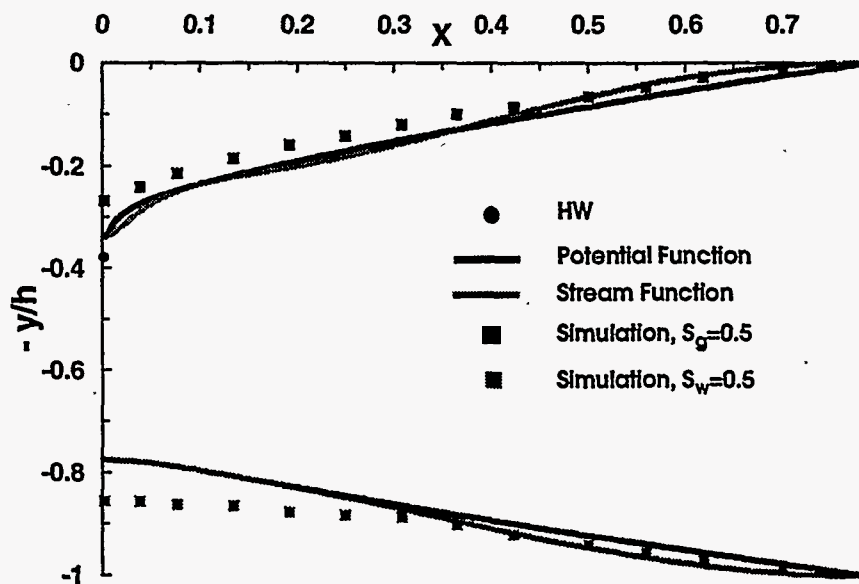


Figure 6.3: Comparison of the Shape of Interface between Simulation and the Semi-Analytical Method for both Gas and Water Crests ($X=\pi x/4x_e$)

6.4 Concluding Remarks

Critical rates for simultaneous gas and water cresting can be accurately predicted by the proposed method based on our earlier semi-analytical solution for a horizontal well at any depth in the reservoir.

Simulation runs and analytical predictions indicate that permeability anisotropy has a marginal effect on critical cresting rates. Furthermore, they show that critical rates decrease with an increase in the anisotropy ratio for horizontal wells located far away from the upper and lower reservoir boundaries.

References

- [1] Fayers, F. J. et al.: *Productivity and Injectivity of Horizontal Wells*, 2nd Annual Report to US Dept. of Energy, Stanford University, 27-46, (1995)
- [2] Piper, L. D. and Gonzalez Jr., F. M.: "Calculation of the Critical Oil Production Rate and Optimum Completion Interval," paper SPE 16206 presented at the SPE Production Operations Symposium, Oklahoma, March 8-10, (1987)
- [3] Wheatley, M. J. : "An Approximate Theory of Oil/Water Coning," SPE 14210 presented at the SPE 60th Annual Meeting, Las Vegas, September 22-25, (1985)
- [4] Chaperon, I.: "Theoretical Study of Coning Toward Horizontal and Vertical Wells in Anisotropic Formations: Subcritical and Critical Rates," paper SPE 15377 presented at the SPE 61st Annual Technical Conference and Exhibition, New Orleans, October 5-8, (1986)
- [5] Butler, R. M.: *Horizontal Wells for the Recovery of Oil, Gas and Bituman*, Petroleum Society Monograph No. 2, CIM, Calgary, 127-131, (1994)

